UNICA

UNIVERSITÀ
DEGLI STUDI
DI CAGLIARI

Ph.D. DEGREE IN
Industrial Engineering

Cycle XXXVI

TITLE OF THE Ph.D. THESIS

Methodologies for a simultaneous estimation of power grid parameters and systematic measurement errors

Scientific Disciplinary Sector

ING-INF/07

Ph.D. Student:	Ing. Carlo Sitzia
Supervisor	Prof. Ing. Sara Sulis
Co-Supervisor	Prof. Ing. Paolo Attilio Pegoraro

Final exam. Academic Year 2022/2023
Thesis defence: February 2024 Session

Contents

Introduction

Modern transmission and distribution systems are currently going through major changes. In particular, a massive penetration of new systems of production or consumption of energy (like distributed generation, electric vehicles or bidirectional charging stations) is underway. These changes require operators to rethink management, control and protection applications, with the main objective of following the evolution of power systems. It is indeed worth underlining that a "smart" management can bring important benefits to the efficiency and reliability of transmission and distribution grids.

Management and control of power systems are affected by an inevitable lack of knowledge about the actual operating conditions of the grid.

A key aspect that has an impact on most of the grid applications is the presence of uncertainty, in terms of modeling and behavior, in the knowledge of the power network parameters. In particular, the actual values of line parameters (i.e., resistances or reactances) may differ from those stored in Energy Management System (EMS) database. This difference can depend on a number of causes, like degradation due to the age, modeling inaccuracies and working conditions of the lines. Aware of this problem, researchers have dedicated, over the years, increasing attention on the problem of the estimation of the grid parameters. In this context, an accurate estimation helps system operators achieve effective monitoring and control applications.

In this regard, an important element in the availability of the system operators is the measurement infrastructure. Specifically, a key aspect of the monitoring architecture is the metrological behavior of the devices installed in the grid. In the last decades, an increasing interest, above all for the transmission systems but also for the distribution systems, raised on the employment of a new generation of instruments: the Phasor Measurement Units (PMUs). This kind of devices is able to provide accurate measurements of voltage and current phasors, frequency and rate of change of frequency at a high rate and synchronized with respect to Coordinated Universal Time (UTC). PMUs, thanks to the above mentioned characteristics, represent a powerful tool for overcoming

some of the limitations and difficulties associated with traditional monitoring and control systems. Nevertheless, despite the high accuracy of PMUs and all the benefits that their use can bring to power system monitoring, synchronized phasor (synchrophasor) measurements too are affected by the uncertainty sources of the measurement chain, which includes the Instrument Transformers (ITs). Therefore, for an effective exploitation of measured synchrophasors, it is necessary to design appropriate evaluation processes, taking into account the uncertainties of the entire measurement chain, which includes ITs (e.g., Current Transformer (CT) and Voltage Transformer (VT)). All the applications leveraging PMUs data must take into account the effects of uncertainty and, when possible, minimize them.

The measurement challenges described above motivated the research activity presented in this thesis, mainly focused on the estimation of power grid parameters. In particular, a methodology (applicable to both transmission and distribution grids) for a simultaneous estimation of power grid parameters and systematic measurement errors has been proposed. The methodology, depending on the applications, can be applied for both single-phase and three-phase systems.

The thesis is organized as follows:

- In Chapter 1, a literature review on the line parameters estimation in transmission and distribution systems is presented, also including the problem of transformer parameters estimation.

- In Chapter 2, a simultaneous estimation of both power grid parameters and systematic measurement errors exploiting PMU measurements is presented. In particular, detailed grid modeling and equations are reported for both single-phase and three-phase systems. The assumptions associated with the measurement error models are described in detail.

- In Chapter 3, the assumptions made on the measurement chain and on the modeling of the grid are analyzed. In particular, the presence of possible mismatch between assumptions and actual conditions is also considered, to evaluate the impact of this realistic condition on the estimates and to discuss possible solutions.

- In Chapter 4, the experimental validation of the estimation method through grid emulators (i.e., OPAL-RT) is discussed. This validation completes the validation process, which was initially carried out mainly via simulations.

- In Chapter 5, the inclusion of the discussed estimation methods in one of the most important power system management and control applications,

the fault location, has been analyzed. Also in this context, the impact of applying the proposed estimation procedure has been studied by means of a Real Time Digital Simulator (RTDS).

- Finally, motivation, analyses and main findings of the thesis are summarized in the Conclusions.

Chapter 1

Parameters estimation for transmission and distribution systems

1.1 Problem statement and motivations

Accurate knowledge of actual operating conditions is crucial for monitoring, management and control tasks. This knowledge is based on information about power network parameters. The line parameters of transmission and distribution systems are indeed critical inputs for several applications. Among others, it is possible to mention power-flow computations [1], state estimation [2], and fault location [3]. Since expensive measurement campaigns are necessarily infrequent, such parameters are usually computed based on assumptions regarding data such as length and conductors geometry, but factors like significant weather variations or aging, see for example [4], are not adequately taken into account. Thus, there is a inherent uncertainty on the parameter values available in the databases of Transmission System Operator (TSO) and Distribution System Operator (DSO) considered in the power network models, and these values can present deviations from actual values even in the order of tens of percent [5, 6]. This uncertainty can cause problems not only to the applications on which the correct functioning of Energy Management System (EMS) is based, but also to the economy and reliability of power dispatching control [7].

1.2 Literature review

1.2.1 Line parameters estimation

Line parameters estimation has been addressed with any type of measurements, mainly offline, but, an evaluation of line parameters based on a real-time monitoring would be of great help in improving and keeping updated with a certain periodicity the network model. In this regard, Phasor Measurement Units (PMUs) can be a powerful tool, with a reporting rate (RR) up to hundreds of measurements per second, permitting defining an estimation problem through time-aligned phasors. Nonetheless, it is worth underlining that phasor measurements are affected by the uncertainty sources of the entire measurement chain, which includes also the effects of Instrument Transformers (ITs). The network parameters estimation tools need to take all of this into account.

Focusing on the estimation process, the most commonly used model for the representation of the line is the π-model. In general, considering the π-model of a line, the parameters of interest are the resistance, reactance and the shunt admittance but, according to the specific case, it is possible to neglect some parameters.

In literature, the simplest approach to estimate line parameters based on PMUs is to obtain the values directly from PMU measurements. This is possible thanks to the relationships that can be derived from the π-model, which permit expressing the line parameters as a function of the voltage and current phasors that are directly monitored by PMUs. The direct calculation of line parameters is used in [8], where the calculation of the uncertainty bounds of transmission line parameters estimation is also presented. In [9], the same direct formulation, considering real PMU measurements, is used to evaluate the variability of line parameters (not considering previous calibration of ITs, and thus, without compensating the systematic errors). Such analysis shows the presence of a discrepancy with respect to the theoretical bounds found considering uncorrelated measurements. As a consequence, the presence of correlation in real measurements is highlighted via statistical analysis. In [10], line parameters estimation is addressed considering the positive sequence model of the transmission line and the presence of only PMU errors. This approach is applied in [11] too, where the identification of susceptances and reactances is addressed. Also in [12], the estimation of line parameters, considering series and shunt compensators, is addressed assuming the presence of PMU errors only. In [13–15], line parameters estimation methods are proposed for distribution grids, considering an error contribution introduced by PMUs.

In [5, 16], line parameters estimation is addressed considering multiple time

instants and modeling IT errors as zero-mean random noise, thus neglecting the contribution of systematic errors. Also in [17], where a single-phase line parameters estimation is proposed, PMU and IT errors are modeled as zero-mean Gaussian noise in the magnitude and phase-angle of each measurement. In the line parameters estimation problem discussed in [18] and [19] the entire measurement chain is taken into account, but random errors are the only type of error considered to influence the measurement process.

In literature, several papers address line parameters estimation problem using the Least Square (LS) method, using multiple time instants and under normal operating conditions. Among these, [20] presents a single-phase line parameters estimation based on field measurements, but, also in this case, the presence of systematic measurement errors in the estimation problem is not expected. Differently, in [21] three different LS methods have been compared using on field measurements and highlighting the problems due to the presence of systematic IT errors. Similar considerations are outlined in [22], where the limit of neglecting, in a real distribution grid, the contribution of IT errors is discussed. [23] presents a new method for line parameters estimation that considers the addition of extra parameters in the estimation model. In particular, these extra parameters account for the bias errors in the non-calibrated ITs.

In [24], a three-phase line parameters estimation for transmission systems is addressed using on-site measurements and a three-phase π-model for the lines. In this paper, as in [21] and [22], it is emphasized that IT accuracy must be considered. In [25], a PMU-based method for the calibration of voltage transformers is proposed, with the main purpose to find the optimal location of "good quality" measurements that bring calibration errors below a specific threshold. [26] proposes a method to estimate line parameters exploiting calibrated ITs at the start node and, in particular, these ITs are used to propagate the accuracy along the network under analysis.

In [27], the estimation problem of both systematic measurement errors and line parameters is faced neglecting current phase-angle and voltage-amplitude systematic errors. [28] presents, in a single-line approach, the estimation of systematic errors and line parameters assuming that ITs at the sending node are calibrated. In a preliminary step, a detection of uncalibrated ITs is also proposed. Also in [29], line parameters estimation along with the correction of uncalibrated instrument transformers is proposed, finding the presence of uncalibrated ITs with a bias error detection test.

In [30], a technique intended to estimate, for distribution systems, line parameters together with the systematic errors in the measurement chain is presented. The method, relying on a PMU monitoring system, is based on a linear approximation of the measurement functions and errors, and is validated on a

small portion of a grid. In [31], a new iterative algorithm that allows dealing with large line parameter deviations is proposed. It allows the simultaneous estimation of multiple impedances on multiple branches in distribution systems. Moreover, the systematic errors in the measurement chain are considered in the estimation problem, thus allowing the algorithm to estimate them as well. The method in [31] is extended for three-phase systems in [32], where constraints deriving from injected currents and zero injection are introduced and used together with voltage drops to improve the accuracy of the estimation.

1.2.2 Transformer parameters estimation

Accurate values of line parameters, as already underlined, are critical for several EMS applications, but, for a proper grid management, accurate information on the transformers parameters is also necessary. In this context, the presence of tap changers and, in particular, the value of the actual tap ratio of a power transformer is a key factor, sometimes difficult to obtain.

The tap changer plays a relevant role in monitoring and control of voltages and is a critical component, for example, in voltage stability operations [33] since it influences the margins of voltage stability. The tap changer is one of the most susceptible parts in the power transformer due to the fact that its elements suffer from both electrical and mechanical stresses [34], [35] (e.g., frequent operation changes lead to accelerating wear and tear) and its uncertainty can impact on applications of great importance like state estimation (see, as an example, [36, 37]).

In the context of transmission grids, many papers take into account the problem of estimating the tap changer behavior in equivalent single-phase power grids. For instance, [38] addresses the tap position identification problem and [39] presents an iterative state estimation method which includes, in the state vector, the tap positions. In [36] an augmented state estimation is proposed including additional state variables such as voltage turn ratios or phase shift angles of the transformers. This state estimation is addressed by means of a measurement model transformed to a conventional nodal frame formulation that introduces one fictitious bus and one fictitious branch for each transformer. Other papers consider the simultaneous estimation of line and transformer parameters due to the fact that an accurate knowledge of the value of tap changer parameters affects the effectiveness of network parameters estimation tools. In [40], a combined estimation of line and transformer parameters is proposed using a supervisory control and data acquisition (SCADA) system. For estimation purposes, the relationships between the state vector and the parameters of interest are considered in order to estimate linearly the single-phase values of tap

ratio, impedance and transversal susceptance. [41] presents a phasor-only augmented state estimator with current channel scaling factors. The estimation of tap position and line parameters is possible if a current PMU measurement is available and if sufficient measurement redundancy is ensured. A similar method is tested on a real system in [42]. However, in this context, the specific assessment of the impact of the measurement chain errors on the estimation results is not possible.

In [43, 44] the estimation of line and transformer parameters is addressed by means of PMUs (assumed at both ends of each line), adding measurement errors to the voltage and current synchrophasors obtained from load flow solutions. In [45] a PMU-based method for the identification of positive-sequence series transmission line and power transformer parameters is proposed. The developed method is capable to estimate also negative and zero sequence parameters but, in the measurement chain, only random errors are considered.

Besides the uncertainty of the tap changer ratio, also the model of the tap-changing transformer has an impact on monitoring and control applications. In this regard, two are the most used tap-changing transformer models in literature and in software packages implementation (see, for details, [46–48]). In particular, these two tap-changing transformer models are described as a π-model where the transformer short circuit impedance is provided by the nominal winding or by the tapped winding. The transformer parameters can be usually obtained from the data provided by manufacturers but, despite that, the nameplate data [49] do not provide specific information on the windings. In fact, manufacturers are not required to provide to customers this type of information.

In this context, some papers address the topic of a correct modeling of the transformer equipped with tap changer. In [50], it is emphasized how the use of a traditional tap-changing transformer model can lead to incongruities, while [33] presents, in the context of voltage stability studies, an improved π-model of the transformer that considers the possible impedance in each transformer winding. In [51], a general model for tap-changing transformer is presented. The model introduces an additional parameter, i.e. k, which represents the ratio among nominal and tapped winding impedances. The focus of this paper is to emphasize how the use of traditional models can lead to critical situations in case of transformers operating at extreme tap positions.

Starting from the aforementioned issues concerning the inaccurate knowledge of power grid parameters, this thesis aimed to develop and validate a methodology for estimating the power grid parameters and systematic measurement errors.

Chapter 2

Proposed Methodology: Modeling the grid and the measurement chain

In the context of estimation procedures for power network parameters, this thesis presents a PMU-based method for the estimation of line and transformer parameters (i.e., tap changer ratios) with the simultaneous compensation of amplitude and phase-angle systematic errors of voltage and current synchrophasor measurements. No assumption is made on the presence of pre-calibrated devices. In particular, the problem has been addressed considering the uncertainty of the measurement chain, which includes the errors introduced by PMUs and ITs. In the thesis, the general assumption about these errors is that random errors are mainly associated with PMUs, while systematic errors are mainly associated with ITs.

The algorithm presented in this thesis is based on a method presented in literature for the line parameters estimation in distribution systems. This method was conceived in both single-phase [30]-[31] and three-phase [52]-[32] versions. The proposed methodology, differently from [30–32, 52], has been designed to also work for transmission systems and to include the estimation of the transversal susceptances in the model. Moreover, the proposal is able to take into account and estimate power transformer parameters.

The problem of network parameters estimation is addressed initially with a single branch approach and then on multiple branches at the same time. This provides the algorithm with greater flexibility because it allows applicability to networks of different size. The algorithm can be applied indifferently to transmission or distribution grids and to either equivalent single-phase or three-

phase systems.

2.1 Single-phase method

In this section, the fundamental assumptions and analyses concerning the developed method are presented. For the sake of a simpler introduction to the method, firstly, an equivalent single-phase model of a three-phase system is considered for lines [53, 54] and tap-changing transformers [55].

2.1.1 Single-phase line model

As general assumptions of the method, a π-model (as shown in Fig. 2.1) is taken into account for a generic line (i, j) of a power system and a synchrophasor measurement unit is assumed to be available at each node.

This last assumption allows measuring two voltage synchrophasor measurements (indicated as v_i and v_j for the start and end nodes, respectively) and two branch current synchrophasor measurements ($i_{i,j}$ and $i_{j,i}$ flowing from the start and end nodes). PMU measurements, due to their nature, can be time-aligned and thus, it is possible to define a coordinated set of measurements associated with the same time instant t.

The line parameters of interest, for the π-model in Fig. 2.1, are the line impedance $z_{i,j} = R_{i,j} + jX_{i,j}$ and the shunt susceptance $B_{\mathrm{sh},i,j}$ (which, in this case, it is assumed equally divided into the two sides of the branch). It is then possible to define a measurement model that links the set of measured values, affected by uncertainties and line parameters, which are not exactly known. Each synchrophasor measurement can be expressed as a function of the reference values (indicated hereafter by the superscript ^{R}) and of the measurement errors. The voltage and current measurements are indicated as follows:

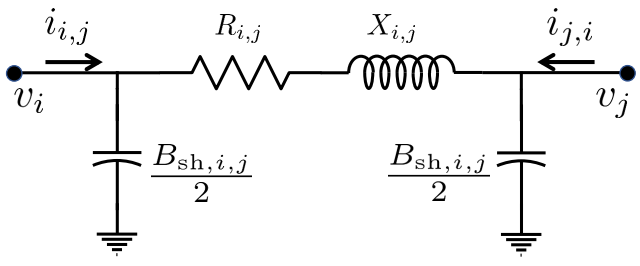

Figure 2.1: Equivalent single-phase π-model of a generic line with parameters and available measurements.

$$\begin{aligned} v_h &= V_h e^{j\varphi_h} = V_h^r + jV_h^x \\ &= (1 + \xi_h^{\text{sys}} + \xi_h^{\text{rnd}}) V_h^R e^{j(\varphi_h^R + \alpha_h^{\text{sys}} + \alpha_h^{\text{rnd}})} \\ i_{i,j} &= I_{i,j} e^{j\theta_{i,j}} = I_{i,j}^r + jI_{i,j}^x \\ &= (1 + \eta_{i,j}^{\text{sys}} + \eta_{i,j}^{\text{rnd}}) I_{i,j}^R e^{j(\theta_{i,j}^R + \psi_{i,j}^{\text{sys}} + \psi_{i,j}^{\text{rnd}})} \end{aligned} \tag{2.1}$$

where the subscript $_h$ represents the generic node of the branch (i, j) and, thus, V_h and φ_h are, respectively, the voltage magnitude and phase-angle measurements corresponding to node h. Focusing on the branch current $i_{i,j}$ flowing from node i toward the node j, $I_{i,j}$ and $\theta_{i,j}$ are its measured magnitude and phase-angle (similar considerations can be done for the branch current $i_{j,i}$). In (2.1), superscripts ^{r} and ^{x} are used for the real and imaginary parts of the corresponding phasors. The measurement errors affecting each measurement can be either systematic or random, indicated with superscripts $^{\text{sys}}$ and $^{\text{rnd}}$, respectively. In particular, the symbols ξ_h and $\eta_{i,j}$ refer to ratio errors of voltage and current, while α_h and $\psi_{i,j}$ are the phase displacement errors for v_h and $i_{i,j}$, respectively. Systematic and random errors are two different types of errors, with systematic errors that do not vary across repeated measurements, while random errors are different for each observation.

Since relationships on power systems are valid only on actual values of voltages and currents, it is useful to rewrite the reference values as a function of measured ones. To do that, it is assumed that, due to the typical IT and PMU accuracies, the absolute values of all the considered errors are much lower than one (i.e. $|\xi|, |\alpha|, |\eta|, |\psi| \ll 1$) and thus, it is possible to define the reference values v_h^R and $i_{i,j}^R$ as:

$$v_h^R \simeq \left(1 - \xi_h^{\text{sys}} - \xi_h^{\text{rnd}}\right) \left(V_h^r + jV_h^x\right) \left(1 - j\alpha_h^{\text{sys}} - j\alpha_h^{\text{rnd}}\right) \tag{2.2a}$$

$$i_{i,j}^R \simeq \left(1 - \eta_{i,j}^{\text{sys}} - \eta_{i,j}^{\text{rnd}}\right) \left(I_{i,j}^r + jI_{i,j}^x\right) \left(1 - j\psi_{i,j}^{\text{sys}} - j\psi_{i,j}^{\text{rnd}}\right) \tag{2.2b}$$

In (2.2), the relationships between measured and actual values are obtained using the approximation $(1 + x)^{-1} \simeq 1 - x$ for $x \simeq 0$ and the linearization of the exponential functions by means $e^{-jx} \simeq 1 - jx$. Applying a first order approximation to (2.2), it is then possible to express the final relationships:

$$v_h^R \simeq \left(V_h^r + jV_h^x\right) \left(1 - \xi_h^{\text{sys}} - \xi_h^{\text{rnd}} - j\alpha_h^{\text{sys}} - j\alpha_h^{\text{rnd}}\right) \tag{2.3a}$$

$$i_{i,j}^R \simeq \left(I_{i,j}^r + jI_{i,j}^x\right) \left(1 - \eta_{i,j}^{\text{sys}} - \eta_{i,j}^{\text{rnd}} - j\psi_{i,j}^{\text{sys}} - j\psi_{i,j}^{\text{rnd}}\right) \tag{2.3b}$$

A fundamental assumption of the presented estimation approach is that systematic errors cannot be omitted in the evaluation process and thus they are treated as unknown parameters to be estimated together with the line parameters. Focusing on Fig. 2.1, the line parameters can be expressed as a function

of their values available in System Operator (SO) database (indicated with the superscript ^{0}) and their deviations from these values. The expressions are indicated as:

$$\begin{aligned} z_{i,j} &= R^0_{i,j}\left(1+\gamma_{i,j}\right) + jX^0_{i,j}\left(1+\beta_{i,j}\right) \\ B_{\mathrm{sh},i,j} &= B^0_{\mathrm{sh},i,j}\left(1+\delta_{i,j}\right) \end{aligned} \tag{2.4}$$

where $\gamma_{i,j}$, $\beta_{i,j}$ and $\delta_{i,j}$ are the relative deviations of SO database values of resistance, reactance and transversal susceptance, respectively.

The proposed algorithm, in all of its formulations, is based on the constraints given by Kirchhoff's laws. The latters allow writing the equations among the line parameters, the measured values and measurement errors. The constraint equations derived from the voltage drop and the current balance equations are defined as:

$$\left(v_i^R - v_j^R\right) = z_{i,j}\left(i_{i,j}^R - j\frac{B_{\mathrm{sh},i,j}}{2}v_i^R\right) \tag{2.5}$$

$$\left(i_{i,j}^R + i_{j,i}^R\right) = j\frac{B_{\mathrm{sh},i,j}}{2}\left(v_i^R + v_j^R\right) \tag{2.6}$$

2.1.2 Tap-changing transformer model

Besides the unavoidable uncertainty on parameters, the possibility of having an accurate knowledge of the transformer behavior is complicated by the presence of the tap changers. Specifically, accurate knowledge on the actual tap ratio of the transformers in the power systems can be challenging to achieve. In fact, tap changer ratios are inevitably affected by uncertainty and this results into a high variability [56], which impacts on fundamental analysis tools in monitoring and control applications. Among these tools, also line parameters estimation methods can be affected by an inaccurate knowledge of tap changer ratios.

Thus, in this thesis, a method for the simultaneous estimation of line and transformer parameters is also addressed. Also in this case, the first approach to the problem is carried out using a single-phase model [46], shown in Fig. 2.2.

The transformer is associated with a branch (l,k) assumed to be equipped with PMUs at both ends. Similarly to what defined in Section 2.1.1 (replacing the pairs of indexes i,j with l,k), also for the π-model of the transformer, it is possible to express voltage measurements v_l and v_k (the associated reference values are v_l^R and v_k^R) and current measurements $i_{l,k}$ and $i_{k,l}$ (the associated reference values are $i_{l,k}^R$ and $i_{k,l}^R$) as in (2.3) relying on the same assumptions. The transformer resistance is assumed negligible with respect to the transformer reactance. For this reason, the transformer parameters can be defined as:

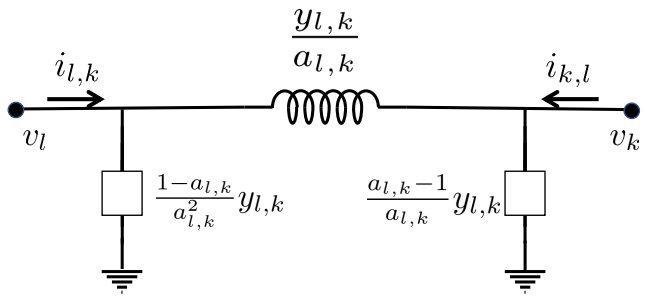

Figure 2.2: Equivalent single-phase π-model of a tap-changing transformer with parameters and available measurements.

$$\begin{aligned} z_{l,k} &= \frac{1}{y_{l,k}} = jX^0_{l,k}\left(1+\beta_{l,k}\right) \\ a_{l,k} &= a^0_{l,k}\left(1+\tau_{l,k}\right) \end{aligned} \tag{2.7}$$

where $X^0_{l,k}$ is the value of the transformer reactance available in the SO database, while $a^0_{l,k}$ represents the nominal tap changer ratio. Finally, $\beta_{l,k}$ and $\tau_{l,k}$ are the relative deviations of $X_{l,k}$ and $a_{l,k}$ with respect to $X^0_{l,k}$ and $a^0_{l,k}$, respectively.

In the presented procedure, tap changer ratio variations are considered unknowns to estimate. Considering the inertia of the mechanism, in what follows, these variations will be considered occurring on a much longer timescale than PMU reporting rate. Similarly to the complex equations (2.5)-(2.6) introduced for the line, it is possible to apply the Kirchhoff's laws also for the tap-changing transformer and define the following equations:

$$v^R_l - a_{l,k} v^R_k = a^2_{l,k} z_{l,k} i^R_{l,k} \tag{2.8}$$

$$i^R_{k,l} = -a_{l,k}\left(i^R_{l,k}\right) \tag{2.9}$$

2.1.3 Estimation framework

Following the assumptions of Sections 2.1.1 and 2.1.2 and thanks to the adopted approximations, it is possible to define a system of linear equations that link the measured values of voltage and current phasors with the unknown parameters to be estimated, which are:

- line parameters deviations for a generic line (i, j);
- reactance and tap ratio deviations for the transformer equipped with the tap changer (l, k);

- all the systematic measurement errors (magnitude and phase-angle) associated with the measured voltages and currents.

Firstly, it is possible to build the system of linear equations for a generic line corresponding to branch (i, j). In particular, replacing (2.3) and (2.4) in (2.5) and (2.6), and neglecting second order terms, four real valued equations can be obtained.

For the voltage drop constraint (2.5), the following two equations, for the real and imaginary parts, can be written:

$$\begin{aligned}
&V_i^r - V_j^r - I_{i,j}^r R_{i,j}^0 + I_{i,j}^x X_{i,j}^0 - \tfrac{B_{\mathrm{sh},i,j}^0}{2}\left(V_i^r X_{i,j}^0 + V_i^x R_{i,j}^0\right) \\
&\quad \simeq \left(\xi_i^{\mathrm{sys}} + \xi_i^{\mathrm{rnd}}\right)\left[V_i^r - \tfrac{B_{\mathrm{sh},i,j}^0}{2}\left(V_i^r X_{i,j}^0 + V_i^x R_{i,j}^0\right)\right] + \\
&\quad + \left(\alpha_i^{\mathrm{sys}} + \alpha_i^{\mathrm{rnd}}\right)\left[-V_i^x - \tfrac{B_{\mathrm{sh},i,j}^0}{2}\left(V_i^r R_{i,j}^0 - V_i^x X_{i,j}^0\right)\right] + \\
&\quad - \left(\xi_j^{\mathrm{sys}} + \xi_j^{\mathrm{rnd}}\right) V_j^r + \left(\alpha_j^{\mathrm{sys}} + \alpha_j^{\mathrm{rnd}}\right) V_j^x + \\
&\quad + \left(\eta_{i,j}^{\mathrm{sys}} + \eta_{i,j}^{\mathrm{rnd}}\right)\left(-I_{i,j}^r R_{i,j}^0 + I_{i,j}^x X_{i,j}^0\right) + \\
&\quad + \left(\psi_{i,j}^{\mathrm{sys}} + \psi_{i,j}^{\mathrm{rnd}}\right)\left(I_{i,j}^r X_{i,j}^0 + I_{i,j}^x R_{i,j}^0\right) + \\
&\quad + \gamma_{i,j} R_{i,j}^0 \left(I_{i,j}^r + \tfrac{B_{\mathrm{sh},i,j}^0}{2} V_i^x\right) + \\
&\quad + \beta_{i,j} X_{i,j}^0 \left(-I_{i,j}^x + \tfrac{B_{\mathrm{sh},i,j}^0}{2} V_i^r\right) + \\
&\quad + \delta_{i,j} \frac{B_{\mathrm{sh},i,j}^0}{2}\left(V_i^r X_{i,j}^0 + V_i^x R_{i,j}^0\right)
\end{aligned} \tag{2.10}$$

$$\begin{aligned}
&V_i^x - V_j^x - I_{i,j}^r X_{i,j}^0 - I_{i,j}^x R_{i,j}^0 + \tfrac{B_{\mathrm{sh},i,j}^0}{2}\left(V_i^r R_{i,j}^0 - V_i^x X_{i,j}^0\right) \\
&\quad \simeq \left(\xi_i^{\mathrm{sys}} + \xi_i^{\mathrm{rnd}}\right)\left[V_i^x + \tfrac{B_{\mathrm{sh},i,j}^0}{2}\left(V_i^r R_{i,j}^0 - V_i^x X_{i,j}^0\right)\right] + \\
&\quad + \left(\alpha_i^{\mathrm{sys}} + \alpha_i^{\mathrm{rnd}}\right)\left[V_i^r + \tfrac{B_{\mathrm{sh},i,j}^0}{2}\left(-V_i^r X_{i,j}^0 + V_i^x R_{i,j}^0\right)\right] + \\
&\quad - \left(\xi_j^{\mathrm{sys}} + \xi_j^{\mathrm{rnd}}\right) V_j^x - \left(\alpha_j^{\mathrm{sys}} + \alpha_j^{\mathrm{rnd}}\right) V_j^r + \\
&\quad + \left(\eta_{i,j}^{\mathrm{sys}} + \eta_{i,j}^{\mathrm{rnd}}\right)\left(-I_{i,j}^r X_{i,j}^0 - I_{i,j}^x R_{i,j}^0\right) + \\
&\quad + \left(\psi_{i,j}^{\mathrm{sys}} + \psi_{i,j}^{\mathrm{rnd}}\right)\left(-I_{i,j}^r R_{i,j}^0 + I_{i,j}^x X_{i,j}^0\right) + \\
&\quad + \gamma_{i,j} R_{i,j}^0 \left(I_{i,j}^x - \tfrac{B_{\mathrm{sh},i,j}^0}{2} V_i^r\right) + \\
&\quad + \beta_{i,j} X_{i,j}^0 \left(I_{i,j}^r + \tfrac{B_{\mathrm{sh},i,j}^0}{2} V_i^x\right) + \\
&\quad + \delta_{i,j} \frac{B_{\mathrm{sh},i,j}^0}{2}\left(V_i^x X_{i,j}^0 - V_i^r R_{i,j}^0\right)
\end{aligned} \tag{2.11}$$

The same assumptions, substitutions and approximations can be also applied to the current-balance constraint (2.6), defining two real valued equations (for the real and imaginary parts) as:

$$
\begin{aligned}
&I^r_{i,j} + I^r_{j,i} + \frac{B^0_{\mathrm{sh},i,j}}{2}\left(V^x_i + V^x_j\right) \\
&\qquad \simeq I^r_{i,j}\left(\eta^{\mathrm{sys}}_{i,j} + \eta^{\mathrm{rnd}}_{i,j}\right) - I^x_{i,j}\left(\psi^{\mathrm{sys}}_{i,j} + \psi^{\mathrm{rnd}}_{i,j}\right) + \\
&\qquad + I^r_{j,i}\left(\eta^{\mathrm{sys}}_{j,i} + \eta^{\mathrm{rnd}}_{j,i}\right) - I^x_{j,i}\left(\psi^{\mathrm{sys}}_{j,i} + \psi^{\mathrm{rnd}}_{j,i}\right) + \\
&\qquad + \tfrac{B^0_{\mathrm{sh},i,j}}{2}\left[\left(\xi^{\mathrm{sys}}_i + \xi^{\mathrm{rnd}}_i\right)V^x_i + \left(\xi^{\mathrm{sys}}_j + \xi^{\mathrm{rnd}}_j\right)V^x_j + \right. \\
&\qquad \left. + V^r_i\left(\alpha^{\mathrm{sys}}_i + \alpha^{\mathrm{rnd}}_i\right) + V^r_j\left(\alpha^{\mathrm{sys}}_j + \alpha^{\mathrm{rnd}}_j\right) - \left(V^x_i + V^x_j\right)\delta_{i,j}\right]
\end{aligned}
\tag{2.12}
$$

$$
\begin{aligned}
&I^x_{i,j} + I^x_{j,i} - \frac{B^0_{\mathrm{sh},i,j}}{2}\left(V^r_i + V^r_j\right) \\
&\qquad \simeq I^x_{i,j}\left(\eta^{\mathrm{sys}}_{i,j} + \eta^{\mathrm{rnd}}_{i,j}\right) + I^r_{i,j}\left(\psi^{\mathrm{sys}}_{i,j} + \psi^{\mathrm{rnd}}_{i,j}\right) + \\
&\qquad + I^r_{j,i}\left(\eta^{\mathrm{sys}}_{j,i} + \eta^{\mathrm{rnd}}_{j,i}\right) + I^x_{j,i}\left(\psi^{\mathrm{sys}}_{j,i} + \psi^{\mathrm{rnd}}_{j,i}\right) + \\
&\qquad + \tfrac{B^0_{\mathrm{sh},i,j}}{2}\left[-V^r_i\left(\xi^{\mathrm{sys}}_i + \xi^{\mathrm{rnd}}_i\right) - V^r_j\left(\xi^{\mathrm{sys}}_j + \xi^{\mathrm{rnd}}_j\right) + \right. \\
&\qquad \left. + V^x_i\left(\alpha^{\mathrm{sys}}_i + \alpha^{\mathrm{rnd}}_i\right) + V^x_j\left(\alpha^{\mathrm{sys}}_j + \alpha^{\mathrm{rnd}}_j\right) + \left(V^r_i + V^r_j\right)\delta_{i,j}\right]
\end{aligned}
\tag{2.13}
$$

Then, focusing on the generic branch (l,k) associated with a tap-changing transformer, it is possible to define two pairs of real valued equations for both voltage drop and current-balance constraints. In particular, replacing the voltages v^R_l, v^R_k, the currents $i^R_{l,k}$, $i^R_{k,l}$ and the transformer parameters (2.7) in (2.8), and neglecting second order terms, it is possible to write, for the voltage drop constraint (2.8), the equations as:

$$
\begin{aligned}
&V^r_l - a^0_{l,k}\left(V^r_k\right) + (a^0_{l,k})^2 X^0_{l,k} I^x_{l,k} \\
&\quad \simeq \left(\xi^{\mathrm{sys}}_l + \xi^{\mathrm{rnd}}_l\right)V^r_l - \left(\alpha^{\mathrm{sys}}_l + \alpha^{\mathrm{rnd}}_l\right)V^x_l + \\
&\quad - \left(\xi^{\mathrm{sys}}_k + \xi^{\mathrm{rnd}}_k\right)a^0_{l,k}V^r_k + \left(\alpha^{\mathrm{sys}}_k + \alpha^{\mathrm{rnd}}_k\right)a^0_{l,k}V^x_k + \\
&\quad + \left(\eta^{\mathrm{sys}}_{l,k} + \eta^{\mathrm{rnd}}_{l,k}\right)(a^0_{l,k})^2 X^0_{l,k} I^x_{l,k} + \left(\psi^{\mathrm{sys}}_{l,k} + \psi^{\mathrm{rnd}}_{l,k}\right)(a^0_{l,k})^2 X^0_{l,k} I^r_{l,k} + \\
&\quad - \beta_{l,k}(a^0_{l,k})^2 X^0_{l,k} I^x_{l,k} + \tau_{l,k}\left[a^0_{l,k}V^r_k - 2(a^0_{l,k})^2 I^x_{l,k} X^0_{l,k}\right]
\end{aligned}
\tag{2.14}
$$

$$
\begin{aligned}
&V^x_l - a^0_{l,k}V^x_k - (a^0_{l,k})^2 X^0_{l,k} I^r_{l,k} \\
&\quad \simeq \left(\xi^{\mathrm{sys}}_l + \xi^{\mathrm{rnd}}_l\right)V^x_l + \left(\alpha^{\mathrm{sys}}_l + \alpha^{\mathrm{rnd}}_l\right)V^r_l + \\
&\quad - \left(\xi^{\mathrm{sys}}_k + \xi^{\mathrm{rnd}}_k\right)a^0_{l,k}V^x_k - \left(\alpha^{\mathrm{sys}}_k + \alpha^{\mathrm{rnd}}_k\right)a^0_{l,k}V^r_k + \\
&\quad - \left(\eta^{\mathrm{sys}}_{l,k} + \eta^{\mathrm{rnd}}_{l,k}\right)(a^0_{l,k})^2 X^0_{i,j} I^r_{l,k} + \left(\psi^{\mathrm{sys}}_{l,k} + \psi^{\mathrm{rnd}}_{l,k}\right)(a^0_{l,k})^2 X^0_{l,k} I^x_{l,k} + \\
&\quad + \beta_{l,k}(a^0_{l,k})^2 X^0_{l,k} I^r_{l,k} + \tau_{l,k}\left[a^0_{l,k}V^x_k + 2(a^0_{l,k})^2 I^r_{l,k} X^0_{l,k}\right]
\end{aligned}
\tag{2.15}
$$

Finally, considering the same substitutions and approximations for the current balance constraint equation (2.9), it is possible to define two real-valued

equations:

$$\begin{aligned} I^r_{k,l} + a^0_{l,k} I^r_{l,k} \simeq & \left(\eta^{\text{sys}}_{k,l} + \eta^{\text{rnd}}_{k,l}\right) I^r_{k,l} - \left(\psi^{\text{sys}}_{k,l} + \psi^{\text{rnd}}_{k,l}\right) I^x_{k,l} + \\ & + \left(\eta^{\text{sys}}_{l,k} + \eta^{\text{rnd}}_{l,k}\right) a^0_{l,k} I^r_{l,k} - \left(\psi^{\text{sys}}_{l,k} + \psi^{\text{rnd}}_{l,k}\right) a^0_{l,k} I^x_{l,k} + \\ & - \tau_{l,k} a^0_{l,k} I^r_{l,k} \end{aligned} \tag{2.16}$$

$$\begin{aligned} I^x_{k,l} + a^0_{l,k} I^x_{l,k} \simeq & \left(\eta^{\text{sys}}_{k,l} + \eta^{\text{rnd}}_{k,l}\right) I^x_{k,l} + \left(\psi^{\text{sys}}_{k,l} + \psi^{\text{rnd}}_{k,l}\right) I^r_{k,l} + \\ & + \left(\eta^{\text{sys}}_{l,k} + \eta^{\text{rnd}}_{l,k}\right) a^0_{l,k} I^x_{l,k} + \left(\psi^{\text{sys}}_{l,k} + \psi^{\text{rnd}}_{l,k}\right) a^0_{l,k} I^r_{l,k} + \\ & - \tau_{l,k} a^0_{l,k} I^x_{l,k} \end{aligned} \tag{2.17}$$

In (2.10)-(2.17) the left-hand side terms are the known terms, which are composed of measured and nominal values (indicated with the superscript ^{0}), those on the right-hand side are function not only of the considered measurement errors but also of line (or transformer) parameters deviations. In the right side, besides the random errors, there are the systematic magnitude and phase-angle errors, e.g. of ITs, that, in addition to line and power transformer parameters, need to be estimated.

The four equations (2.10)-(2.13) for a generic line (i, j) and, similarly, the equations (2.14)-(2.17) for the generic power transformer branch (l, k) represent a set of new equivalent measurements related to the unknown parameters and the random measurement errors. Considering a generic branch (i, j) and a single measurement instant t associated with the time-tag of PMUs, it possible to define a system of equations as follows:

$$\begin{aligned} \mathbf{b}_{i,j,t} = \mathbf{H}_{i,j,t} & \begin{bmatrix} \xi^{\text{sys}}_i \\ \alpha^{\text{sys}}_i \\ \xi^{\text{sys}}_j \\ \alpha^{\text{sys}}_j \\ \eta^{\text{sys}}_{i,j} \\ \psi^{\text{sys}}_{i,j} \\ \eta^{\text{sys}}_{j,i} \\ \psi^{\text{sys}}_{j,i} \\ \gamma_{i,j} \\ \beta_{i,j} \\ \delta_{i,j} \end{bmatrix} + \mathbf{E}_{i,j,t} \begin{bmatrix} \xi^{\text{rnd}}_i \\ \alpha^{\text{rnd}}_i \\ \xi^{\text{rnd}}_j \\ \alpha^{\text{rnd}}_j \\ \eta^{\text{rnd}}_{i,j} \\ \psi^{\text{rnd}}_{i,j} \\ \eta^{\text{rnd}}_{j,i} \\ \psi^{\text{rnd}}_{j,i} \end{bmatrix} \\ & = \mathbf{H}_{i,j,t}\mathbf{x}_{i,j} + \mathbf{E}_{i,j,t}\boldsymbol{e}_{i,j,t} = \mathbf{H}_{i,j,t}\mathbf{x}_{i,j} + \boldsymbol{\epsilon}_{i,j,t} \end{aligned} \tag{2.18}$$

In (2.18), $\mathbf{b}_{i,j,t}$ is the 4×1 vector of known terms at time t, $\mathbf{H}_{i,j,t}$ is the measurement matrix that links the equivalent measurements to the unknown parameters to be estimated. Finally, $\mathbf{E}_{i,j,t}$ is the transformation matrix (Jacobian matrix) relating equivalent measurements random error vector $\boldsymbol{\epsilon}_{i,j,t}$ to the

PMU random errors in $\mathbf{e}_{i,j,t}$, while the state vector $\mathbf{x}_{i,j}$ groups the 11 unknowns ($\gamma_{i,j}$, $\beta_{i,j}$ and $\delta_{i,j}$ plus the magnitude and phase-angle systematic errors for v_i, v_j, $i_{i,j}$ and $i_{j,i}$) of the branch (i,j).

Similar considerations and conclusions can be drawn also for the generic tap-changing transformer branch (l,k). The only difference with respect to the line (i,j) is that the state vector $\mathbf{x}_{l,k}$ has 10 unknowns due to the model in Fig. 2.2, which has $\beta_{l,k}$ and $\tau_{l,k}$ as parameters of interest.

If only the timestamp t is considered, the estimation problem defined in (2.18), is undetermined (as underlined in [57]) since there are 4 equations in 11 unknowns. In this context, the idea was to consider multiple time instants $t_1, ..., t_{N_t}$ and their associated measurement sets to define a new system of equations:

$$\begin{aligned}\mathbf{b}_{i,j} &= \begin{bmatrix}\mathbf{b}_{i,j,t_1}\\ \vdots \\ \mathbf{b}_{i,j,t_{N_t}}\end{bmatrix} = \begin{bmatrix}\mathbf{H}_{i,j,t_1}\\ \vdots \\ \mathbf{H}_{i,j,t_{N_t}}\end{bmatrix}\mathbf{x}_{i,j} + \begin{bmatrix}\mathbf{E}_{i,j,t_1}\\ \vdots \\ \mathbf{E}_{i,j,t_{N_t}}\end{bmatrix}\mathbf{e}_{i,j} \\ &= \mathbf{H}_{i,j}\mathbf{x}_{i,j} + \boldsymbol{\epsilon}_{i,j}\end{aligned} \tag{2.19}$$

This can be achieved thanks to PMUs, which, due to their high RR (which can reach hundreds of measurements per second), can provide different snapshots of the same load condition, i.e. repeated observations of basically the same network condition. Thus, for the estimation problem, it is possible to consider two types of measurements:

- measurements that represent different load or generator conditions, associated with different "cases" (in what follows, the number of cases considered will be indicated as C).
- repeated measurements of the same network condition (for each of the C cases) that, due to the small time interval (corresponding to 1 s or less), can been averaged to reduce the random error contribution on the measurements.

By averaging the measurement data, the problem (2.19) that has a number of time instants $N_t = M \cdot C$ (i.e., C cases and M repeated observations for each case), can be considered composed only of C cases.

Then, in addition to the equations in (2.19), prior information about the IT class (from the manufacturer's specifications) and assumed maximum network parameters variability can be used to define an augmented and overdetermined estimation problem as:

$$\mathbf{b}_{i,j,\text{tot}} = \begin{bmatrix} \mathbf{b}_{i,j} \\ \mathbf{0}_{11\times 1} \end{bmatrix} = \begin{bmatrix} \mathbf{H}_{i,j} \\ \mathbf{I}_{11} \end{bmatrix} \mathbf{x}_{i,j} + \begin{bmatrix} \boldsymbol{\epsilon}_{i,j} \\ \mathbf{e}_{\text{prior}} \end{bmatrix} = \mathbf{H}_{i,j,\text{tot}} \mathbf{x}_{i,j} + \boldsymbol{\epsilon}_{i,j,\text{tot}} \tag{2.20}$$

where $\mathbf{0}_{11\times 1}$ is a vector of zeros of length 11, which defines the pseudo-measurements associated to the prior information (i.e., no deviations is assumed), while $\mathbf{I}_{11}$ is the identity matrix of size 11. Finally, $\boldsymbol{\epsilon}_{i,j,\text{tot}}$ includes not only the equivalent random errors but also the random variables that represent prior errors.

The problem in (2.20) can be solved, as will be discussed in detail in the Section 2.1.3, by means of Weighted Least Square (WLS) estimation, where the weight matrix $\mathbf{W}_{i,j,\text{tot}}$ is chosen as the inverse of the covariance matrix of measurements and prior errors:

$$\boldsymbol{\Sigma}_{\boldsymbol{\epsilon}_{i,j,\text{tot}}} = \begin{bmatrix} \boldsymbol{\Sigma}_{\boldsymbol{\epsilon}_{i,j}} & \mathbf{0} \\ \mathbf{0} & \Sigma_{\mathbf{e}_{\text{prior}}} \end{bmatrix} \tag{2.21}$$

The resulting covariance matrix includes, on the first diagonal term, the covariance matrix of all the equivalent measurements (assumed, in absence of specific information, decorrelated for all cases), obtained applying the uncertainty propagation law [58] to the matrix representing the PMU uncertainty $\boldsymbol{\Sigma}_{\mathbf{e}_{i,j}}$, as follows:

$$\boldsymbol{\Sigma}_{\boldsymbol{\epsilon}_{i,j}} = \mathbf{E}_{i,j} \boldsymbol{\Sigma}_{\mathbf{e}_{i,j}} \mathbf{E}_{i,j}^{\intercal} \tag{2.22}$$

where $^{\intercal}$ indicates the transpose operator. It is worth highlighting that $\mathbf{E}_{i,j}$ is a rectangular full row rank matrix, and thus, the matrix $\boldsymbol{\Sigma}_{\boldsymbol{\epsilon}_{i,j}}$ is invertible. The second diagonal term $\Sigma_{\mathbf{e}_{\text{prior}}}$ in (2.21) includes all the prior variances of the unknowns. Thus, the resulting WLS problem is:

$$(\mathbf{H}_{i,j,\text{tot}}^{\intercal} \mathbf{W}_{i,j,\text{tot}} \mathbf{H}_{i,j,\text{tot}}) \hat{\mathbf{x}}_{i,j} = \mathbf{H}_{i,j,\text{tot}}^{\intercal} \mathbf{W}_{i,j,\text{tot}} \mathbf{b}_{i,j,\text{tot}} \tag{2.23}$$

where $\hat{\mathbf{x}}_{i,j}$ is the estimated vector.

Estimation on a set of branches

Considering multiple branches altogether (defining a branch set Γ of cardinality N_{br}) at the same time, the problem can be defined considering all the voltage constraints (2.5) and the current equations (2.6) for all the branches $(i,j) \in \Gamma$. In this case, the unknowns are all the systematic measurement errors and line parameters deviations of the N_{br} branches involved, all grouped in the augmented state vector $\mathbf{x}_\Gamma$. Thus, the system in (2.19) grows to become a

$4 \times N_{br}$ set of equations with n unknowns:

$$\mathbf{b}_{\Gamma,t} = \begin{bmatrix} \mathbf{b}_{(i_1,j_1),t} \\ \vdots \\ \mathbf{b}_{(i_{N_{br}},j_{N_{br}}),t} \end{bmatrix} = \mathbf{H}_{\Gamma,t}\mathbf{x}_\Gamma + \mathbf{E}_{\Gamma,t}\boldsymbol{e}_{\Gamma,t} = \mathbf{H}_{i,j,t}\mathbf{x}_\Gamma + \boldsymbol{\epsilon}_{\Gamma,t} \tag{2.24}$$

where subscript $_\Gamma$ indicates that unknowns, equations and measurements correspond to a given set of branches. An important aspect to consider and highlight is that, when different branches are considered at the same time, the nodes adjacent to multiple branches share systematic measurement errors of the voltages. This leads to a reduction of the measurement/constraints ratio and, as will be shown in the next sections, an overall improvement of the estimation performance.

The estimation problem defined by (2.24), as already mentioned, is typically under-determined. However, multiple time instants $t_1, \cdots, t_{N_t}$, that is multiple synchronized measurement sets, can be used and a new over-determined linear system can be defined as follows:

$$\begin{aligned} \mathbf{b}_\Gamma &= \begin{bmatrix} \mathbf{b}_{\Gamma,t_1} \\ \vdots \\ \mathbf{b}_{\Gamma,t_{N_t}} \end{bmatrix} = \begin{bmatrix} \mathbf{H}_{\Gamma,t_1} \\ \vdots \\ \mathbf{H}_{\Gamma,t_{N_t}} \end{bmatrix} \mathbf{x}_\Gamma + \begin{bmatrix} \mathbf{E}_{\Gamma,t_1} & & \\ & \ddots & \\ & & \mathbf{E}_{\Gamma,t_{N_t}} \end{bmatrix} \begin{bmatrix} \mathbf{e}_{\Gamma,t_1} \\ \vdots \\ \mathbf{e}_{\Gamma,t_{N_t}} \end{bmatrix} \\ &= \mathbf{H}_\Gamma\mathbf{x}_\Gamma + \mathbf{E}_\Gamma\boldsymbol{e}_\Gamma = \mathbf{H}_\Gamma\mathbf{x}_\Gamma + \boldsymbol{\epsilon}_\Gamma \end{aligned} \tag{2.25}$$

where it is important to highlight that the unknown vector $\mathbf{x}_\Gamma$ is common to all the time instants, whereas measurement matrix and random errors change with the timestamp. Also in this case, it is possible to exploit the high RR of the PMU to use different cases and repeated measurements of the same case and the prior information about the unknowns involving all the branches considered (IT accuracy class and maximum parameters variability). Considering the N_{br} branches and $N_\Gamma \leq 2N_{br}$ nodes in Γ, combining C different operating cases (while averaging repeated measurements) and adding prior information about unknowns, an over-determined and augmented linear system is obtained:

$$\begin{aligned} \mathbf{b}_{\text{tot}} &= \begin{bmatrix} \mathbf{b}_\Gamma \\ \mathbf{0}_{n\times 1} \end{bmatrix} = \begin{bmatrix} \mathbf{H}_\Gamma \\ \mathbf{I}_n \end{bmatrix} \mathbf{x} + \begin{bmatrix} \boldsymbol{\epsilon}_\Gamma \\ \mathbf{e}_{\text{prior}} \end{bmatrix} \\ &= \mathbf{H}_{\text{tot}}\mathbf{x}_\Gamma + \boldsymbol{\epsilon}_{\text{tot}} \end{aligned} \tag{2.26}$$

with $\mathbf{b}_\Gamma \in \mathbb{R}^m$, $\mathbf{H}_\Gamma \in \mathbb{R}^{m\times n}$, $\mathbf{H}_{\text{tot}} \in \mathbb{R}^{(m+n)\times n}$, $\mathbf{b}_{\text{tot}} \in \mathbb{R}^{m+n}$, where m is the number of involved Kirchhoff's constraints. I_n and $0_{n\times 1}$ are the n-size identity matrix and the n-zeros vector, respectively, with the same meanings of (2.20). Then, $m = 4 \times N_{br} \times C$ and the number of unknowns includes both $2 \times N_\Gamma + 4 \times N_{br}$ systematic errors of the measurement chain and $3 \times N_{br}$ line

parameter deviations (if γ, β and δ line parameters are all present in the model of each branch). In general, it is important to emphasize that this approach can consider also branches where shunt susceptance can be neglected. The unknown variables are then estimated by means of WLS, where the weight matrix is chosen as the inverse of covariance matrix of measurements:

$$\mathbf{\Sigma}_{\boldsymbol{\epsilon}_{\text{tot}}} = \begin{bmatrix} \mathbf{\Sigma}_{\boldsymbol{\epsilon}_\Gamma} & \mathbf{0} \\ \mathbf{0} & \mathbf{\Sigma}_{\mathbf{e}_{\text{prior}_\Gamma}} \end{bmatrix} \tag{2.27}$$

which includes

- $\mathbf{\Sigma}_{\boldsymbol{\epsilon}_\Gamma} \in \mathbb{R}^{m \times m}$, the covariance matrix of all the equivalent measurements, defined by applying the law of propagation of uncertainty [58] to the matrix representing the PMU measurement uncertainties $\mathbf{\Sigma}_{\mathbf{e}_\Gamma}$ (assumed decorrelated for all cases):

$$\mathbf{\Sigma}_{\boldsymbol{\epsilon}_\Gamma} = \mathbf{E}_\Gamma \mathbf{\Sigma}_{\mathbf{e}_\Gamma} \mathbf{E}_\Gamma^\intercal \tag{2.28}$$

- $\mathbf{\Sigma}_{\mathbf{e}_{\text{prior}_\Gamma}} \in \mathbb{R}^{n \times n}$ is the diagonal matrix including all the prior variances of the unknowns.

The estimated state vector $\hat{\mathbf{x}_\Gamma}$ is thus the solution of the WLS problem, i.e.:

$$(\mathbf{H}_{\text{tot}}^\intercal \mathbf{W}_{\text{tot}} \mathbf{H}_{\text{tot}}) \hat{\mathbf{x}}_\Gamma = \mathbf{H}_{\text{tot}}^\intercal \mathbf{W}_{\text{tot}} \mathbf{b}_{\text{tot}} \tag{2.29}$$

where

$$\mathbf{W}_{\text{tot}} = \mathbf{\Sigma}_{\boldsymbol{\epsilon}_{\text{tot}}}^{-1} \tag{2.30}$$

When multiple branches are considered at the same time[1], it is also beneficial to introduce additional constraints associated with the injected currents on the nodes (if available). In particular, two cases can be observed: the first one is the case of a node that is a zero injection (ZI) node [31], where the injected current is zero, while, the second one is the case in which the injected current is not zero. In general, for both cases, Kirchhoff's current law can be used, applying an additional complex equation, i.e. two linear real-valued equations for the generic injection (or ZI) node j. For instance, when node j is a ZI node, the equations become:

$$\sum_{h \in \Omega_j} I_{j,h}^r \simeq \sum_{h \in \Omega_j} I_{j,h}^r (\eta_{j,h}^{\text{sys}} + \eta_{j,h}^{\text{rnd}}) - \sum_{h \in \Omega_j} I_{j,h}^x (\psi_{j,h}^{\text{sys}} + \psi_{j,h}^{\text{rnd}}) \tag{2.31a}$$

$$\sum_{h \in \Omega_j} I_{j,h}^x \simeq \sum_{h \in \Omega_j} I_{j,h}^x (\eta_{j,h}^{\text{sys}} + \eta_{j,h}^{\text{rnd}}) + \sum_{h \in \Omega_j} I_{j,h}^r (\psi_{j,h}^{\text{sys}} + \psi_{j,h}^{\text{rnd}}) \tag{2.31b}$$

[1]Hereafter, the problem of line parameters and systematic measurement errors estimation that considers multiple branches at the same time will be named "multi-branch" approach.

In (2.31), $I^r_{j,h}$ and $I^x_{j,h}$ are the real and imaginary parts of the generic measured branch current phasor $i_{j,h}$, and Ω_j is the set of nodes adjacent to node j. It has to be underlined that, if the node j is an injection node, the measured injected current and its systematic and random errors must be also considered in the equation.

Estimation problem framed as Tikhonov regularization

In the context of a grid parameters estimation, as already underlined in [57], a proper management of data coming from different operating conditions is needed. In fact, [31] shows that a larger number of operating conditions (i.e., constraint equations) has a positive effect on the estimation performance. In this section, it is shown how the problem in (2.29) can be generalized as a particular case of Tikhonov regularization [54]. This generalization permits improving the estimation performance of line parameters and systematic measurement errors by properly considering, in the estimation process, multiple load (or generator) conditions.

The augmented problem (2.26) can be transformed in a LS problem by means of the whitening process:

$$\begin{aligned} &\forall\, \mathbf{W}_{\text{Ch}} \in \mathbb{R}^{m\times m} : \mathbf{W}_{\text{Ch}}^{\intercal}\mathbf{W}_{\text{Ch}} = \boldsymbol{\Sigma}_{\boldsymbol{\epsilon}_\Gamma}^{-1} \\ &\mathbf{b}_{\mathbf{w}} \triangleq \mathbf{W}_{\text{Ch}}\mathbf{b}_\Gamma \Longrightarrow \boldsymbol{\Sigma}_{\mathbf{b}_{\mathbf{w}}} = \mathbf{I} \end{aligned} \tag{2.32}$$

In (2.32), the whitening matrix is chosen as $\mathbf{W}_{\text{Ch}} = {\mathbf{U}_{\text{Ch}}}^{-\intercal}$, where $\mathbf{U}_{\text{Ch}}$ is the upper triangular matrix obtained by means of the Cholesky decomposition of the matrix $\boldsymbol{\Sigma}_{\boldsymbol{\epsilon}_\Gamma}$. Furthermore, defining the diagonal matrix $\mathbf{L} = \boldsymbol{\Sigma}_{\mathbf{e}_{\text{prior}}}^{-\frac{1}{2}}$, the equivalent least square problem can be obtained as:

$$\hat{\mathbf{x}}_{\text{WLS}} = \arg\min_{\mathbf{x}} \left\| \begin{bmatrix} \mathbf{W}_{\text{Ch}}\mathbf{H}_\Gamma \\ \mathbf{L} \end{bmatrix} \mathbf{x} - \begin{bmatrix} \mathbf{W}_{\text{Ch}}\mathbf{b}_\Gamma \\ \mathbf{0}_{n\times 1} \end{bmatrix} \right\|_2^2 \tag{2.33}$$

Then, it is possible to define:

$$\begin{aligned} \mathbf{y} &= \mathbf{L}\mathbf{x} \\ \mathbf{A} &= \mathbf{W}_{\text{Ch}}\mathbf{H}_\Gamma\mathbf{L}^{-1} \end{aligned} \tag{2.34}$$

and add a regularization parameter $\mu \in \mathbb{R}^+$, which leads the LS problem:

$$\hat{\mathbf{y}}_\mu = \arg\min_{\mathbf{y}} \left\| \begin{bmatrix} \mathbf{A} \\ \sqrt{\mu}\mathbf{I}_n \end{bmatrix} \mathbf{y} - \begin{bmatrix} \mathbf{b}_{\mathbf{w}} \\ \mathbf{0}_{n\times 1} \end{bmatrix} \right\|_2^2 \tag{2.35}$$

Equation (2.35) is equivalent to the standard form of the Tikhonov regulariza-

tion problem:

$$\hat{\mathbf{y}}_\mu = \arg\min_{\mathbf{y}} \|\mathbf{A}\mathbf{y} - \mathbf{b_w}\|_2^2 + \mu \|\mathbf{y}\|_2^2 \tag{2.36}$$

and, then, once $\hat{\mathbf{y}}_\mu$ is estimated, the state $\hat{\mathbf{x}}$ can be found inverting the first equation in (2.34). Finally, it is possible to frame the augmented WLS problem as a particular case of the Tikhonov regularization where $\mu = 1$ and

$$\hat{\mathbf{x}}_{\text{WLS}} = \mathbf{L^{-1}}\hat{\mathbf{y}}_{\mu=1} \tag{2.37}$$

thus retrieving the solution of the WLS from $\hat{\mathbf{y}}_{\mu=1}$.

A suitable management, in the estimation process, of multiple operative conditions C can be exploited in order to leverage the high RR of PMUs. As previously mentioned, the two equations (2.35) and (2.36) are different formulations of the same problem: the first one is formulated as an augmented LS problem, while the second one is addressed as a penalized problem that involve two terms:

- The term $\|\mathbf{A}\mathbf{y} - \mathbf{b_w}\|_2^2$ is the squared norm of the residual vector and represents an index of how well the solution vector $\mathbf{y}$ fits the measurement vector $\mathbf{b_w}$.
- The term $\|\mathbf{y}\|_2^2$ is the square of the regularization term norm. It represents the "energy" of the solution vector $\mathbf{y}$ (i.e., $\mathbf{x}$ weighed with prior information).

It is worth highlighting that in both formulations, it is possible to set μ (regularization parameter) to take into account the a-priori information on the problem to be solved. Then, applying the normal equations to (2.36), it is possible to define the following equation:

$$\left(\mathbf{A}^\intercal\mathbf{A} + \mu\mathbf{I}_n\right)\hat{\mathbf{y}}_\mu = \mathbf{A}^\intercal\mathbf{b_w} \tag{2.38}$$

and after that, it is possible to apply the Singular Value Decomposition (SVD) to the matrix $\mathbf{A}$ (i.e., $\mathbf{A} = \mathbf{U}\mathbf{\Sigma}\mathbf{V}^\intercal$) to express the analytical solution of the problem as the regularization parameter μ changes:

$$\begin{aligned}\hat{\mathbf{y}}_\mu &= \mathbf{V}\left(\mathbf{\Sigma}^\intercal\mathbf{\Sigma} + \mu\mathbf{I}_n\right)^{-1}\mathbf{\Sigma}^\intercal\mathbf{U}^\intercal\mathbf{b_w} \\ &= \sum_{\sigma_j>0} f_j \frac{\mathbf{u}_j^\intercal\mathbf{b_w}}{\sigma_j}\mathbf{v}_j = \sum_{\sigma_j>0} g_j\mathbf{v}_j = \hat{\mathbf{y}}_{\text{Tikhonov}}\end{aligned} \tag{2.39}$$

where

$$f_j = \frac{\sigma_j^2}{\sigma_j^2 + \mu} \tag{2.40}$$

In (2.39), $\mathbf{u}_j$ is the jth vector of matrix $\mathbf{U}$, as well as $\mathbf{v}_j$ for matrix $\mathbf{V}$, while $\hat{\mathbf{y}}_\mu$ is obtained by means of a linear combination of $\mathbf{v}_j$ through the Fourier coefficients $\mathbf{u}_j^\intercal \mathbf{b}_\mathbf{w}$. f_j is a "low-pass" filter that cuts down all the components corresponding to $\sigma_j^2 \ll \mu$. With this framework, it is possible to analyze the trends of the estimation performance if different network operating conditions and values of μ are considered.

2.1.4 Analysis, tests and results: the single-phase method settings and performance

Test assumptions

To assess the validity of the proposed approach, simulation tests have been performed in MATLAB environment using the IEEE 14 bus test system in Fig. 2.3 (see, for details, Appendix I). Different number of cases $C \in \{10, 20, ..., 1000\}$ and $M = 10$ repeated measurements for each case have been considered, also varying the number of involved branches.

To validate statistically the results, Monte Carlo (MC) simulations, with $N_{\mathrm{MC}} = 5000$, have been performed. Each MC simulation is composed of $M \times C$ measurement instants sharing the same systematic error, then each MC trial has a different systematic error. Random errors for each measurement instant and each case have been extracted and added to the true values (considered as reference values and indicated with superscripts ^{R}) of the voltage and current synchrophasor measurements. These reference values of voltages and currents have been obtained from a power-flow. Once the measurement errors are added to these reference values, the M repeated measurements of the same operating condition are averaged, obtaining a system of $4 \times C \times N_{br}$ equations. The test set-up follows these assumptions:

- Maximum deviations of line parameters $R_{i,j}$, $X_{i,j}$ and $B_{\mathrm{sh},i,j}$ have been assumed equal to $\pm 15\,\%$.
- ITs are assumed, both VTs [59] and CTs [60], to be of Class 0.5, thus using a maximum error of 0.5 % for voltage and current ratios, a maximum CT phase-angle error of 0.9 crad (10^{-2} rad) and a maximum VT phase-angle error of 0.6 crad. For every test, the errors have been extracted from uniform distributions in order to define, for each MC trial, the actual systematic errors.
- As for the PMUs, accurate values for real PMUs in steady-state conditions have been considered. In particular, a maximum ratio error of 0.1 % and a maximum phase-angle error of 0.1 crad have been used for both voltage

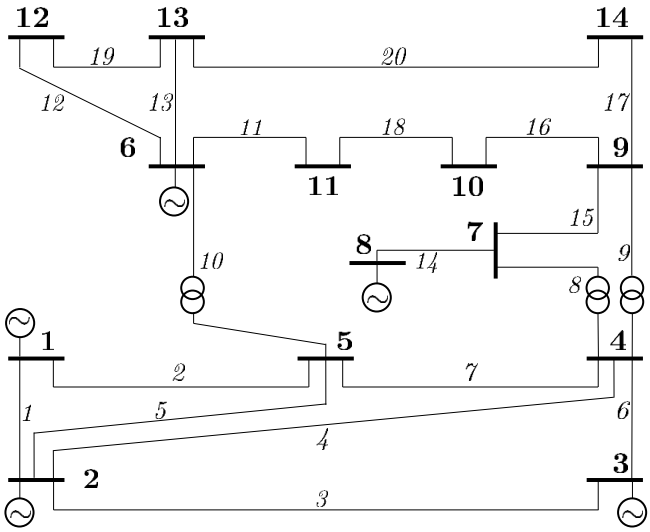

Figure 2.3: Unifilar diagram of the IEEE 14 bus test system.

and current measurements. This configuration will be hereafter referred to as "PMU01".

- Load/generator variability, among different cases, of $\pm 10\,\%$ with respect to nominal values (for both active and reactive powers) has been considered.

The above base test configuration is adopted in the following tests, unless different assumptions are explicitly made. First the performance assessment focuses on line parameters and then a specific paragraph is dedicated to the tests involving tap-changing transformers.

Analysis of regularization parameter impact and proposed configuration

To investigate the role of the regularization parameter, several tests have been performed. The first 6 branches and the corresponding buses of the IEEE 14 bus test system [61] shown in Fig. 2.3, and referred to as IEEE 14 in the figures, have been considered to perform the analysis by varying μ and C.

To assess the performance of the estimation algorithm, the relative root square error (RRSE) is used:

$$\mathrm{RRSE} = \frac{\|\hat{\mathbf{y}}_\mu - \mathbf{y}\|_2}{\|\mathbf{y}\|_2} \tag{2.41}$$

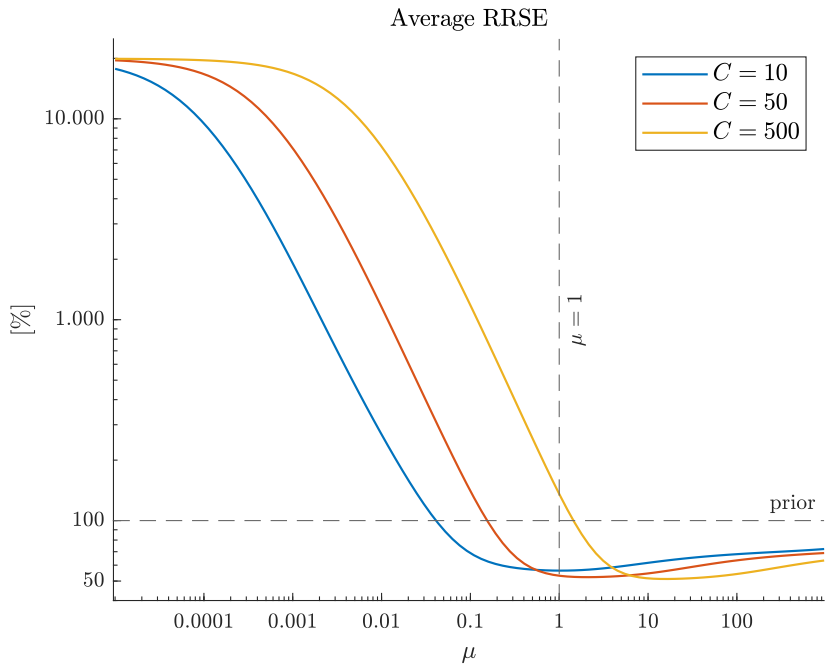

Figure 2.4: IEEE 14 - 6 branches, average RRSE as a function of μ with a varying number of operating conditions.

Figure 2.4 reports the evolution (in log-log scale) of RRSE (averaged on the results of the $N_{\text{MC}} = 5000$ simulations) as a function of μ (with $\mu \in [0, ..., 1000]$) and three different scenarios $C \in \{10, 50, 500\}$.

As it can be seen from the figure, if no prior information is used (i.e., when the value of $\mu = 0$) the estimates are basically unreliable. Moreover, some important remarks can be highlighted observing Fig. 2.4:

- RRSE values drop down when μ increases and, for the three scenarios considered, the minimum is lower and shifted to the right with the increasing of C. The flatness of the curve around this minimum means that the method is robust with respect to an uncertainty on the a-priori information about unknowns.

- For low values of μ, it is possible to observe that the estimation problem starts as under-determined and, with an increasing number of the operating conditions, becomes over-determined. Anyway, without weighting prior information with well-suited values of μ, higher values of C lead to worse estimates.

- For $C = 10$, it is possible to observe that $\mu = 1$ is very close to μ_{min} (the value corresponding to the minimum) but, if more cases are considered

the estimation becomes unreliable (e.g., when 500 cases are considered, the RRSE obtained by means of classic WLS goes beyond 100% and, thus, prior error).

This behavior is not related to a conditioning problem since, as already stated in [57], a higher number of C brings a lower condition number. Indeed, when higher values of C are considered, the singular values profile shifts towards higher values and, as a consequence, a greater μ is needed in order to comply with the discrete Picard condition, which states ([62], [63]): Fourier coefficients in (2.39) have to decrease faster than the corresponding singular values σ_j in order to have a limited solution in (2.35).

Thus, in the context of the proposed methodology of network parameters and systematic measurement errors estimation, the presented framework can be leveraged to obtain a more accurate estimation and improve the knowledge on the power system model.

Following from the above analysis, it is useful to tune the value of μ and adapt it to the specifics of the current problem. To do that, different tests in different configurations have been carried out and they have shown that the increase in σ_j follows the number of equations, i.e. the number of rows of matrix $\mathbf{A}$ (with $\mathbf{A} \in \mathbb{R}^{m \times n}$). For this reason, the proposed regularization parameter [54] has been empirically chosen as:

$$\mu_{\text{sqrt}} = \sqrt{\frac{m}{n}} \tag{2.42}$$

To provide an idea of how the proposed regularization parameter is tuned to this problem, Fig. 2.5 shows the trends of the Picard condition plots (considering $C = 500$). In the figure, the ideal solution that does not consider measurement errors is indicated with red circles, while g_j coefficients obtained with $\mu = 0$ (without prior), with WLS formulation (considering $\mu = 1$) and with μ_{sqrt} (proposed solution) are indicated with purple, blue and green asterisks, respectively. Thus, it is evident how the proposed regularization parameter contains the coefficients surge better than other methods.

For sake of completeness, the proposed regularization method has been compared with classic algorithms ([62], [64]) used for the choice of μ in the Tikhonov problem, which are:

- *L-curve* criterion (LCC), a graphical tool consisting in a log-log plot that represents the trend of the regularization term norm as a function of the norm of the residual vector. This method chooses as regularization parameter the corner value (trade-off between the two terms in (2.36)) of this curve.
- *Generalized Cross Validation* (GCV), a statistically based approach.

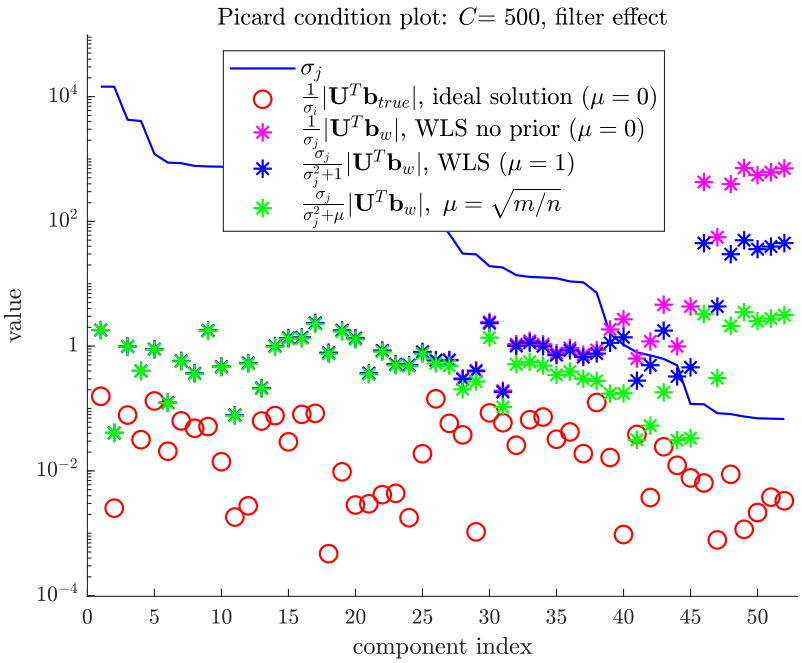

Figure 2.5: IEEE 14 - 6 branches, filtering effect.

- *Discrepancy Principle* (DP), the only method based on the knowledge of the error norm. This method chooses the regularization parameter so that the residual norm is close to the error norm [65] as:

$$\mu_{\text{DP}} : \|\mathbf{b_w} - \mathbf{A}\hat{\mathbf{y}}_{\mu_{\text{DP}}}\|_2 \approx \tau \, \|\boldsymbol{\epsilon}_{\mathbf{w}_{\text{meas}}}\|_2 \, , \; \tau \geq 1 \tag{2.43}$$

  where $\boldsymbol{\epsilon}_{\text{meas}}$ is the measurement error vector, while $\boldsymbol{\epsilon}_{\mathbf{w}_{\text{meas}}} = \mathbf{W}_C\boldsymbol{\epsilon}_{\text{meas}}$ represents the whitened measurement error vector (which have the identity matrix as covariance matrix). The method in [66] has been applied to this problem to have an estimation of the measurement error norm and the problem in (2.43) has been solved by means of the method in [67].

Moreover, for sake of a complete comparison, also the benchmark method, which takes the optimal regularization parameter μ_{opt} in all the MC trials, has been considered. The optimal value is defined as:

$$\mu_{\text{opt}} = \arg\min_{\mu} \text{RRSE}_{\mu} \tag{2.44}$$

where RRSE_{μ} is the RRSE corresponding to μ. As clear from the definition, the optimal μ is used only as a reference and, in practice, it is not available since its computation requires prior knowledge of the true values $\mathbf{y}$.

Figure 2.6 reports the trends for the average RRSE varying the number of cases from 10 to 500. The WLS method ($\mu = 1$) shows an improvement of per-

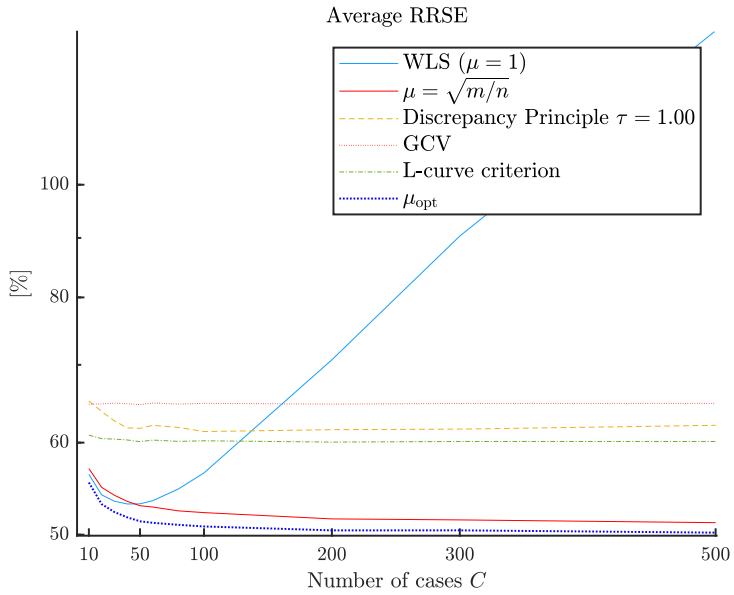

Figure 2.6: IEEE 14 - 6 branches, average RRSE (5000 MC trials performed) whit different numbers of operating conditions.

formance at the beginning with a minimum for $C = 50$ but, for higher number of cases C, the estimates become unreliable (see, as a further confirmation of this behavior, Fig. 2.4). While the classic regularization methods LCC, GCV and DP do not reach good estimation performance, the proposed regularization method is the only one that, for different values of C, is close to the benchmark solution. A flowchart schematically representing the proposed procedure in all the above described aspects is shown in Fig. 2.7.

Performance test results

After refining the procedure, several tests have been carried out to assess the estimation performance. In all the results reported in this thesis, the evaluation metric used to assess the estimation performance of both the grid parameters and the systematic errors is the root mean square error (RMSE):

$$\text{RMSE} = \sqrt{\sum_{m=1}^{N_{\text{MC}}} \frac{(\hat{\nu}_m - \nu_m)^2}{N_{\text{MC}}}} \tag{2.45}$$

In (2.45), $\hat{}$ indicates the estimated quantity and ν is a placeholder that can be associated with each unknown of the state vector $\mathbf{x}$ (or $\mathbf{x}_{hd}$, with $(h, d) = (i, j)$ or (l, k) according to previously introduced notation and depending on the considered branch type). On one hand, focusing on a generic line associated

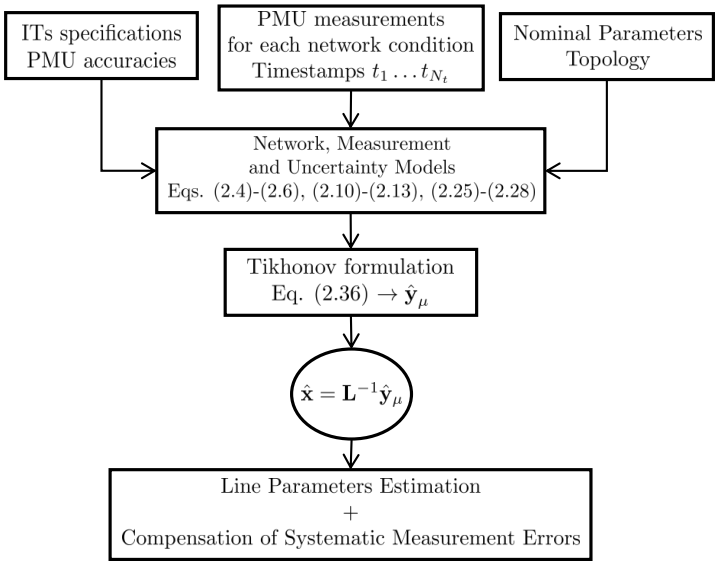

Figure 2.7: Flow chart of the proposed procedure.

with the pair of nodes (i, j), ν can be equal to ξ_i, α_i, ξ_j, α_j, $\eta_{i,j}$, $\psi_{i,j}$, $\eta_{j,i}$, $\psi_{j,i}$, $\gamma_{i,j}$, $\beta_{i,j}$ or $\delta_{i,j}$. On the other hand, for a generic transformer associated with the branch (l, k), ν can be equal to ξ_l, α_l, ξ_k, α_k, $\eta_{l,k}$, $\psi_{l,k}$, $\eta_{k,l}$, $\psi_{k,l}$, $\beta_{l,k}$ or $\tau_{l,k}$. In the following tests, unless otherwise specified (e.g. by using the above 2-node indices notation), each branch will be indicated with a single ordinal number q, as done in Fig. 2.3, and thus the associated line parameters will be $\gamma_q, \beta_q, \delta_q$.

The portion of the grid from node 1 to node 5 of Fig. 2.3 (the high voltage nodes) has been used for the first series of tests, considering the multi-branch approach. From the results shown in Fig. 2.6, it is possible to see that classic regularization methods are basically unreliable and, thus, the methods WLS ($\mu = 1$), the proposed one (μ_{sqrt}-method) and the ideal solution μ_{opt} have been compared. The results obtained with μ_{opt} are also considered as a performance upper bound. However, it is important to recall that μ_{opt} is found based on RRSE, thus depending on an average among all the unknowns. RRSE is indeed a summary index that considers all the errors of the unknown parameters altogether. For this reason, the RMSEs achieved with μ_{opt} for some quantities or some branches may not be the lowest.

Both results, WLS and μ_{sqrt}-method, are presented choosing the best scenario for each method, i.e. the value of C that allows best performance [2]. In addition, the basic scenario $C = 10$ is also used with the WLS (with $\mu = 1$)

[2]The ideal results with μ_{opt} are presented using the same C as μ_{sqrt}.

method to have a clear comparison of the estimation results. In this regard, Table 2.1 shows the considered scenarios and the corresponding RRSE results averaged among all MC trials.

Table 2.1: IEEE 14 - 6 branches, best average RRSE (5000 MC trials) for different methods

Method	**Average RRSE [%]**
WLS ($\mu = 1$), $C = 10$ [53]	56.35
WLS ($\mu = 1$), $C_{\text{best}} = 40$	53.14
$\mu = \sqrt{m/n}$, $C_{\text{best}} = 500$	51.21
μ_{opt}, $C = 500$	50.20

In what follows, for the evaluations of the results, the RMSE obtained for each unknown will be compared with the corresponding prior standard deviation. Table 2.2 reports the summary of the prior values for all the parameters, obtained as the maximum deviation of the associated parameter divided by $\sqrt{3}$. It is worth underlining that, if different maximum deviations are considered (as in the sections below), prior standard deviations in Table 2.2 change accordingly.

Table 2.2: Summary of prior

Parameter	**Prior standard deviation**
$\gamma_{i,j}, \beta_{i,j}, \delta_{i,j}$	5.77 %
$\xi_h, \eta_{i,j}$ (or $\eta_{l,k}$)	0.29 %
α_h	0.35 crad
$\psi_{i,j}$ (or $\psi_{l,k}$)	0.52 crad
$\beta_{l,k}$	5.77 %
$\tau_{l,k}$	0.58 %

Considering the same scenarios as in Table 2.1, Fig. 2.8 shows the estimation RMSE for the branch resistance of the first 6 branches of the grid. It is possible to underline that the results considering $\mu = 1$ and $C = 40$, indicated with blue plus signs, have an average improvement of about 32.2 % with respect to the scenario $\mu = 1$ and $C = 10$ (green plus signs). The best WLS configuration with $\mu = 1$ is outperformed, with an additional improvement of 25.5 %, by the proposed regularization method (red asterisks). Furthermore, it is possible to mention that, also in this case, the proposed regularization method is very close to the benchmark results (empty blue circles). As mentioned above, μ_{opt} depends on RRSE and is not the best value for each estimated quantity. This explains why, as shown in Fig. 2.8, μ_{sqrt}-method is even slightly better of μ_{opt}-method for γ [2], but for other unknowns this is not the case.

[2]In what follows, if notation is reported without indexes, it refers to the parameter type.

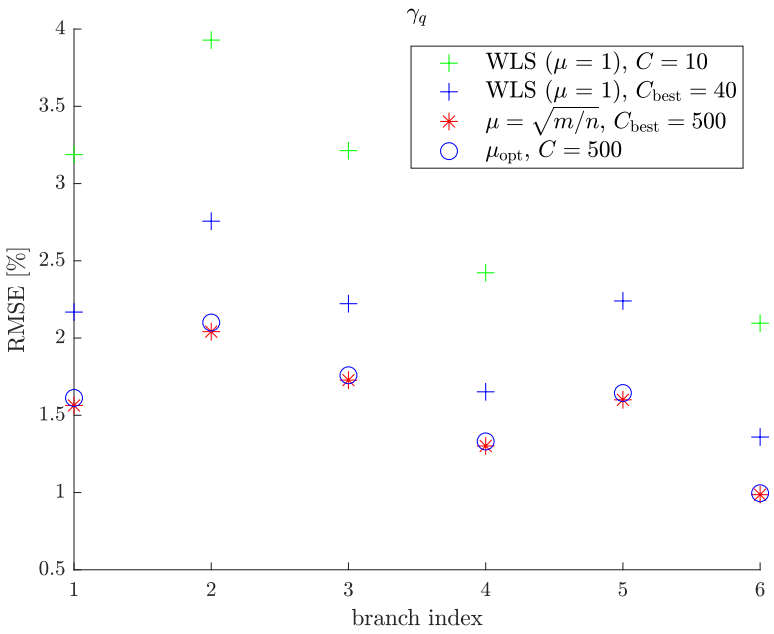

Figure 2.8: IEEE 14 - 6 branches, estimation results for γ parameters.

A comprehensive picture of the proposed regularization method is reported in Fig. 2.9, where the results for all parameter types are shown. In fact, the proposed method (bars in foreground with solid line edge) improves all the results obtained with $\mu = 1$ and $C = 40$ (bars in background with dotted dashed edge). As an example, the average percent error reductions of the proposed method are 34.9 % and 57.2 % for β_q and δ_q, respectively.

The RMSEs results for ξ are shown in Fig. 2.10 as a function of the number of cases and for all the regularization methods presented in Section 2.1.3. It is possible to say that the results for WLS, i.e. $\mu = 1$, (green plus signs) and DP with $\tau = 1.00$ (blue triangles) go beyond the prior values (black dashed line). The results confirm that the WLS method can lead to unreliable results when the number of cases increases. Focusing again on the ξ estimates, Table 2.3 shows the comparison between the single-branch and multi-branch approaches for ξ_1, considering both $\mu = 1$ and $\mu = \sqrt{m/n}$ and with $C \in \{10, 500\}$. Besides the improvement that can be achieved when multi-branch method is considered, it is possible to observe that the regularization with $\mu = \sqrt{m/n}$ brings clear benefits when C is high and, it prevents the occurrence of critical conditions also in the single-branch approach, as already observed in Fig. 2.10.

Further studies have been carried out considering the multi-branch approach

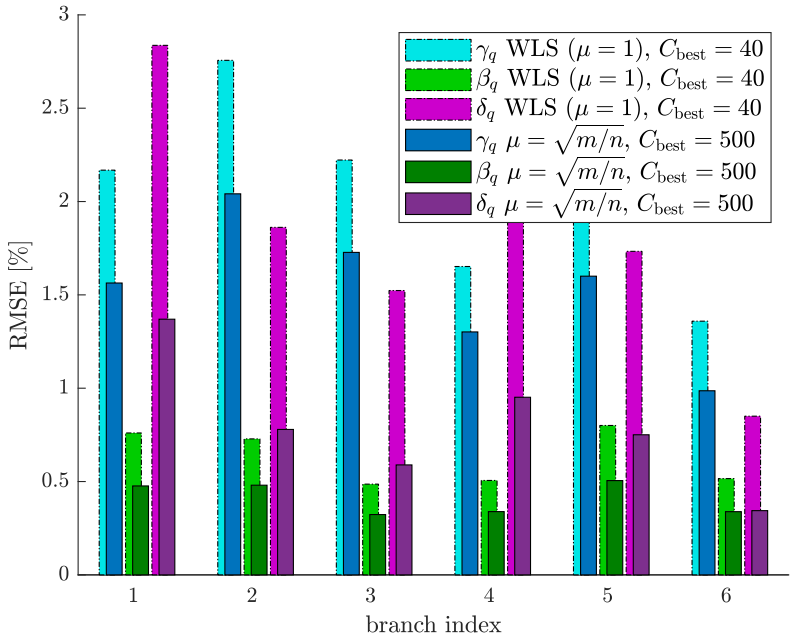

Figure 2.9: IEEE 14 - 6 branches, estimation results for all line parameters.

Table 2.3: IEEE 14 - node 1, RMSE (5000 MC trials) for ξ_1 - comparison between multi-branch and single-branch approaches

Method	**C**	**RMSE [%]**	
		Multi-branch	Single-branch
$\mu = \sqrt{m/n}$	10	0.16	0.22
$\mu = \sqrt{m/n}$	500	0.16	0.21
WLS ($\mu = 1$)	10	0.16	0.22
WLS ($\mu = 1$)	500	1.01	0.46

on the entire IEEE 14 bus test system, considering a variable number of $C \in \{10, 20, ..., 1000\}$ and comparing μ_{sqrt} and WLS methods. For the considered methods, the best scenario is chosen and C_{best} varies according to the configuration (i.e., $C_{\text{best}} = 30$ for WLS and $C_{\text{best}} = 200$ for μ_{sqrt}). In particular, Fig. 2.11 reports β_q estimates ($q = \{1, .., 6\}$) for both methods and two multi-branch configurations. N_{br} is the number of branches considered at the same time in the estimation process, i.e., the cardinality of the branch set Γ. $N_{br} = 6$ indicates the first 6 branches, while the entire network corresponds to $N_{br} = 20$).

Figure 2.11 shows the benefits of using a wider set of constraints, deriving from the increased number of branches and cases. As a confirmation of this

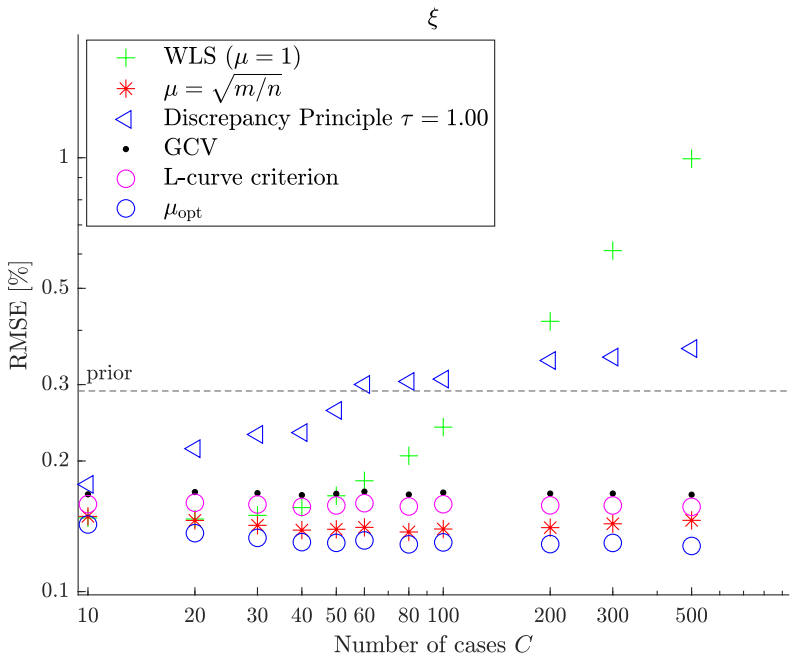

Figure 2.10: IEEE 14 - 6 branches, ξ estimation results as a function of the number of cases for all the considered methods.

statement, the average improvement from the WLS (with $\mu = 1$, $C = 10$ and $N_{br} = 6$) to $\mu = \sqrt{m/n}$, $C_{\text{best}} = 200$ and considering $N_{br} = 20$ (indicated with blue asterisks) is of about 66.6 %.

To summarize the obtained estimation results, Fig. 2.12 shows the RMSE values for all the line parameters, considering $N_{br} = 20$ and using only the best scenario C_{best} for both WLS with $\mu = 1$ (top of the figure) and μ_{sqrt} method (bottom of the figure). It is important to highlight that a significant estimation improvement can be obtained with the proposed method: γ_q, β_q and δ_q have an average RMSE improvement with respect to the WLS method of about 16 %, 23.9 % and 44.4 %, respectively.

Finally, a comparison of the estimation results between the proposed method and two different methods (from literature) using the above described measurement set-up is shown in Table 2.4. The two considered methods compared with the proposed one are:

- A direct estimation method (Method A) for the line parameters estimation based on the classic equations reported in [8] (the same used in [9]). It is important to underline that, for a fair comparison, the estimates have been obtained by averaging repeated measurements like in the proposed method.

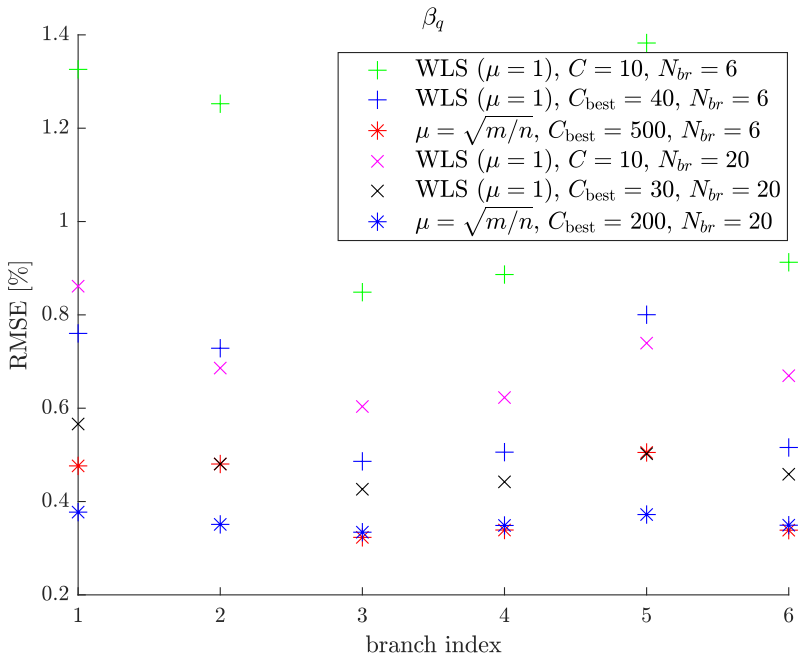

Figure 2.11: β estimation results with multi-branch approach applied to a portion and to the entire network using different methods and configurations.

- The method presented in [28, Sec. IV] (Method B), intended to obtain the simultaneous estimation, in a single-branch approach, of the line parameters and of the measurement errors introduced by the ITs at the arrival node.

Table 2.4 shows the line parameters estimation results for branch 1 (considering $C \in \{10, 200\}$), but similar results can be obtained also for other branches. RMSEs of resistance, reactance and systematic measurement errors at the end node (since Method A does not include the estimation of systematic errors and Method B does not allow the estimation of systematic errors of the start node) have been reported. The symbol '$-$' in Table 2.4 indicates that the corresponding parameter is not available for the considered method. To prove the robustness of the proposed method with respect to measurement accuracy, in addition to PMU01, also a configuration that considers a maximum amplitude error of 0.2 % and a maximum phase-angle error of 0.2 crad (indicated with "PMU02") has been taken into account. As a general comment, it is possible to observe that the proposed method is more accurate than the others for every condition and configuration. Focusing on γ_1 estimates for Method A, these are always beyond the prior value since the systematic errors affect the estimation and its RMSE varies slightly with C and PMU accuracy. Method B, unlike Method

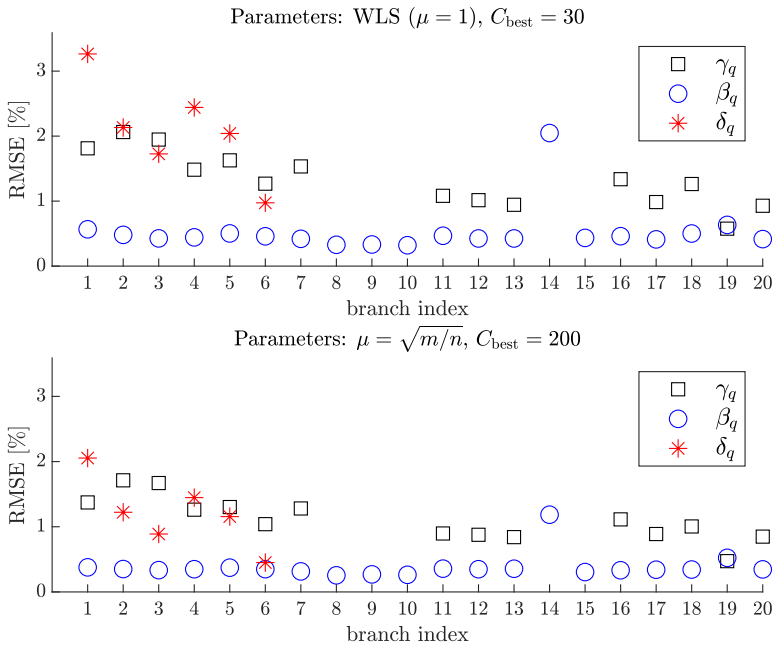

Figure 2.12: IEEE 14 - entire network, estimation results for all the line parameters.

A, takes advantage of an increase of C for the estimation of line parameters but not for that of systematic errors (which is larger than prior values). As a further confirmation of the quality of the proposal, the proposed method is more robust than Method B when PMU accuracy degrades, i.e. moving from PMU01 to PMU02. Thus, it is possible to conclude that properly considering the uncertainty sources and using a multi-branch approach are key factors to improve the estimation performance.

Tests and results for the tap-changing transformer

In this section, the validation of the proposed procedure carried out for the tap-changing transformer is presented. To do that, a series of simulation tests have been performed on the IEEE 14 bus test system (Fig. 2.3), considering the single-branch and multi-branch approaches. All the tests have been executed simulating $C = 10$ cases and $M = 10$ repeated measurements for each case. $N_{\text{MC}} = 5000$ trials have been performed. For each case, the reference conditions are evaluated and voltages and currents are obtained by means of a power-flow, where the actual tap changer conditions (i.e., tap changer ratios) are also established. Systematic and random errors are then added, for each measurement instant, to the reference values to obtain magnitude and phase-

Table 2.4: IEEE 14 - branch 1, comparison of different methods

Method	**C**	**PMU accuracy**	**RMSE** γ_1 [%]	β_1 [%]	ξ_2 [%]	α_2 [crad]	$\eta_{2,1}$ [%]	$\psi_{2,1}$ [crad]
Proposed Method	10	PMU01	2.53	0.88	0.10	0.10	0.20	0.37
		PMU02	3.73	1.53	0.11	0.14	0.21	0.38
	200	PMU01	1.38	0.38	0.10	0.09	0.20	0.36
		PMU02	2.08	0.76	0.11	0.11	0.20	0.37
Method A [8]	10	PMU01	13.15	5.16	-	-	-	-
		PMU02	13.16	5.16	-	-	-	-
	200	PMU01	13.08	5.10	-	-	-	-
		PMU02	13.08	5.10	-	-	-	-
Method B [28, Sec. IV]	10	PMU01	7.34	2.48	0.37	0.42	0.36	0.56
		PMU02	14.99	5.71	0.55	0.65	0.53	0.68
	200	PMU01	2.55	0.97	0.29	0.36	0.29	0.53
		PMU02	4.84	3.05	0.31	0.46	0.30	0.53

angle of each synchrophasor measurement. The following assumptions have been applied in order to obtain a realistic setup:

1. As for the line parameters, maximum deviations of $R_{i,j}$, $X_{i,j}$ and $B_{\mathrm{sh},i,j}$ are assumed equal to $\pm 10\,\%$ (in this case, the corresponding prior standard deviation is equal to $5.77\,\%$).

2. As for the ITs, they are assumed to be of Class 0.5, while for $a_{l,k}$ a maximum deviation of $\pm 1\,\%$ is assumed.

3. As for the PMUs, the configuration "PMU01" is used.

4. As for the operating conditions, a $\pm 10\,\%$ load/generator variability with respect to nominal values (for both active and reactive powers) is considered among different cases.

For every test, the errors and the deviations have been extracted from uniform distributions. To assess the performance of the estimation process, the RMSE (2.45) is used.

The first series of tests have been carried out on single branches of the system. In particular, the branches equipped with a tap changer have been considered (i.e., branches 8, 9 and 10 in Fig. 2.3). To understand the impact of estimating also the tap changer ratio along with the line parameters and the systematic errors, a comparison has been made between the method including the tap changer in the estimation process (named "Tap estimation") and the method

that consider the ratio like a known value, without uncertainty (named "No Tap estimation"). Tap estimation method takes into account possible variations in the actual tap ratio and performs a ratio estimation as shown in Section 2.1.3. Table 2.5 shows the impact of the tap estimation on the evaluation of ξ_l, ξ_k, α_l and α_k. It is possible to notice that the Tap estimation method can bring a noticeable reduction of the errors, up to more than 30 % with respect to No Tap Estimation method. As for the parameter ξ, in case of Tap estimation a clear reduction of the errors is obtained, whereas, the model mismatch jeopardizes the No Tap estimation results.

Table 2.5: RMSE of systematic voltage errors estimation - single-branch estimation

Branch	RMSE			
	ξ_l [%]	α_l [crad]	ξ_k [%]	α_k [crad]
$(4,7)$ Tap estimation	0.24	0.25	0.24	0.25
$(4,7)$ No Tap estimation	0.35	0.25	0.35	0.25
$(4,9)$ Tap estimation	0.24	0.25	0.25	0.25
$(4,9)$ No Tap estimation	0.35	0.25	0.35	0.25
$(5,6)$ Tap estimation	0.25	0.26	0.25	0.27
$(5,6)$ No Tap estimation	0.35	0.27	0.34	0.27

Then, a second series of tests has been performed on single branches, or on an extended set of branches of this grid, or on the entire IEEE 14 bus test system. As a first result, Table 2.6 shows the RMSE obtained for parameter $\tau_{l,k}$ with or without the estimation of the tap changer ratio. The comparison of the results obtained by applying both the single-branch (applied to the branches with the tap changer) and multi-branch approach (applied to the entire IEEE 14 bus test system) is reported. It is possible to notice that the RMSEs of the single-branch approach are more than halved when compared with the prior errors. Moreover, the multi-branch method halves the RMSEs with respect to the single-branch approach and, when compared with the prior errors, it brings to reductions of more than 75 %.

As a further example of the results obtainable when the multi-branch approach is applied, Fig. 2.13 shows the RMSEs of the evaluation of ξ. In the figure are reported the results obtained on the entire network ("All branches" results) and on a set of branches including all the branches of the grid except those with tap changer ("reduced branch set" results).

It is possible to observe that estimating the tap ratios and using the entire

Table 2.6: Tap ratio error $\tau_{l,k}$ estimation

Branch	**RMSE [%]**		
#, (l,k)	Single-branch	Multi-branch	Prior
8, $(4,7)$	0.26	0.13	0.57
9, $(4,9)$	0.26	0.13	0.57
10, $(5,6)$	0.26	0.13	0.57

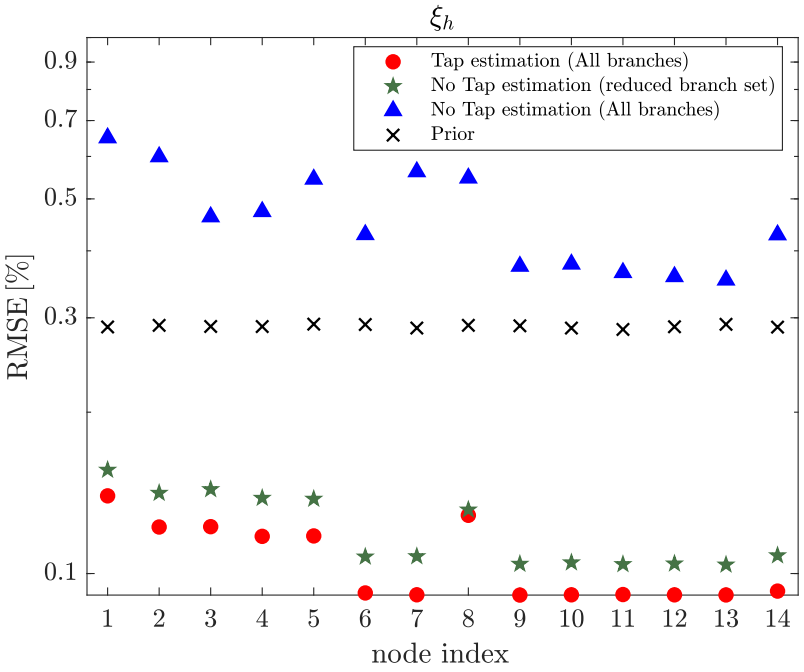

Figure 2.13: Voltage amplitude systematic errors - results obtained with and without tap estimation with respect to prior.

network (red circle markers) leads a remarkable reduction of the errors with respect to the prior (black crosses). The No Tap estimation method (blue triangles) suffers again from improper modeling and all the nodes are affected, showing how its application cannot be generalized to all types of branch (representing lines and transformers). It is important to underline that the No Tap estimation method, which does not consider uncertainty in the tap ratio, behaves better if applied only on all the branches that do not include tap changers (green stars). Nonetheless, on this reduced set of branches, the method is still worse than Tap Estimation method, since it does not include all the available constraints. This type of results highlights the importance of executing a preliminary study on the network to monitor, in order to choose what type of

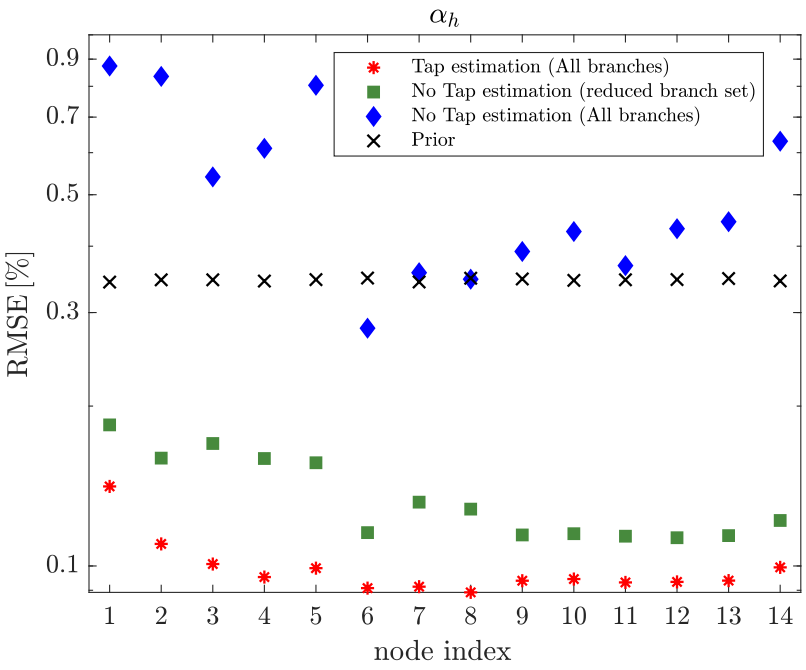

Figure 2.14: Voltage phase-angle systematic errors - results obtained with and without tap estimation with respect to prior.

estimation method could be applied most successfully.

Figure 2.14 shows the same kind of comparison in terms of the errors obtained in the evaluation of the phase-angle voltage systematic errors. Also in this case, the errors obtained with Tap Estimation (indicated with red asterisks) are the lowest, resulting in average improvements of about 71 % with respect to prior errors and of about 26 % with respect to the errors obtained applying the No Tap estimation method on a reduced set of branches (green squares).

2.2 Three-phase method

In power system analysis, the methods are typically validated, in a first stage, using equivalent single-phase models and balanced operative conditions. However, when unbalanced systems are considered or more details models are sought, a three-phase approach needs to be introduced. In this regard, after the first validation analysis reported in Section 2.1, this section presents the extension of the presented methodology for the simultaneous estimation of network parameters and systematic measurement errors to three-phase systems [68]. This approach permits having on one hand the estimation of real parameters of the physical system (like, for example, the parameters of the cables of a branch).

On the other hand, the estimation of the systematic errors associated with the ITs, which is performed through the proposed estimation method, is inherently related to the three-phase model because measurements are obtained on a per-phase basis. Indeed, it is worth noticing that this permits the identification of a specific degradation of the metrological performance of a single IT or of the parameters in a given system phase, which is possible only if a three-phase model is used.

2.2.1 Three-phase line model

As for a complete line model, a three-phase π-model (as shown in Fig. 2.15) has been considered.

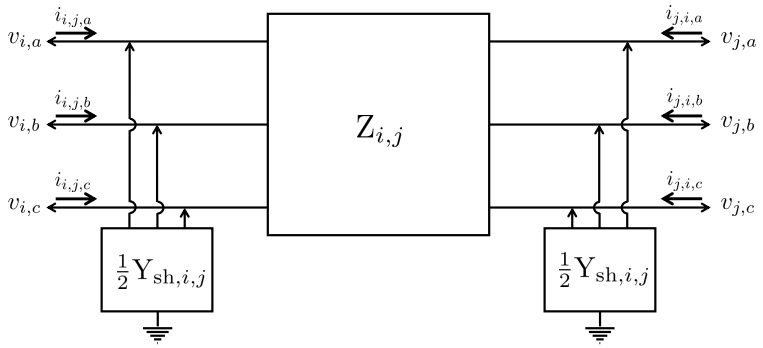

Figure 2.15: Equivalent three-phase π-model of a generic branch with parameters and available measurements.

This model can be represented by means of two 3×3 matrices: $\mathbf{Z}_{i,j}$ and $\mathbf{Y}_{\mathrm{sh},i,j}$, which are the impedance and shunt admittance matrices, respectively. These matrices can be expressed as:

$$\mathbf{Z}_{i,j} = \begin{bmatrix} z_{i,j,aa} & z_{i,j,ab} & z_{i,j,ac} \\ z_{i,j,ab} & z_{i,j,bb} & z_{i,j,bc} \\ z_{i,j,ac} & z_{i,j,bc} & z_{i,j,cc} \end{bmatrix} \tag{2.46}$$

$$\mathbf{Y}_{\mathrm{sh},i,j} = \begin{bmatrix} y_{\mathrm{sh},i,j,aa} & y_{\mathrm{sh},i,j,ab} & y_{\mathrm{sh},i,j,ac} \\ y_{\mathrm{sh},i,j,ab} & y_{\mathrm{sh},i,j,bb} & y_{\mathrm{sh},i,j,bc} \\ y_{\mathrm{sh},i,j,ac} & y_{\mathrm{sh},i,j,bc} & y_{\mathrm{sh},i,j,cc} \end{bmatrix} \tag{2.47}$$

In (2.46) and (2.47), in the entries of both matrices, the subscripts $_i$ and $_j$ indicate the start and end nodes of the branch (i, j), while the subscripts $_p$ and $_q$ (with $p, q \in \{a, b, c\}$) indicate the corresponding phases (in order to take into account, in the three-phase matrices, the presence of diagonal elements and also

the mutual parameters). The shunt admittance is assumed, as in (2.4), to be equally divided into the two sides of the three-phase branch and it is assumed to be a pure susceptance ($y_{\mathrm{sh},i,j,pq} = jB_{\mathrm{sh},i,j,pq}$). Consequently, the three-phase matrix $\mathbf{Y}_{\mathrm{sh},i,j}$ is equal to $j\mathbf{B}_{\mathrm{sh},i,j}$. The synchronized measurements, assuming the availability of PMUs on both ends of each branch (i,j), are the three-phase voltage $v_{h,p}$ synchrophasor measurements and the six synchrophasor current measurements $i_{i,j,p}$ and $i_{j,i,p}$ (for both end nodes).

Considering the typical values of PMUs and ITs errors, it is possible to define the reference synchrophasor $v^R_{h,p}$, $i^R_{i,j,p}$ and $i^R_{j,i,p}$ as a function of the measured values $v_{h,p}$, $i_{i,j,p}$ and $i_{j,i,p}$, generalizing (2.3). In addition, the line parameters of interest in the matrices (2.46), (2.47) can be expressed as a function of the values available in the SO database and the deviations from these values. In fact, from a generalization of (2.4) the generic element (p,q) in the matrices $\mathbf{Z}_{i,j}$ and $\mathbf{Y}_{\mathrm{sh},i,j}$ can be expressed as:

$$\begin{aligned} z_{i,j,pq} &= R_{i,j,pq} + jX_{i,j,pq} = R^0_{i,j,pq}(1+\gamma_{i,j,pq}) + jX^0_{i,j,pq}(1+\beta_{i,j,pq}) \\ B_{\mathrm{sh},i,j,pq} &= B^0_{\mathrm{sh},i,j,pq}\,(1+\delta_{i,j,pq}) \end{aligned} \tag{2.48}$$

where $\gamma_{i,j,pq}$, $\beta_{i,j,pq}$ and $\delta_{i,j,pq}$ are the relative deviations of $R_{i,j,pq}$, $X_{i,j,pq}$ and $B_{\mathrm{sh},i,j,pq}$ values, respectively, from the values $R^0_{i,j,pq}$, $X^0_{i,j,pq}$ and $B^0_{\mathrm{sh},i,j,pq}$ available in SO database.

Considering $\mathbf{v}^R_h = \begin{bmatrix} v^R_{h,a} & v^R_{h,b} & v^R_{h,c} \end{bmatrix}^\intercal$ the three-phase voltage phasors vector for node h and $\mathbf{i}^R_{i,j} = \begin{bmatrix} i^R_{i,j_a} & i^R_{i,j_b} & i^R_{i,j_c} \end{bmatrix}^\intercal$ and $\mathbf{i}^R_{j,i} = \begin{bmatrix} i^R_{j,i_a} & i^R_{j,i_b} & i^R_{j,i_c} \end{bmatrix}^\intercal$ the three-phase vector for branch-current phasor vectors leaving node i and j, it is possible to define the constraints for the three-phase formulation of the method by leveraging the Kirkhhoff's laws. In particular, the constraint equations corresponding to the three-phase line voltage drop and current balance equations. These can be defined as:

$$\left(\mathbf{v}^R_i - \mathbf{v}^R_j\right) = \mathbf{Z}_{i,j}\left(\mathbf{i}^R_{i,j} - j\frac{\mathbf{B}_{\mathrm{sh},i,j}}{2}\mathbf{v}^R_i\right) \tag{2.49}$$

$$\left(\mathbf{i}^R_{i,j} + \mathbf{i}^R_{j,i}\right) = j\frac{\mathbf{B}_{\mathrm{sh},i,j}}{2}\left(\mathbf{v}^R_i + \mathbf{v}^R_j\right) \tag{2.50}$$

Then, substituting the reference values $\mathbf{v}^R_h$, $\mathbf{i}^R_{i,j}$ and $\mathbf{i}^R_{j,i}$, rewritten as a function of measured values and their errors, and the parameters (2.48) in the constraint equations (2.49) and (2.50), it is possible to define (applying a first order approximation) a system of linear equations involving the measurement functions, measurement errors and line parameters deviations. In particular, splitting the obtained complex equations in real and imaginary parts and considering the branch (i,j) and a time instant t, a system of 12 real valued equations can be obtained. In the equations, like in Section 2.1, the model errors are given by the effect of random errors (from PMUs) while the systematic measurement

errors and the line parameter deviations are the unknown parameters included in the three-phase state vector. For instance, the latter includes the 3×1 vectors of the systematic ratio and phase-angle errors for the voltage vector $\mathbf{v}_h$, indicated as $\boldsymbol{\xi}_h^{\text{sys}} = \left[\xi_{h,a}^{\text{sys}}\ \xi_{h,b}^{\text{sys}}\ \xi_{h,c}^{\text{sys}}\right]^\intercal$ and $\boldsymbol{\alpha}_h^{\text{sys}} = \left[\alpha_{h,a}^{\text{sys}}\ \alpha_{h,b}^{\text{sys}}\ \alpha_{h,c}^{\text{sys}}\right]^\intercal$, respectively. Furthermore, similar considerations can be made to define the other vectors of unknowns $\boldsymbol{\eta}_{i,j}^{\text{sys}}$, $\boldsymbol{\psi}_{i,j}^{\text{sys}}$, $\boldsymbol{\eta}_{j,i}^{\text{sys}}$ and $\boldsymbol{\psi}_{j,i}^{\text{sys}}$. Focusing on line parameter deviations, it is possible to define, for example, the 6×1 vector including the resistance deviations as $\boldsymbol{\gamma}_{i,j,pq} = [\gamma_{i,j,aa}\ \gamma_{i,j,bb}\ \gamma_{i,j,cc}\ \gamma_{i,j,ab}\ \gamma_{i,j,ac}\ \gamma_{i,j,bc}]^\intercal$ (similar definitions can be used for $\boldsymbol{\beta}_{i,j,pq}$ and $\boldsymbol{\delta}_{i,j,pq}$).

2.2.2 Three-phase tap-changing transformer models

The three-phase formulation of the estimator for tap-changing transformer operating parameters is built on the single-phase version presented in Section 2.1 [55]. In particular, the proposed procedure is performed considering some of the most used Step Voltage Regulators (SVRs) configurations in three-phase systems and can be applied from the single branch to multiple branches or even to the entire network. The SVR is a device usually installed at the substation or along the feeder in order to control the voltage levels and keep these within acceptable limits. More specifically, the SVR is a connection of an autotransformer with a variable turn ratio related to the position of the tap [69]. The position of the tap is obtained through a control circuit that commands the displacement of the device based on the approximated voltage drop.

The three-phase SVRs formulation of the wye and closed-delta connections [70] is developed, allowing the application of the proposed method based on both configurations [71].

In the thesis, following the notation of Section 2.1.2, the SVR is modeled as installed in a branch (l, k) and, thus, the voltage measurements $v_{l,p}$ and $v_{k,p}$ and the current measurements $i_{l,k,p}$ and $i_{k,l,p}$ can be considered. If voltage and current phasors are available at the primary and secondary of the SVR (represented with an impedance matrix $\mathbf{Z}_{\text{SVR},l,k}$), the constraint equations of voltage drop and current balance can be applied. This can be obtained by means of the matrices $\mathbf{A}_{\text{v},l,k}$ and $\mathbf{A}_{\text{i},l,k}$, which represent the voltage gain and the current gain matrices, whose entries are determined by the specific connection. For both wye and closed-delta connections, the relationship between the two gain matrices is defined as:

$$\mathbf{A}_{\text{v},l,k}^{-1} = \mathbf{A}_{\text{i},l,k}^\intercal \tag{2.51}$$

For a wye-connected SVR the following equation holds:

$$\mathbf{A}_{\mathrm{v},l,k} = \begin{bmatrix} a_{l,k,aa} & 0 & 0 \\ 0 & a_{l,k,bb} & 0 \\ 0 & 0 & a_{l,k,cc} \end{bmatrix} \tag{2.52}$$

If a closed-delta connected SVR is considered, (2.52) becomes:

$$\mathbf{A}_{\mathrm{v},l,k} = \begin{bmatrix} a_{l,k,ab} & 1 - a_{l,k,ab} & 0 \\ 0 & a_{l,k,bc} & 1 - a_{l,k,bc} \\ 1 - a_{l,k,ac} & 0 & a_{l,k,ac} \end{bmatrix} \tag{2.53}$$

In (2.52) and (2.53) the nonzero entries of $\mathbf{A}_{\mathrm{v},l,k}$ can be expressed as:

$$a_{l,k,pq} = a^0_{l,k,pq}\,(1 + \tau_{l,k,pq}) \tag{2.54}$$

where $a^0_{l,k,pq}$ is the assumed value of the tap changer ratio and $\tau_{l,k,pq}$ is the relative deviation of the actual value from the assumed one (the variation of the tap changer ratios occur with a longer timescale than the RR of the PMUs). $\tau_{l,k,pq}$ is considered, in the estimation process, as an unknown parameter to be estimated. The impedance matrix for the wye connection of the SVRs is diagonal (as in [70]) and it is defined from the following entries:

$$z_{l,k,pp} = jX^0_{l,k,pp}\,(1 + \beta_{l,k,pp}) \tag{2.55}$$

Similar considerations can be used for the closed-delta connected transformer. In fact, the diagonal nonzero parameters $z_{l,k,ab}$, $z_{l,k,bc}$ and $z_{l,k,ac}$ are associated with the $\beta_{l,k,ab}$, $\beta_{l,k,bc}$ and $\beta_{l,k,ac}$ deviations. For a generic SVR connection, $\mathbf{Y}_{l,k}$ is the 6×6 nodal admittance matrix, defined as:

$$\mathbf{Y}_{l,k} = \begin{bmatrix} \mathbf{A}_{\mathrm{i},l,k}\mathbf{Z}^{-1}_{\mathrm{SVR},l,k}\mathbf{A}^{\intercal}_{\mathrm{i},l,k} & -\mathbf{A}_{\mathrm{i},l,k}\mathbf{Z}^{-1}_{\mathrm{SVR},l,k} \\ -\mathbf{Z}^{-1}_{\mathrm{SVR},l,k}\mathbf{A}^{\intercal}_{\mathrm{i},l,k} & \mathbf{Z}^{-1}_{\mathrm{SVR},l,k} \end{bmatrix} \tag{2.56}$$

Considering (2.56), it is possible to define the constraint equations exploiting the relationship between voltages and currents as:

$$\begin{bmatrix} \mathbf{i}^R_{l,k} \\ \mathbf{i}^R_{k,l} \end{bmatrix} = \mathbf{Y}_{l,k} \begin{bmatrix} \mathbf{v}^R_l \\ \mathbf{v}^R_k \end{bmatrix} \tag{2.57}$$

It is then possible to use (2.56) and (2.57) to write the three-phase voltage drop and current balance equations similarly to Section 2.1.2. In particular, it is possible to exploit $\mathbf{A}_{\mathrm{v},l,k}$ and (2.51) to define the following equations:

$$\mathbf{v}^R_l - \mathbf{A}_{\mathrm{v},l,k}\mathbf{v}^R_k = \mathbf{A}_{\mathrm{v},l,k}\mathbf{Z}_{\mathrm{SVR},l,k}\mathbf{A}^{\intercal}_{\mathrm{v},l,k}\mathbf{i}^R_{l,k} \tag{2.58}$$

$$\mathbf{i}^R_{k,l} = -\mathbf{A}^{\intercal}_{\mathrm{v},l,k}\mathbf{i}^R_{l,k} \tag{2.59}$$

linking the actual values to the actual three-phase parameters.

2.2.3 Three-phase estimation framework

As mentioned in Section 2.2.1, adopting the same assumptions and approximations used in Sections 2.1.1 and 2.1.3 for the single-phase case, it is possible to obtain, for the generic three-phase branch (i, j), 12 real-valued equations (from 6 complex equations) linking through linearized measurement functions equivalent measurements to all the unknown parameters. These linearized equations valid for the generic three-phase branch (i, j) are the extension of the single-phase version given by (2.10)-(2.13) and, thus, they won't be reported. The voltage drop and current balance constraint equations for the three-phase SVR model defined by (2.58) and (2.59) (related to a generic three-phase power transformer at branch (l, k)) are instead detailed in what follows.

Firstly, taking into account the wye-connected SVR, (2.60)-(2.63) represent the real and imaginary parts of the voltage drop and current balance equations written for the generic phases $p \in \{a, b, c\}$:

$$\begin{aligned} V^r_{l,p} - V^r_{k,p} a_{l,k,pp} + I^x_{l,k,p} X_{l,k,pp} a^2_{l,k,pp} \simeq V^r_{l,p} \left(\xi^{\text{sys}}_{l,p} + \xi^{\text{rnd}}_{l,p}\right) - V^x_{l,p} \left(\alpha^{\text{sys}}_{l,p} + \alpha^{\text{rnd}}_{l,p}\right) + \\ - V^r_{k,p} a_{l,k,pp} \left(\xi^{\text{sys}}_{k,p} + \xi^{\text{rnd}}_{k,p}\right) + V^x_{k,p} a_{l,k,pp} \left(\alpha^{\text{sys}}_{k,p} + \alpha^{\text{rnd}}_{k,p}\right) + \\ + I^x_{l,k,p} X_{l,k,pp} a^2_{l,k,pp} \left(\eta^{\text{sys}}_{l,k,p} + \eta^{\text{rnd}}_{l,k,p}\right) + I^r_{l,k,p} X_{l,k,pp} a^2_{l,k,pp} \left(\psi^{\text{sys}}_{l,k,p} + \psi^{\text{rnd}}_{l,k,p}\right) + \\ - I^x_{l,k,p} X_{l,k,pp} a^2_{l,k,pp} \beta_{l,k,pp} + \left(V^r_{k,p} a_{l,k,pp} - 2 I^x_{l,k,p} X_{l,k,pp} a^2_{l,k,pp}\right) \tau_{l,k,pp} \end{aligned} \tag{2.60}$$

$$\begin{aligned} V^x_{l,p} - V^x_{k,p} a_{l,k,pp} - I^r_{l,k,p} X_{l,k,pp} a^2_{l,k,pp} \simeq V^x_{l,p} \left(\xi^{\text{sys}}_{l,p} + \xi^{\text{rnd}}_{l,p}\right) + V^r_{l,p} \left(\alpha^{\text{sys}}_{l,p} + \alpha^{\text{rnd}}_{l,p}\right) + \\ - V^x_{k,p} a_{l,k,pp} \left(\xi^{\text{sys}}_{k,p} + \xi^{\text{rnd}}_{k,p}\right) - V^r_{k,p} a_{l,k,pp} \left(\alpha^{\text{sys}}_{k,p} + \alpha^{\text{rnd}}_{k,p}\right) + \\ - I^r_{l,k,p} X_{l,k,pp} a^2_{l,k,pp} \left(\eta^{\text{sys}}_{l,k,p} + \eta^{\text{rnd}}_{l,k,p}\right) + I^x_{l,k,p} X_{l,k,pp} a^2_{l,k,pp} \left(\psi^{\text{sys}}_{l,k,p} + \psi^{\text{rnd}}_{l,k,p}\right) + \\ + I^r_{l,k,p} X_{l,k,pp} a^2_{l,k,pp} \beta_{l,k,pp} + \left(V^x_{k,p} a_{l,k,pp} + 2 I^r_{l,k,p} X_{l,k,pp} a^2_{l,k,pp}\right) \tau_{l,k,pp} \end{aligned} \tag{2.61}$$

$$\begin{aligned} I^r_{l,k,p} a_{l,k,pp} + I^r_{l,k,p} \simeq I^r_{l,k,p} a_{l,k,pp} \left(\eta^{\text{sys}}_{l,k,p} + \eta^{\text{rnd}}_{l,k,p}\right) + I^r_{l,k,p} \left(\eta^{\text{sys}}_{l,k,p} + \eta^{\text{rnd}}_{l,k,p}\right) + \\ - I^x_{l,k,p} a_{l,k,pp} \left(\psi^{\text{sys}}_{l,k,p} + \psi^{\text{rnd}}_{l,k,p}\right) - I^x_{l,k,p} \left(\psi^{\text{sys}}_{l,k,p} + \psi^{\text{rnd}}_{l,k,p}\right) - I^r_{l,k,p} a_{l,k,pp} \tau_{l,k,pp} \end{aligned} \tag{2.62}$$

$$\begin{aligned} I^x_{l,k,p} a_{l,k,pp} + I^x_{l,k,p} \simeq I^x_{l,k,p} a_{l,k,pp} \left(\eta^{\text{sys}}_{l,k,p} + \eta^{\text{rnd}}_{l,k,p}\right) + I^x_{l,k,p} \left(\eta^{\text{sys}}_{l,k,p} + \eta^{\text{rnd}}_{l,k,p}\right) + \\ + I^r_{l,k,p} a_{l,k,pp} \left(\psi^{\text{sys}}_{l,k,p} + \psi^{\text{rnd}}_{l,k,p}\right) + I^r_{l,k,p} \left(\psi^{\text{sys}}_{l,k,p} + \psi^{\text{rnd}}_{l,k,p}\right) - I^x_{l,k,p} a_{l,k,pp} \tau_{l,k,pp} \end{aligned} \tag{2.63}$$

Then, similar considerations can be done also for the closed-delta connected

transformers, obtaining again 12 real-valued equations (four for each system phase).

A linear system of equations can be obtained considering a time instant t (e.g. corresponding to a PMU timestamp) and the above constraint equations related to a given SVR branch (l,k) (in what follows, only this case will be reported). Then, it is possible to express in matrix notation the linear system, separating systematic errors from random ones as follows:

$$\begin{aligned}\mathbf{b}_{l,k,t} &= \mathbf{H}_{l,k,t}\begin{bmatrix}\boldsymbol{\xi}_l^{\text{sys}}\\ \boldsymbol{\alpha}_l^{\text{sys}}\\ \boldsymbol{\xi}_k^{\text{sys}}\\ \boldsymbol{\alpha}_k^{\text{sys}}\\ \boldsymbol{\eta}_{l,k}^{\text{sys}}\\ \boldsymbol{\psi}_{l,k}^{\text{sys}}\\ \boldsymbol{\eta}_{k,l}^{\text{sys}}\\ \boldsymbol{\psi}_{k,l}^{\text{sys}}\\ \boldsymbol{\beta}_{l,k}\\ \boldsymbol{\tau}_{l,k}\end{bmatrix} + \mathbf{E}_{l,k,t}\begin{bmatrix}\boldsymbol{\xi}_{l,t}^{\text{rnd}}\\ \boldsymbol{\alpha}_{l,t}^{\text{rnd}}\\ \boldsymbol{\xi}_{k,t}^{\text{rnd}}\\ \boldsymbol{\alpha}_{k,t}^{\text{rnd}}\\ \boldsymbol{\eta}_{l,k,t}^{\text{rnd}}\\ \boldsymbol{\psi}_{l,k,t}^{\text{rnd}}\\ \boldsymbol{\eta}_{k,l,t}^{\text{rnd}}\\ \boldsymbol{\psi}_{k,l,t}^{\text{rnd}}\end{bmatrix}\\ &= \mathbf{H}_{l,k,t}\mathbf{x}_{l,k} + \mathbf{E}_{l,k,t}\mathbf{e}_{l,k,t} = \mathbf{H}_{l,k,t}\mathbf{x}_{l,k} + \boldsymbol{\epsilon}_{l,k,t}\end{aligned} \tag{2.64}$$

In (2.64), $\mathbf{b}_{l,k,t}$ is the vector of known terms and $\mathbf{H}_{l,k,t}$ is the measurement matrix linking the measurement functions and the state vector $\mathbf{x}_{l,k}$. The state vector $\mathbf{x}_{l,k}$ includes all the 3×1 vectors of systematic measurement errors of voltage and current synchrophasors ($\boldsymbol{\xi}_l^{\text{sys}} = \left[\xi_{l,a}^{\text{sys}}\ \xi_{l,b}^{\text{sys}}\ \xi_{l,c}^{\text{sys}}\right]^{\intercal}$, ..., $\boldsymbol{\psi}_{k,l}^{\text{sys}} = \left[\psi_{k,l,a}^{\text{sys}}\ \psi_{k,l,b}^{\text{sys}}\ \psi_{k,l,c}^{\text{sys}}\right]^{\intercal}$) and, in addition, the line parameters deviations associated with the SVR (for instance, in case of a wye-connected transformer, $\boldsymbol{\beta}_{l,k} = [\beta_{l,k,aa}\ \beta_{l,k,bb}\ \beta_{l,k,cc}]^{\intercal}$ and $\boldsymbol{\tau}_{l,k} = [\tau_{l,k,aa}\ \tau_{l,k,bb}\ \tau_{l,k,cc}]^{\intercal}$).

Then, it is possible to extend, without loss of generality, the procedure used in Section 2.1.3 to obtain the solution of the system in (2.64). Indeed, the assumption is to have multiple PMU measurements available, corresponding to C power network conditions along with prior knowledge on all the considered unknowns, to define the following overall system of equations:

$$\begin{aligned}\mathbf{b}_{l,k,\text{tot}} &= \begin{bmatrix}\mathbf{b}_{l,k}\\ \mathbf{0}_{r\times 1}\end{bmatrix} = \begin{bmatrix}\mathbf{H}_{l,k}\\ \mathbf{I}_r\end{bmatrix}\mathbf{x}_{l,k} + \begin{bmatrix}\boldsymbol{\epsilon}_{l,k}\\ \mathbf{e}_{\text{prior}}\end{bmatrix}\\ &= \mathbf{H}_{l,k,\text{tot}}\mathbf{x}_{l,k} + \boldsymbol{\epsilon}_{l,k,\text{tot}}\end{aligned} \tag{2.65}$$

where r is the number of unknowns included in the state vector (dependent on the type of the connection of the SVR), $\mathbf{0}_{r\times 1}$ is a r-size vector of zeros that establishes the pseudo-measurements related to the prior information and thus assuming no deviations, and $\mathbf{I}_r$ is the r-size identity matrix of prior values. Vec-

tor $\boldsymbol{\epsilon}_{l,k,\text{tot}}$ includes both $\boldsymbol{\epsilon}_{l,k}$ and $\mathbf{e}_{\text{prior}}$, indicating the equivalent random errors and the random variables associated with the prior values, respectively. Equation (2.65) represents the estimation problem for the generic SVR connection associated with the three-phase branch (l,k). This problem can be solved in WLS sense using a weight matrix $\mathbf{W}_{l,k,\text{tot}} = \boldsymbol{\Sigma}^{-1}_{\boldsymbol{\epsilon}_{l,k,\text{tot}}}$ defined as:

$$\boldsymbol{\Sigma}_{\boldsymbol{\epsilon}_{l,k,\text{tot}}} = \begin{bmatrix} \boldsymbol{\Sigma}_{\boldsymbol{\epsilon}_{l,k}} & \mathbf{0} \\ \mathbf{0} & \boldsymbol{\Sigma}_{\mathbf{e}_{\text{prior}}} \end{bmatrix} \tag{2.66}$$

where the covariance matrix of $\boldsymbol{\epsilon}_{l,k}$ is obtained, similarly to (2.22), by means the law of propagation [58], as:

$$\boldsymbol{\Sigma}_{\boldsymbol{\epsilon}_{l,k}} = \mathbf{E}_{l,k} \boldsymbol{\Sigma}_{\mathbf{e}_{l,k}} \mathbf{E}^{\intercal}_{l,k} \tag{2.67}$$

It is worth highlighting that, if additional information on specific correlations of line parameters uncertainties or accuracy of the devices are available, this can be included and appropriately treated in the estimation problem (as will be discussed in Section 3.2).

Finally, the estimated vector $\hat{\mathbf{x}}_{l,k}$ is obtained as:

$$(\mathbf{H}^{\intercal}_{l,k,\text{tot}} \mathbf{W}_{l,k,\text{tot}} \mathbf{H}_{l,k,\text{tot}}) \hat{\mathbf{x}}_{l,k} = \mathbf{H}^{\intercal}_{l,k,\text{tot}} \mathbf{W}_{l,k,\text{tot}} \mathbf{b}_{l,k,\text{tot}} \tag{2.68}$$

2.2.4 Tests and results: the three-phase method performance

The method in its three-phase formulation has been validated in MATLAB environment by means of different simulation scenarios to emphasize the impact of the grid model on the the estimation accuracy [68]. In particular, the tests have been carried out on the three-phase version of the IEEE 14 bus test system (in Fig. 2.3 it is shown the unifilar diagram with node and branch indexes). The three-phase version of the grid has been obtained considering as positive sequence parameters the data in [72] and, then, determining the remaining sequence parameters (negative and positive sequence networks) following [24].

To validate statistically the estimation results, MC simulations have been performed using $N_{\text{MC}} = 10000$ trials. The tests have been carried out considering as reference values for voltages and currents the outputs of a three-phase power-flow. Thus, the actual values of voltages, currents and tap ratios are established. Once the reference values of the measurements have been defined, random and systematic errors have been added to them. The variability in the network and the uncertainties affecting the monitoring system have been then established. Thus, the default scenario for the set-up of the tests of this section is defined by the following assumptions:

1. As for the line parameters, maximum deviations $\gamma_{i,j,pq}$, $\beta_{i,j,pq}$ and $\delta_{i,j,pq}$

in (2.48) are equal to $\pm 10\,\%$.

2. ITs belong to Class 0.5 and the maximum deviation of $a_{l,k,pq}$ is set to $\pm 1\,\%$ [56] for both wye and closed-delta connected transformers.

3. PMU01, introduced in Section 2.1.4, has been chosen for the base uncertainty configuration.

4. A variability of $\pm 10\,\%$ with respect to nominal values of active and reactive powers has been considered to obtain different load conditions. Focusing on the unbalance among the phases, a maximum variability of $\pm 1\,\%$ (for each node) has been imposed keeping the limit of the voltage asymmetry compatible with the limits identified by the Italian TSO (details on these limits can be founded in [73] and [74]).

5. As for the extraction of the deviations of the involved parameters, the errors have been associated with uniform distributions.

The results have been analyzed by means the RMSEs errors, generalizing (2.45) for three-phase parameters.

Single-branch approach

The firsts series of tests have been carried out, in a single-branch perspective, on the branches equipped with a SVR (i.e., the branches $(4,7)$, $(4,9)$ and $(5,6)$, with indexes 8, 9 and 10, respectively, in Fig. 2.3), considering both SVR configurations. The RMSEs of the results, obtained with (2.45), can be compared with prior errors standard deviation. The estimation results of the proposal (referred to as "Tap estimation") are compared with those of "No Tap estimation" method, which is the method considering the tap changer ratios as known a-priori. In particular, in "No Tap estimation", despite uncertainty affecting tap changer ratios, these latter are not included in the estimation model and, thus, possible voltage regulation uncertainty is neglected.

Table 2.7 shows the estimation results of amplitude and phase-angle displacement errors for the voltages (only for phase a but similar results can be obtained for other phases) of branches $(4,7)$, $(4,9)$ and $(5,6)$. It is worth observing that, if the tap changer is modeled as in Tap estimation, a reduction, with respect to No Tap estimation, of the RMSE up to $50\,\%$ and $30\,\%$ for ratio and phase-angle errors can be obtained. This behavior is explained by the fact that No Tap estimation suffers from the lack of modeling of tap ratios variability, which, if neglected, has a significant impact on systematic error estimates.

In Table 2.7, systematic errors of amplitude and phase-angle of currents are not reported, but it is worth underlining that similar results can be obtained.

Table 2.7: RMSE of systematic voltage errors estimation, single-branch approach and closed delta configuration

Branch Index (l,k)	**Method**	**RMSE** $\xi_{l,a}$ [%]	$\alpha_{l,a}$ [crad]	$\xi_{k,a}$ [%]	$\alpha_{k,a}$ [crad]
8 (4, 7)	Tap estimation	0.25	0.26	0.24	0.26
8 (4, 7)	No Tap estimation	0.48	0.35	0.48	0.36
9 (4, 9)	Tap estimation	0.24	0.26	0.24	0.26
9 (4, 9)	No Tap estimation	0.47	0.33	0.47	0.35
10 (5, 6)	Tap estimation	0.24	0.28	0.25	0.28
10 (5, 6)	No Tap estimation	0.44	0.31	0.43	0.33

In addition to the fact that the results for $\xi_{h,p}$ improve with the inclusion of tap ratios in the estimation model, it is important to highlight that the estimation results for No Tap estimation are beyond the prior values (i.e., 0.29 % for a VT of Class 0.5, as shown in Table 2.2).

Table 2.8 reports the results for the reactance estimation for the SVR branches that are included in the grid. Despite the results for both methods are far below the prior value for $\beta_{l,k,pq}$ (which is 5.77 %), it is possible to observe that an improvement of the estimation results is obtained when tap changer ratios are modeled and estimated, reaching a maximum RMSE reduction of 37 % for branch 10.

Table 2.8: $\beta_{l,k,pq}$ estimation, single-branch estimation and closed delta configuration

Branch index (l,k)	**Method**	**RMSE [%]** $\beta_{l,k,ab}$	$\beta_{l,k,bc}$	$\beta_{l,k,ac}$
8 (4, 7)	Tap estimation	2.76	2.76	2.72
8 (4, 7)	No Tap estimation	3.01	3.02	2.97
9 (4, 9)	Tap estimation	2.03	2.10	2.08
9 (4, 9)	No Tap estimation	2.75	2.81	2.81
10 (5, 6)	Tap estimation	2.31	2.33	2.33
10 (5, 6)	No Tap estimation	3.65	3.64	3.69

Multiple branches approach

Further tests have been carried out in a multiple branches (multi-branch) perspective, in particular considering the entire three-phase network in Fig. 2.3. When a multi-branch approach is considered, the constraints of all the involved

branches must be used. Table 2.9 shows the estimation results of the tap ratios $\tau_{l,k,pq}$ (closed-delta connection) when multi-branch and single-branch approaches are considered. This test has been carried out to remark the impact of a multi-branch approach on the estimation results. In Table 2.9, it is possible to observe that the proposal leads to significant improvements with respect to the prior values (i.e., 0.58 % in Table 2.2), achieving RMSEs of less than 0.2 % and 0.1 % for single-branch and multi-branch approaches, respectively.

Table 2.9: Tap ratio error $\tau_{l,k,pq}$ estimation, multi-branch vs single-branch and closed delta configuration

Branch index (l,k)	**Approach**	**RMSE [%]**		
		$\tau_{l,k,aa}$	$\tau_{l,k,bb}$	$\tau_{l,k,cc}$
8 $(4,7)$	Single-branch	0.18	0.18	0.18
8 $(4,7)$	Multi-branch	0.08	0.08	0.08
9 $(4,9)$	Single-branch	0.18	0.19	0.19
9 $(4,9)$	Multi-branch	0.08	0.08	0.08
10 $(5,6)$	Single-branch	0.19	0.19	0.19
10 $(5,6)$	Multi-branch	0.09	0.09	0.09

Despite the results for wye-connected transformers are not reported, it is interesting to observe that in the same network conditions, the errors are higher than those in Table 2.9. Nevertheless, the single-branch approach still more than halves the RMSE with respect to the prior, and the multi-branch solution, in turn, halves the estimation results obtained with the single-branch approach, achieving reductions with respect to the prior errors of more than 77 %.

As a further confirmation of the estimation results that can be obtained when multi-branch approach is applied, Fig. 2.16 shows the RMSE of systematic voltage amplitude errors $\xi_{h,a}$ estimates when the whole network is considered. In Fig. 2.16, No Tap Estimation method is indicated with blue squares, prior values are indicated with black plus sign and Tap Estimation method with orange asterisks. In addition, No Tap estimation method can be still applied also on the portion of the grid excluding tap changers and this method is indicated with purple dots. Indeed, it is possible to observe that when the estimation is applied assuming tap changer ratios as perfectly known, this method suffers again from the lack of modeling and the RMSE results are higher than prior values for all the nodes of the grid (even far away from the branches equipped with SVRs). On the other side, focusing on the proposed method, it can be highlighted that estimating the tap ratios of the SVRs brings remarkable improvements of the errors with respect to prior values. The above explained behaviors can

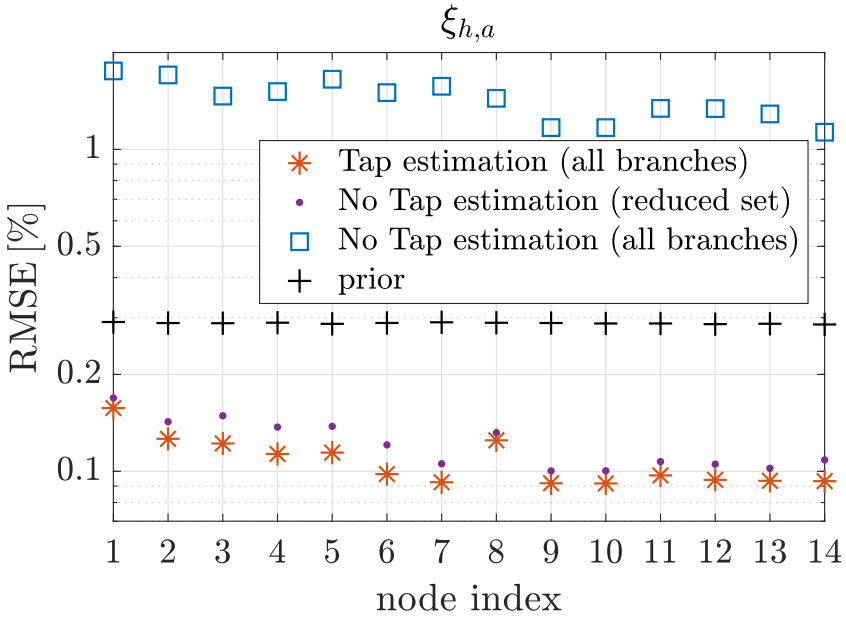

Figure 2.16: Entire network, estimation of voltage amplitude systematic errors - results obtained with and without tap estimation.

be observed also in Fig. 2.17, where the same methods, colors and markers of Fig. 2.16 are considered, focusing on systematic voltage phase-angle errors estimation.

It is important to stress the aspect that, when the method is applied to a reduced set of branches, it is still clearly more accurate than prior but its RMSEs are higher than those obtained when the Tap estimation method is applied to all the branches of the grid. To sum up, lowest RMSEs are obtained when the whole network is considered and a detailed model of the tap changers is included in the estimation model. This allows reaching, for phase-angle errors estimation of Fig. 2.17, an average reduction of about 68 % with respect to the prior. This type of conclusion implies that, for each possible network under study, preliminary analyses should be done to help the choice on the most appropriate configuration of the estimation method to apply.

As another example of the test outcomes, the estimation results for the reactance parameters for branch $(4, 5)$ (i.e., the branch close to branches 8, 9 and 10, equipped with SVRs), with or without the tap changer ratios estimation, can be observed in Fig. 2.18. Different results can be observed if self or mutual reactance parameters are considered: the estimation of self reactances improves of almost two-thirds with respect to the prior, while for the mutual reactance parameters the reduction is of about 30 %. This confirms the advantages of

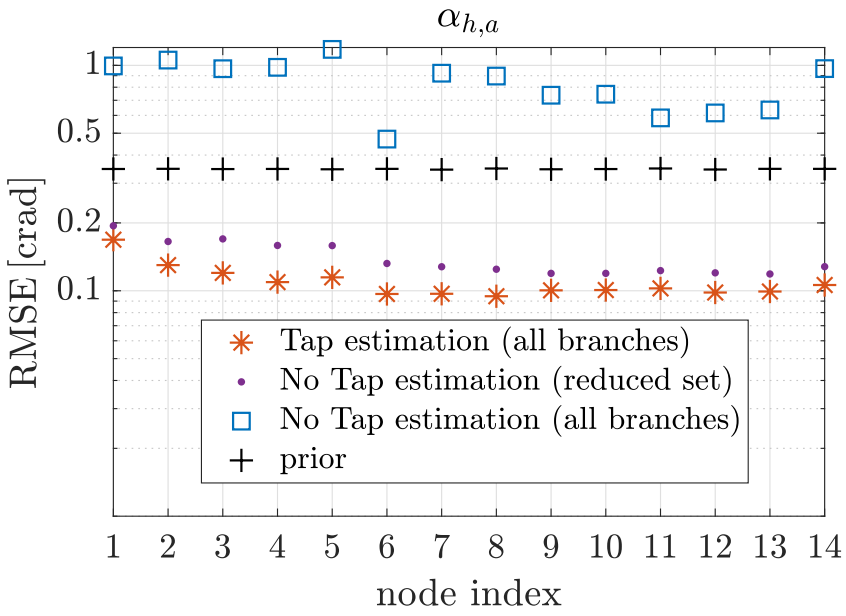

Figure 2.17: Entire network, estimation of voltage phase-angle systematic errors - results obtained with and without tap estimation.

Table 2.10: Estimation performance under different uncertainty scenarios

IT class	**PMU accuracy**	**RMSE**							
		$\gamma_{2,3,aa}$ [%]	$\gamma_{2,3,ab}$ [%]	$\beta_{2,3,aa}$ [%]	$\beta_{,23,ab}$ [%]	$\xi_{2,a}$ [%]	$\alpha_{2,a}$ [crad]	$\xi_{3,a}$ [%]	$\alpha_{3,a}$ [crad]
0.2	PMU01	2.11	2.81	1.39	2.81	0.07	0.08	0.06	0.07
	PMU02	2.63	3.37	1.67	3.47	0.08	0.11	0.07	0.09
0.5	PMU01	2.21	2.83	1.44	2.84	0.13	0.13	0.12	0.12
	PMU02	2.74	3.39	1.77	3.51	0.15	0.17	0.14	0.14

the three-phase formulation in the estimation of all the parameters involved. It is worth observing that, when the complete model of the grid is considered, a reduction, with respect to the configuration considering the reduced set of branches, of about 32 % and 19 % can be reached for self and mutual parameters, respectively.

To investigate the impact of IT and PMU uncertainty on the estimation performance, other tests have been carried out considering different values for the IT class and the maximum PMU errors (considering both PMU01 and PMU02 accuracy levels). ITs of Class 0.2 have been also considered and this translates into a maximum ratio error of 0.2 % and a maximum phase displacement error of 0.3 crad (leading to prior standard deviations of 0.12 % and 0.17 crad for ratio

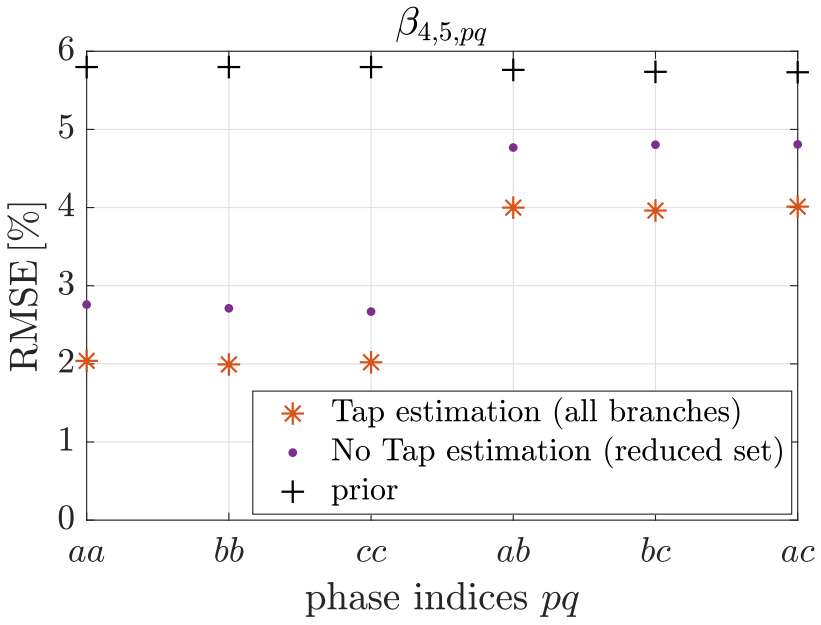

Figure 2.18: RMSE results for the estimation of reactance parameters of branch $(4, 5)$.

and phase errors, respectively). Table 2.10 shows, for phase a and branch $(2, 3)$, RMSE results for both line parameters and VT systematic errors. As expected, the estimation accuracy degrades with higher uncertainties. In particular, since systematic errors are included in the model and estimated, the main impact is related to PMU errors, leading to an increase of the errors of more than 20 % for all the estimated line parameters when maximum PMU errors double.

Some tests have been carried out also to investigate the impact on the estimation performance of an increase of the number of branches involved in a multi-branch approach. The tests have been performed increasing progressively from a single-branch approach to the entire network. Table 2.11 shows, for the parameters of branch $(2, 3)$, the estimation results considering different scenarios: the single-branch approach; a "3 branches" configuration that corresponds to the set of branches 3, 4 and 6; a "6 branches" configuration that involves the branches from index 1 to 6; and the "All branches" configuration that corresponds to the simultaneous estimation on the entire network.

Focusing on Table 2.11, it is possible to observe that, as expected, the estimation improves with the size of the set of branches involved. In particular, the most significant improvement in the line parameters estimation results is found moving from the single-branch approach to the "3 branches" scenario: an error reduction up to about 26 % is achieved when 3 branches are considered,

Table 2.11: Estimation performance on increasing network portion - branch $(2, 3)$

Network portion	**RMSE**							
	$\gamma_{2,3,aa}$ [%]	$\gamma_{2,3,ab}$ [%]	$\beta_{2,3,aa}$ [%]	$\beta_{2,3,ab}$ [%]	$\xi_{2,a}$ [%]	$\alpha_{2,a}$ [crad]	$\xi_{3,a}$ [%]	$\alpha_{3,a}$ [crad]
Single-branch	3.24	4.06	2.20	4.29	0.22	0.26	0.22	0.26
3 branches	2.48	3.16	1.63	3.16	0.19	0.22	0.18	0.21
6 branches	2.43	3.09	1.56	3.12	0.14	0.17	0.15	0.18
All branches	2.21	2.83	1.44	2.84	0.13	0.13	0.12	0.12

while an error reduction of 34 % is obtained using the entire network. For the estimation of systematic errors, the improvement of the results becomes more pronounced with an increasing number of branches. For example, the RMSE of $\alpha_{2,a}$ halves moving from the single-branch approach to the "All branches" scenario. In addition, it is worth highlighting that also the topology of the set of branches considered has an impact on the results. In fact, meshes in the grid introduce additional constraints (each node is shared at least among two branches) helping the overall estimation performance.

Finally, despite a comprehensive comparison of the estimation results with other methods in literature is not possible because of their characteristics, some tests have been carried out comparing, in the same measurement scenario, three estimation methods. In Table 2.12, the proposed method (which is used also with the single-branch approach) is compared with two methods that face the three-phase line parameters estimation using PMU measurements. The first method, named Method C [75], is built on a two-step estimation of shunt admittance and impedance matrices for a single branch and can deal, as the proposed method, also with non-transposed lines. The second method (identified with Method D [24]), starting from the current equations available at both ends of the line, proposes a robust estimator for the shunt and line admittance parameters. It is important to underline that Method C and Method D rely on a significant level of unbalance to improve the accuracy of the estimation. For this reason and to perform a comparison as fair as possible, the maximum variations of the load among the system phases at a given node have been considered with two different levels (column 'Load Unb.'): a default value of ± 1 % and also a variation up to ± 5 % are considered in the following tests. Table 2.12 reports the estimation results for branch $(2, 3)$, using the accuracy scenarios of the sensitivity study reported in Table 2.10. In this table, the symbol '>' is used to highlight the estimation results far beyond the prior values (at least twice the corresponding prior values). As a general comment, it is possible to observe that lowest RMSEs are obtained with the proposed method, whereas

Table 2.12: Comparison of different methods in different uncertainty scenarios - branch $(2, 3)$

Method	**ITs class**	**PMU accuracy**	**Load Unb.** [%]	**RMSE** $\gamma_{2,3,aa}$ [%]	$\gamma_{2,3,ab}$ [%]	$\beta_{2,3,aa}$ [%]	$\beta_{2,3,ab}$ [%]
Proposed Method (All branches)	0.2	PMU01	1	2.11	2.81	1.39	2.81
			5	0.93	1.02	0.59	1.25
	0.5	PMU01	1	2.21	2.83	1.44	2.84
			5	1.08	1.07	0.67	1.33
		PMU02	1	2.74	3.39	1.77	3.51
			5	1.63	1.72	1.04	1.94
Proposed Method (Single-branch)	0.2	PMU01	1	3.14	4.06	2.13	4.23
			5	1.47	1.64	0.97	2.07
	0.5	PMU01	1	3.22	4.07	2.19	4.29
			5	1.71	1.72	1.08	2.22
		PMU02	1	3.55	4.54	2.52	4.63
			5	2.56	2.81	1.72	3.35
Method C [75]	0.2	PMU01	1	>	>	>	>
			5	2.36	2.38	1.50	3.20
	0.5	PMU01	1	>	>	>	>
			5	3.30	3.42	2.09	4.62
		PMU02	1	>	>	>	>
			5	4.99	4.96	3.11	6.77
Method D [24]	0.2	PMU01	1	10.48	10.08	6.50	>
			5	2.14	2.22	1.40	2.92
	0.5	PMU01	1	>	>	8.40	>
			5	2.99	3.16	1.96	4.15
		PMU02	1	>	>	>	>
			5	4.45	4.55	2.86	6.05

Methods C and D suffer, above all, from the presence of low levels of unbalance. For instance, the proposed method achieves the best results in the multi-branch approach and, as expected, benefits from a higher level of unbalance.

The three-phase formulation, besides allowing the estimation of three-phase line parameters and the systematic errors of each phase measurement (permitting thus to find some ITs in critical metrological conditions), allows also a better estimation of the positive sequence parameters of the branch when a realistic level of unbalance is present in the grid. As a demonstration of the above mentioned statement, Table 2.13 shows the average estimation RMSEs across all the branches for the positive sequence values of resistance and reactance line

parameters. In particular, a comparison of the results obtainable with both versions of the proposed algorithm has been carried out. The two versions are: the three-phase version of the algorithm described in this section and, in this case, the positive sequence values are obtained from the three-phase parameters, and the single-phase one, from which positive sequence values are obtained directly applying the algorithm in Section 2.1.3).

Table 2.13: Comparison of positive sequence parameters estimation with single-phase and three-phase approaches

Method	**Average RMSE [%]**	
	γ_+	β_+
Single-phase	2.47	1.23
Three-phase	1.59	0.76

To do that, the results in Table 2.13 are obtained with the wye configuration because an equivalence is possible with [55]. In Table 2.13, γ_+ and β_+ represent the average positive sequence estimation RMSEs (averaged among all the branches of the grid) for line resistance and reactance, respectively. The results confirm that, when symmetry is no guaranteed, the three-phase formulation overcomes the performance of the positive sequence approach. More specifically, the improvement of the estimation performance of the three-phase method with respect to the single-phase version is of about 36 % and 38 % for γ_+ and β_+, respectively.

Validation with experimental data

Additional tests have been performed to assess the proposed method estimation performance with a more realistic uncertainty scenario. To do that, real PMU measurement errors, obtained trough a laboratory characterization of commercial PMUs (like those in [76] and [77]), have been used for the tests. Table 2.14 shows the estimation results for line parameters and systematic voltage errors of phase a for branches $(2, 3)$, $(4, 5)$ and $(9, 14)$, using the above mentioned PMU errors after the introduction of IT systematic errors according to the assumed Class 0.5. The results are obtained with the proposed method when the entire grid is considered. It is possible to note that the RMSE results are similar to those obtained with simulated PMU errors and are even better, since the used commercial PMUs have lower uncertainty than that assumed for the simulations. The RMSEs are much lower than prior standard deviations, thus confirming the validity of the presented approach in reducing the uncertainty of both network parameters and IT errors.

Table 2.14: Estimation performance with experimental PMU errors

Branch index (i,j)	**RMSE**							
	$\gamma_{i,j,aa}$ [%]	$\gamma_{i,j,ab}$ [%]	$\beta_{i,j,aa}$ [%]	$\beta_{i,j,ab}$ [%]	$\xi_{i,a}$ [%]	$\alpha_{i,a}$ [crad]	$\xi_{j,a}$ [%]	$\alpha_{j,a}$ [crad]
3 $(2,3)$	1.81	2.36	1.10	2.29	0.11	0.11	0.11	0.11
7 $(4,5)$	2.19	2.62	1.53	3.41	0.11	0.10	0.11	0.11
17 $(9,14)$	1.62	1.91	1.39	3.27	0.09	0.10	0.09	0.10

Chapter 3

Assumptions on measurement chain and grid: Impact and solutions

Following the findings previously discussed, this Chapter presents the results of the analyses carried out to understand how the assumptions on the measurement chain and on the grid modeling could be improved in order to enhance the estimation performance. The main purpose of the Chapter is to present how the presented estimation method for line parameters and systematic measurement errors has been generalized. First of all, the model of the measurement chain errors (for both IT and PMU) has been refined to take into account different possible metrological behaviors. Focusing on CT, a more realistic model has been defined and its impact on the performance of the parameters estimation has been evaluated. As for the PMUs, a more realistic error model has been applied in the proposed method, considering possible correlation in phase-angle measurements.

Then, from the grid modeling point of view, the following aspects have been considered:

- A more general model of the tap-changing transformer has been analyzed and a compromise solution to include this model in the proposed estimation method has been introduced.
- The presence of a possible mismatch between the assumed maximum line parameters variability and the actual one (i.e., incorrect prior information on line parameter uncertainty) has been taken into account and its impact has been studied deeply.

3.1 Refined model of current transformer

In literature, various papers have dealt with line parameters estimation for both transmission and distribution grids. Nevertheless, a detailed description of the measurement errors occurring in the entire measurement chain has not been deeply considered. In fact, in a measurement chain composed of ITs and PMUs, the first ones are typically responsible for the main uncertainty contributions [78], but they are often neglected or just considered through purely random error sources.

In this context, in [54, 68] the estimation of line parameters and systematic errors has been proposed assuming that both VTs and CTs introduce systematic ratio and phase displacement errors. As for the possible distribution for these errors, in absence of specific information, the only justifiable choice is to extract error values from uniform distributions (i.e., starting from information provided by the accuracy class) and assume no correlation among these errors.

In this regard, due to the fact that the node voltages in normal operating conditions are close to the rated values [79], for VTs the above assumption is reasonable. In fact, the accuracy class for measuring VTs (both conventional [59] and low-power [80]) prescribes maximum ratio and phase errors that hold for primary voltage magnitude varying between 80 % and 120 % of the rated value.

When CTs are considered instead, the primary current can vary significantly with respect to the rated values. For this reason and for the presence of intrinsic nonlinear effects in the CT model, the assumption of fixed systematic errors (i.e., constant errors) associated with CTs is not, in general, a good choice [81], [82]. For a given class of accuracy for CTs indeed, the standards [60] and [83] allow larger errors in the lowest part of the measurement range.

To deal with the complex behavior of CTs, a model of the CT more detailed than that considered in the previous sections has been defined and included in the line parameters estimation method [84]. In particular, a more detailed representation of the uncertainty of CTs has been obtained trough numerical simulations and experimental tests, then the impact of this more complex model on the estimates has been studied. The final model assumed for the CT behavior has been presented in [85], where the limitations found in [84] have been overcome. The proposed solution is a refined model of CT behavior, which takes into account the possible presence of a nonlinear behavior in the lowest part of the measurement range. The obtained model has been also based on experimental tests carried out on CTs from different manufacturers. The errors found have been indeed exploited to define a parametric model of CT errors that can be included in the estimation model. Considering this model, the estimation

results show that the estimates of the series line parameters $R_{i,j}$ and $X_{i,j}$ are not significantly affected by the CT, while CTs have a relevant impact on shunt susceptance estimation.

3.1.1 Current transformer errors

The impact of CTs on PMUs measurements, if taken into account, is typically considered superimposing systematic errors to the reference synchrophasors, but this approach, as above discussed, is just an approximation. In what follows, a refined CT error model, obtained based on both simulation and experimental results, is presented.

CT errors model

To model the complex CT behavior, the classical Steinmetz equivalent circuit (shown in Fig. 3.1) is used [86]. In Fig. 3.1, the secondary leakage inductance L_l, the secondary resistance R_2 and the parallel resistor (which takes into account the eddy current loss) of a Class 0.5 CT are referred to the secondary side. In addition, i_1 and i_2 are the primary and secondary currents, while K_n is the nominal ratio. The Tellinen hysteresis model is considered to take into account the relationship between mutual flux linkage λ_m and magnetizing current i_m.

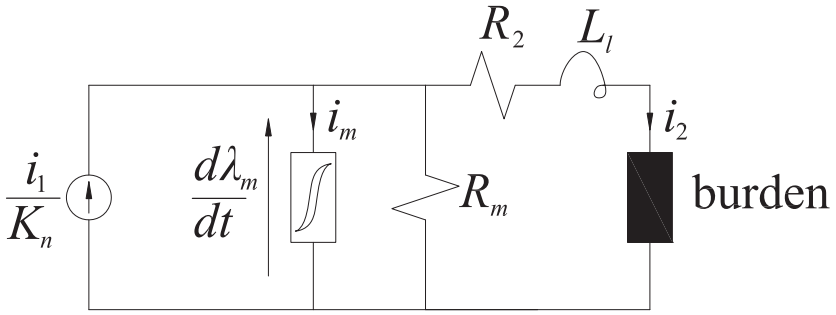

Figure 3.1: Equivalent circuit of a current transformer.

It is worth noticing that, as also known in literature [82], [87] and [81], the accuracy of a CT at the fundamental frequency is just weakly affected by the other (considerably weaker) components that may be present in the primary current. For this reason, in these analyses, ratio and phase errors are considered as related to the amplitude of the fundamental component only. As a first step, the errors variability can be found feeding, with different amplitude levels, the CT with sinusoidal currents at rated frequency and extracting the difference (in magnitude and phase) between the phasors $K_n i_2$ and i_1 (which represent the reconstructed current and the actual one, respectively), thus obtaining overall

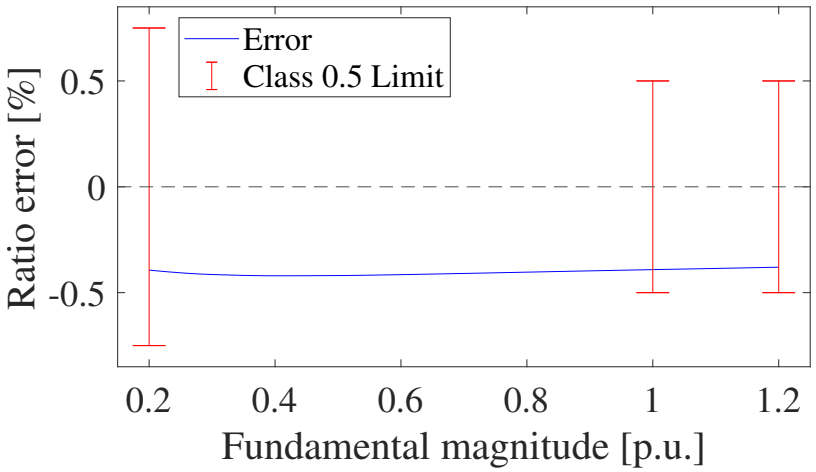

Figure 3.2: Ratio error as a function of the fundamental magnitude.

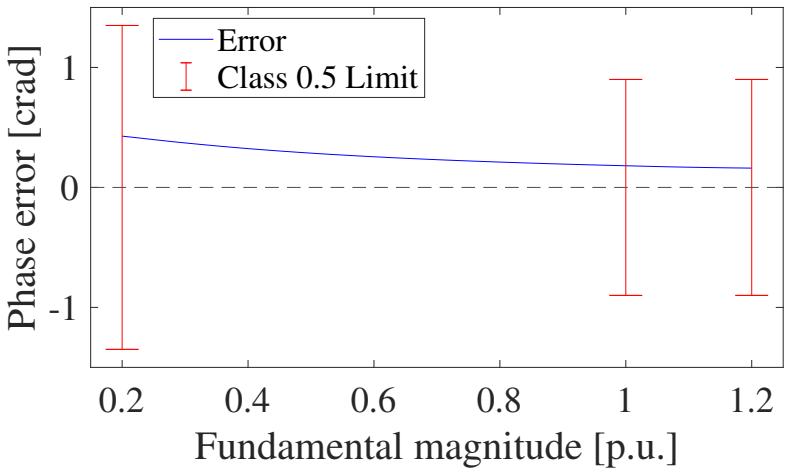

Figure 3.3: Phase error as a function of the fundamental magnitude.

trends similar to those shown in Fig. 3.2 and Fig. 3.3 for η and ψ errors, respectively. In Fig. 3.2 and Fig. 3.3, the errors have been computed considering the hysteresis parameters that reflects those of a typical Class 0.5 CT operating at rated burden, with primary current ranging between 20 % and 120 % of the rated value. In the figures, the red lines represent the limits of a CT of Class 0.5 (ratio and phase errors).

Focusing on the level of the errors in the figures, as expected, the values of ratio error $\eta(I/I^0)$ and phase error $\psi(I/I^0)$ (functions of the ratio of current magnitude I on its nominal value I^0) are within the accuracy limits reported in

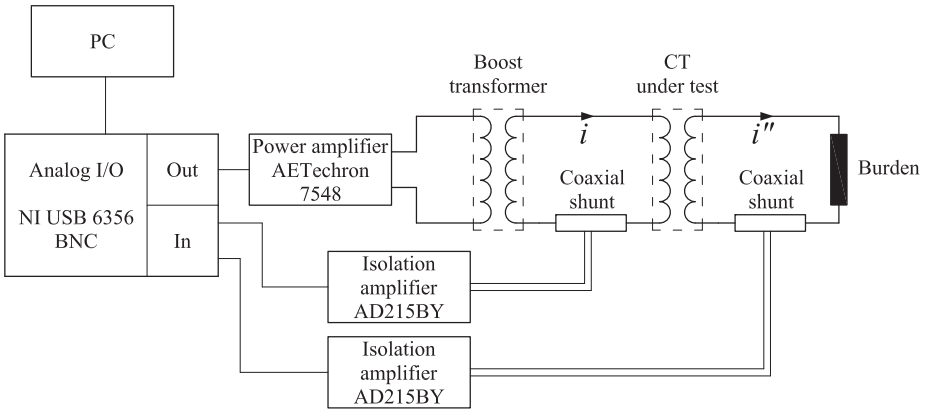

Figure 3.4: Measurement setup for the characterization of CTs.

the standards. In particular, $\eta(I/I^0)$ is basically constant ($-0.4\,\%$ with negative bias, as often happens for a CT loaded with full burden). $\psi(I/I^0)$ shows, due to the inductive nature of i_m, a significant increase at low values of I: moving from 0.16 crad when $I = I^0$ to 0.43 crad at 20 % of the rated value. From a physical point of view, this happens due to the typical behavior of ferromagnetic materials at low flux density values, where i_m is less than proportional to λ_m and thus to the current i_1.

Experimental CT errors

In this section, the complex CT behavior is deeply investigated by means of a series of experimental tests. Also in this study, similarly to what previously shown in Section 3.1.1 for CT errors simulated from the Steinmetz model, the influence of the presence of harmonics is neglected and η and ψ can be considered as functions of the sole fundamental primary current magnitude I. Following this simplification, η and ψ (functions of the actual current I at 50 Hz) have been measured for three different types of Class 0.5 CTs operating at rated burden (i.e., 10 VA with 5 A nominal secondary current). All three CTs have been connected in order to have at the primary side $I^0 = 50$ A. It is worth underlining that the same behavior would have been observed in other configurations (what matters is I/I^0). For each CT type, two samples have been characterized in order to have an idea of the spread of their performances.

Tests have been carried out with the experimental set-up shown in Fig. 3.4. The primary winding of the CT is supplied trough an industrial power amplifier (i.e., AETechron 7548) that is connected to a transformer to increase the maximum current output capability. The CT under test has primary and secondary currents measured by means of calibrated coaxial shunts (100 A and

10 A nominal currents for primary and secondary, respectively). The voltage signals are too small for being properly acquired and, thus, their outputs have been connected to calibrated high-linearity Analog Devices AD215BY isolation amplifiers. A PC connected to a National Instruments NI USB-6356 board with 16 bit resolution (adjustable analog input range, synchronized acquisition and generation capability) manages the aspects of signal generation, data acquisition and processing.

Tests have been carried out applying sinusoidal currents to the primary winding of the CT under test, ranging from $0.2\,I^0$ to $1.2\,I^0$ with steps of $0.05\,I^0$. Primary and secondary steady-state current waveforms $i(t)$ and $i''(t)$ have been acquired considering 100 periods and 200 kHz rate. In this case, due to the synchronized acquisition and generation, phasors components can be extracted without spectral leakage phenomena (the impact of noise is mitigated by means of the averaging process over the acquired 100 periods [88]). The trends of ratio and phase errors, functions of I/I^0, have been obtained and they are shown in Fig. 3.5 and in Fig. 3.6, respectively. The noise standard deviations of the obtained error curves have been quantified and, due to the low values, neglected.

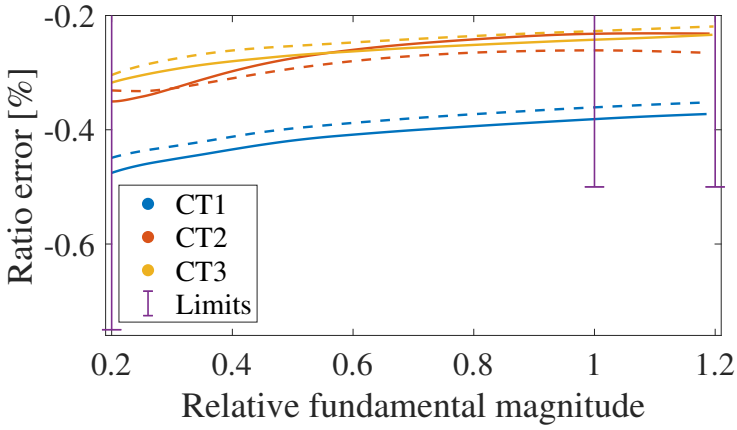

Figure 3.5: Ratio error as a function of I/I^0 for the tested CTs.

Ratio and phase errors are obtained by means of interpolation between experimental values using smoothing spline. In Fig. 3.5 and Fig. 3.6, solid and dashed line of the same color denote the two samples of the same CT type and, despite the fact that there are some differences, the trends are the same. The results show that the obtained errors are in line with the limits of the standard [60]. In particular, focusing on the ratio errors $\eta(I/I^0)$, it is possible to see that they are all negatively biased (similarly to the trends of Fig. 3.2) and, in general, they show limited variations over the investigated current range (about 0.1 %).

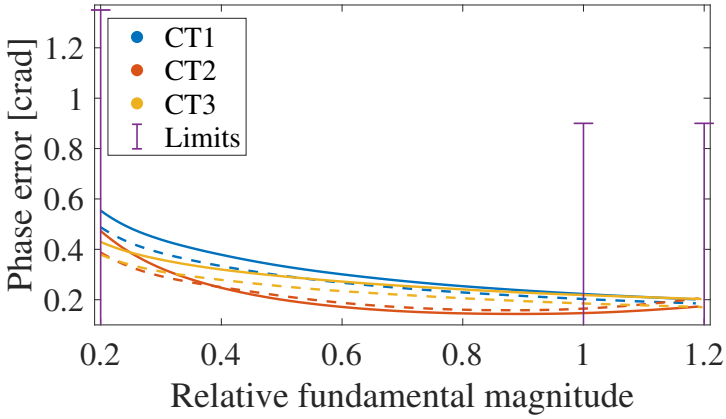

Figure 3.6: Phase error as a function of I/I^0 for the tested CTs.

The trends for $\psi(I/I^0)$ reveal smallest errors near the rated current in the range between 0.14 and 0.22 crad and, as expected, an almost monotonic increase in the lowest region of the measurement range: between 0.38 and 0.56 crad at 20 % of the rated current value.

In principle, on one hand, if one knew the functions of the errors $\eta(I/I^0)$ and $\psi(I/I^0)$, it would be possible to compensate the systematic contributions of CTs. On the other hand, this demands for a time-consuming and expensive individual characterization of all the CTs installed in the grid, which should be also kept continuously updated.

3.1.2 Impact of current transformer errors on parameter estimation

To investigate the impact of realistic CT errors on the proposed estimation method, tests have been first carried out by means simulations, in MATLAB environment, on a modified and reduced version of the 95 nodes UKGDS system [89] shown in Fig. 3.7 (with a base impedance $Z_\mathrm{b} = 1.21\,\Omega$). The grid has been modified by considering the active and reactive powers on node 9 as the equivalent of the entire network downstream of the node itself. In particular, the single-phase test network summarized in Table 3.1 has been modeled (see for details Appendix II). In addition to the series line parameters also the transversal shunt susceptance parameters have been considered, using typical *per length* capacitance values for Distribution System (DS) lines.

The tests have been carried out considering different operating conditions to test the performance of the method with different load levels (i.e., different values of CT errors). In particular, for each of the CTs installed in the grid,

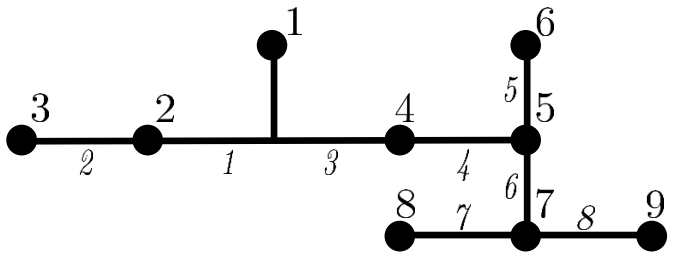

Figure 3.7: Modified version of the 95 UKGDS system.

Table 3.1: Nominal linedata values

Branch	$R^0_{i,j}$ **[pu]**	$X^0_{i,j}$ **[pu]**	$B^0_{sh,i,j}$ **[pu]**
1	0.055	0.057	0.000073
2	0.039	0.10	0.000052
3	0.049	0.051	0.000065
4	0.098	0.33	0.00013
5	0.17	0.076	0.00023
6	0.21	0.20	0.00028
7	0.24	0.11	0.00032
8	0.26	0.18	0.00035

the rated current I^0 has been chosen from the typical primary current ratings of CTs for DSs, assuming a nominal load profile (henceforth named "Nominal") that has led the choice of the CTs. In the tests, to have a comprehensive view of the reachable estimation performance under different operating conditions, a distributed generation (DG) plant has been assumed installed in node 9, defining two base cases "High Load" and "Low Load". The first one is the scenario where the DG is off and, in each branch, it is possible to see $I^R/I^0 > 70\,\%$, while the second one represents a scenario where the DG is on (up to 60 % of the load in node 9) and some branches belonging to the main feeder have currents $\leq 40\,\%$ of the rated current.

Each test involves $N_{\mathrm{MC}} = 5000$ and the estimation model is based on a number of PMU measurements $N_t = 10 \cdot C$ (with $C \in \{10, 200\}$). The following assumptions have been applied:

- $R_{i,j}$, $X_{i,j}$, and $B_{\mathrm{sh},i,j}$ vary in the range of $\pm 15\,\%$ across N_{MC} trials.
- ITs belong to Class 0.5. CT errors are extracted according to simulated CT

errors in Fig. 3.2 and Fig. 3.3 of Section 3.1.1, considering the class limits at different levels of current magnitude. Two maximum scaling factors ν_{mag} and ν_{ph} for amplitude and phase-angle, respectively, are chosen in order to amplify the error curves without violating class prescriptions. Then, for each of the N_{MC} trials, two uniform random variables μ_{mag} and $\mu_{\text{ph}} \in [-1, 1]$ are extracted. Thus, for a given timestamp and current $i_{i,j}^R$ having magnitude $I_{i,j}^R$ the resulting systematic errors are:

$$\eta_{i,j}^{\text{sys}} = \mu_{\text{mag}}\nu_{\text{mag}}\,\eta\left(\frac{I_{i,j}^R}{I^0}\right) \tag{3.1}$$

$$\psi_{i,j}^{\text{sys}} = \mu_{\text{ph}}\nu_{\text{ph}}\,\psi\left(\frac{I_{i,j}^R}{I^0}\right) \tag{3.2}$$

- Three PMU accuracy levels are used: "PMU01" , "PMU02" and the last one is "TVE1", which has maximum errors of 0.707 % and 0.707 crad, leading to the maximum Total Vector Error (TVE) of 1 %.

- Load and generator powers have been scattered within ±10 % among the C different cases of each MC trial.

Figures 3.8 and 3.9 show the test results for PMU01 and $C = 200$, for the line parameters of all the branches of the grid in Fig. 3.7 under Low Load and High Load scenarios, respectively.

It is possible to underline that, the RMSE values for series line parameters γ and β in the Low Load scenario are higher than High Load case and, among them, branches 4, 6, and 8 (which are the branches on the main feeder) have the lowest errors. In particular, although the estimates for the branches $4, 6$ and 8 are better than other branches in both scenarios, moving from High Load to Low Load scenario, a degradation of the estimates occurs. This behavior can be explained by the fact that lower power-flows lead to lower voltage drops and, thus, the errors affecting the measurement chain have higher impact. Focusing on δ estimation results, it is possible to observe a different behavior: the RMSEs are, in some branches, larger than prior values (in this case $15/\sqrt{3} = 8.66\,\%$) especially for branches 4, 6, and 8. This behavior is more pronounced in Low Load scenario where higher and dispersed CT phase displacements errors are involved (as can be seen in Fig. 3.2 and Fig. 3.3). As a further demonstration of the above mentioned behaviors, other tests have been carried out in both Low Load and High Load conditions, assuming CT errors as in [54], [68] (i.e., maximum errors corresponding to the class limits at rated current for every load condition). Tests have demonstrated that γ and β estimation results do not depend significantly on the used CT model, since very close results have been found. Shunt susceptance, instead, is mainly estimated thanks to the current balance

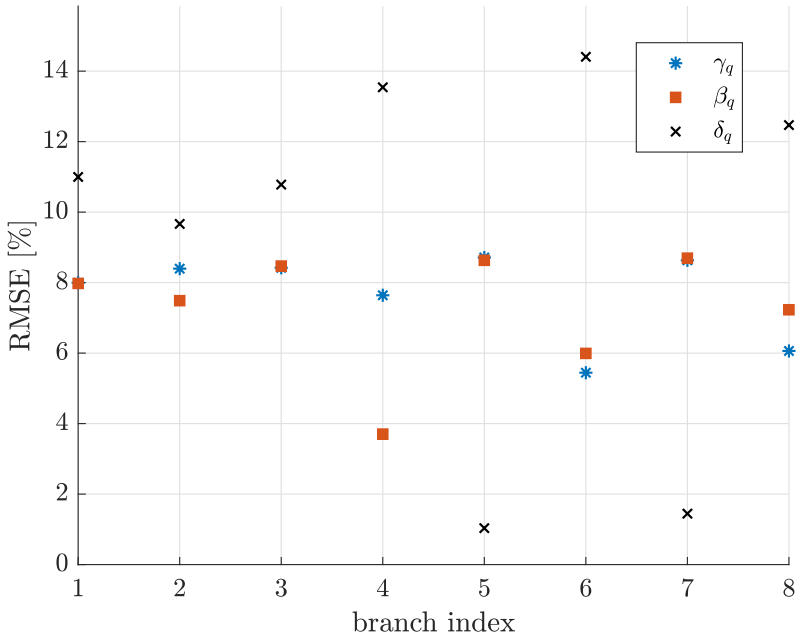

Figure 3.8: Estimation results for Low Load condition (PMU01 and $C = 200$).

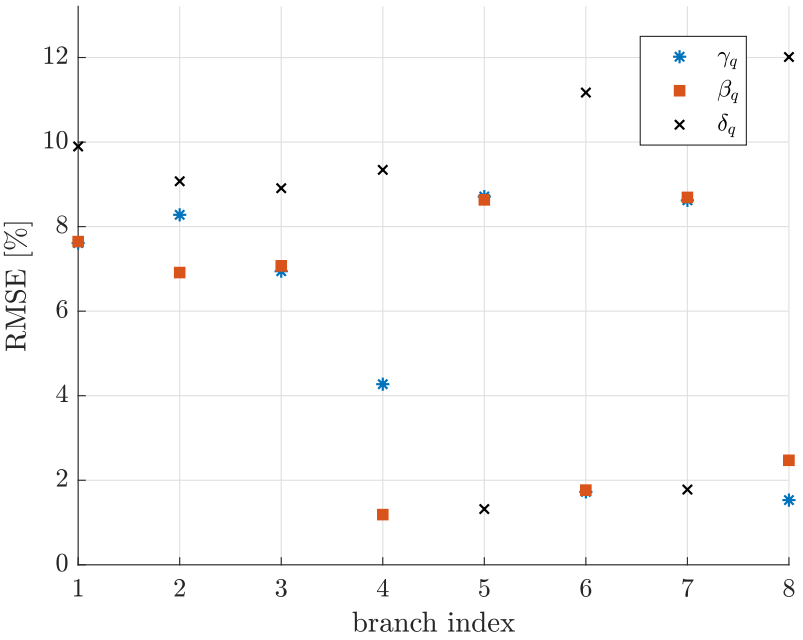

Figure 3.9: Estimation results for High Load condition (PMU01 and $C = 200$).

Table 3.2: Comparison of different network and measurement configurations

PMU accuracy	**Load condition**	C	**RMSE**							
			γ_4 [%]	β_4 [%]	δ_4 [%]	γ_8 [%]	β_8 [%]	δ_8 [%]	δ_5 [%]	δ_7 [%]
PMU01	Low Load	10	8.30	6.42	10.04	7.89	8.33	10.57	1.12	1.56
		200	7.64	3.70	13.54	6.06	7.23	12.47	1.03	1.45
	High Load	10	6.57	2.90	8.77	4.28	5.58	9.46	1.42	1.94
		200	4.27	1.19	9.34	1.53	2.47	12.01	1.32	1.78
PMU02	Low Load	10	8.50	7.66	8.68	8.44	8.61	8.58	1.30	1.80
		200	8.29	5.89	8.93	7.71	8.24	8.80	1.08	1.49
	High Load	10	7.63	4.30	8.63	6.09	7.20	8.63	1.65	2.26
		200	6.28	2.21	8.64	3.45	4.93	8.80	1.36	1.82
TVE1	Low Load	10	8.58	8.30	8.59	8.63	8.69	8.40	1.72	2.23
		200	8.57	8.00	8.58	8.54	8.66	8.32	1.39	1.79
	High Load	10	8.20	5.86	8.63	7.52	8.15	8.62	2.07	2.73
		200	8.02	5.02	8.63	6.85	7.76	8.63	1.66	2.13

constraint and its estimation accuracy is a fingerprint of CT mismatch with respect to the assumptions of the method. In particular, CT errors are not constant across multiple cases and this can jeopardize δ estimation. Indeed, δ RMSEs for branches 4, 6, and 8 in Fig. 3.8 and Fig. 3.9 are far beyond the prior values, while this phenomenon is not observed when the simpler CT error model is applied.

Finally, Table 3.2 shows a summary of the estimation results (γ_q, β_q and δ_q are the deviations for resistance, reactance and susceptance for the generic branch with index q, respectively) varying load conditions and test assumptions (i.e., PMU accuracy level and C). The results confirm, basically, the previous conclusions but, in addition, it is possible to observe that when the PMU accuracy gets worse, δ_4 and δ_8 RMSEs decrease. This can be explained by the fact that the degradation of PMU performance and thus the presence of higher errors masks the mismatch due to non-constant CT errors across the C cases. A further confirmation of this behavior can be seen moving from $C = 10$ to $C = 200$, where δ_4 and δ_8 estimation accuracy worsens whereas other parameters improve. For instance, considering PMU01, the improvement in γ_8 estimation between Low Load and High Load condition varies from 48 % for $C = 10$ to 75 % for $C = 200$.

The reported results show that a degradation of the estimation performance with respect to the ideal case of constant CT systematic errors is unavoidable in practice, particularly when load variability and lightly loaded branches are

involved. For this reason, in the following section, a proposal to enhance the estimation method presented in Chapter 2 is introduced.

3.1.3 Integration of a more complex CT model: Proposed solution

The method described in Sections 2.1.3 and 2.2.3 does not consider possible variations, across different timestamps, of current ratio and phase systematic errors (i.e., it assumes constant systematic errors). If N_t timestamps (C cases and M repeated measurements of each case) are considered, the estimation problem deals with different load conditions and, thus, CT errors depend on I/I^0 leading to nonlinear functions for systematic errors $\eta^{\text{sys}} = \eta(I/I^0)$ and $\psi^{\text{sys}} = \psi(I/I^0)$. In this regard, the proposal is to change the measurement model in order to follow the possible variations of the systematic errors and reflect the actual complex behavior of the CT. Equation (2.1) for $i_{i,j}$ (same model can be applied for $i_{j,i}$) changes as follows:

$$i_{i,j} = I_{i,j}e^{j\theta_{i,j}} = (1 + \eta^{\text{sys}}_{i,j}(I_{i,j}/I^0_{i,j}) + \eta^{\text{rnd}}_{i,j})I^R_{i,j}e^{j(\theta^R_{i,j}+\psi^{\text{sys}}_{i,j}(I_{i,j}/I^0_{i,j})+\psi^{\text{rnd}}_{i,j})} \quad (3.3)$$

In (3.3), $I^0_{i,j}$ is the rated current for the CT used to measure $i_{i,j}$, while $\eta^{\text{sys}}_{i,j}()$ and $\psi^{\text{sys}}_{i,j}()$ are the ratio and phase error functions and, with the same approximations and linearizations of Section 2.1.3, it is possible to define:

$$i^R_{i,j} = I^R_{i,j}e^{j\theta^R_{i,j}} \simeq I_{i,j}e^{j\theta_{i,j}}\left[1 - \eta^{\text{sys}}_{i,j}(I_{i,j}/I^0_{i,j}) - \eta^{\text{rnd}}_{i,j} - j\psi^{\text{sys}}_{i,j}(I_{i,j}/I^0_{i,j}) - j\psi^{\text{rnd}}_{i,j}\right] \quad (3.4)$$

To include the model of systematic CT errors in the estimation model, it is necessary to generalize the representation of the errors. It is would be thus useful to include a parametric representations for the generic functions $\eta^{\text{sys}}_{i,j}()$ and $\psi^{\text{sys}}_{i,j}()$.

The inclusion of additional unknowns in the state vector would permit accurately tracking the actual trends, but this choice significantly decreases the constraints/unknowns ratio. Furthermore, more parameters in the estimation problem can lead to an overfit of the problem and, at the end, undermine the robustness of the estimates. For the above defined reasons and as a compromise solution, it has been proposed to approximate $\eta^{\text{sys}}_{i,j}()$ and $\psi^{\text{sys}}_{i,j}()$ as piece-wise linear functions, defined by just two parameters each.

In particular, for each of the N_t timestamps it is possible to define the approximated error model (indicated with $\tilde{}$):

$$\tilde{\eta}^{\text{sys}}_{i,j}\left(\frac{I_{i,j,t}}{I^0_{i,j}}\right) =$$

$$\begin{cases} \eta_{i,j,\bar{\kappa}_{i,j}}\% + m_{\eta,i,j}\left(\frac{\bar{\kappa}_{i,j}}{100} - \frac{I_{i,j,t}}{I^0_{i,j}}\right) & \text{if } \frac{\underline{\kappa}_{i,j}}{100} I^0_{i,j} < I_{i,j,t} < \frac{\bar{\kappa}_{i,j}}{100} I^0_{i,j} \\ \eta_{i,j,\bar{\kappa}_{i,j}}\% & \text{if } I_{i,j,t} \geq \frac{\bar{\kappa}_{i,j}}{100} I^0_{i,j} \end{cases} \tag{3.5}$$

$$\tilde{\psi}^{\text{sys}}_{i,j}\left(\frac{I_{i,j,t}}{I^0_{i,j}}\right) =$$

$$\begin{cases} \psi_{i,j,\bar{\lambda}_{i,j}}\% + m_{\psi,i,j}\left(\frac{\bar{\lambda}_{i,j}}{100} - \frac{I_{i,j,t}}{I^0_{i,j}}\right) & \text{if } \frac{\underline{\lambda}_{i,j}}{100} I^0_{i,j} < I_{i,j,t} < \frac{\bar{\lambda}_{i,j}}{100} I^0_{i,j} \\ \psi_{i,j,\bar{\lambda}_{i,j}}\% & \text{if } I_{i,j,t} \geq \frac{\bar{\lambda}_{i,j}}{100} I^0_{i,j} \end{cases} \tag{3.6}$$

where the ratio error $\eta_{i,j,\bar{\kappa}_{i,j}}\%$ and phase-angle error $\psi_{i,j,\bar{\lambda}_{i,j}}\%$ are the errors of the considered CT at $\bar{\kappa}_{i,j}\%$ and $\bar{\lambda}_{i,j}\%$ of the rated current, respectively. The proposed CT model is thus composed of two regions:

- as for low currents, $\underline{\kappa}_{i,j}/100$ is the lowest considered current ratio for magnitude errors ($\underline{\lambda}_{i,j}/100$ is that associated with phase displacement) and there is a linear trend with slope $m_{\eta,i,j}$ ($m_{\psi,i,j}$ for phase displacement).
- as for high currents, the errors are constant (defined by an horizontal line) starting from the function knee at current ratio $\bar{\kappa}_{i,j}/100$ (or $\bar{\lambda}_{i,j}/100$).

Then, replacing (3.5) and (3.6) into (3.4) and following the same approach and the same steps discussed in Section 2.1.3 for the single-phase version of the algorithm, it is possible to define a new state vector $\mathbf{x}'_{i,j}$ as:

$$\mathbf{x}'_{i,j} = \begin{bmatrix} \xi^{\text{sys}}_i \\ \alpha^{\text{sys}}_i \\ \xi^{\text{sys}}_j \\ \alpha^{\text{sys}}_j \\ \eta_{i,j,\bar{\kappa}_{i,j}}\% \\ m_{\eta,i,j} \\ \psi_{i,j,\bar{\lambda}_{i,j}}\% \\ m_{\psi,i,j} \\ \eta_{j,i,\bar{\kappa}_{j,i}}\% \\ m_{\eta,j,i} \\ \psi_{j,i,\bar{\lambda}_{j,i}}\% \\ m_{\psi,j,i} \\ \gamma_{i,j} \\ \beta_{i,j} \\ \delta_{i,j} \end{bmatrix} \tag{3.7}$$

In (3.7), two additional unknowns are included for each current measurement, allowing to manage the non constant CT errors across multiple cases. State vector $\mathbf{x}'_{i,j}$ can be estimated in WLS sense, similarly to (2.23).

If the inclusion of additional unknowns in the state vector is easily obtained, more complex is instead the definition and treatment of prior information for these additional unknowns. All the unknowns can be assumed to be zero with a given level of uncertainty and, if the new variables $m_{\eta,i,j}$ and $m_{\psi,i,j}$ are supposed to be zero, it means that prior errors are considered constant. Prior standard deviation of $\eta_{i,j,\bar{\kappa}_{i,j}}\%$ can be obtained from CT class specifications (in the tests $\bar{\kappa}_{i,j} = 100$ is considered for all considered branches). Thus, this means that, assuming uniform prior distribution, prior standard deviation of $\eta_{i,j,\bar{\kappa}_{i,j}}\%$ is equal to the CT class divided by $\sqrt{3}$. Focusing instead on the slope parameter $m_{\eta,i,j}$, its range can be extracted for a given $\bar{\kappa}_{i,j}$ taking into account all the error curves that can be defined for every $\eta_{i,j,\bar{\kappa}_{i,j}}\%$. In fact, each of these curves is characterized by a slope value and, as a consequence, the prior is defined by the range spanned by this value. Also in this case, uniform distribution is assumed in the absence of additional information. A similar procedure is adopted for phase displacement, defining $\psi_{i,j,\bar{\lambda}_{i,j}}\%$ and $m_{\psi,i,j}$ prior standard deviations. It is important to recall that the prior uncertainty definition takes part in the weighing matrix, which helps only in narrowing the ranges of the unknowns possible values according to available prior information. Once prior information is defined, WLS estimation can be, for instance, used to find the estimated state vector $\hat{\mathbf{x}}'_{i,j}$, allowing then the definition of the systematic error associated with each CT considering all the timestamps $t_1, \ldots, t_{N_t}$ as follows:

$$\hat{\eta}^{\text{sys}}_{i,j} = \hat{\eta}_{i,j,\bar{\kappa}_{i,j}}\% + \hat{m}_{\eta,i,j}\left(\frac{\bar{\kappa}_{i,j}}{100} - \frac{I_{i,j,t_l}}{I^0_{i,j}}\right) \tag{3.8}$$

$$\hat{\psi}^{\text{sys}}_{i,j} = \hat{\psi}_{i,j,\bar{\lambda}_{i,j}}\% + \hat{m}_{\psi,i,j}\left(\frac{\bar{\lambda}_{i,j}}{100} - \frac{I_{i,j,t_l}}{I^0_{i,j}}\right) \tag{3.9}$$

The above defined model will be named DynCTlin in the following tests. Another possibility could be the use, instead of a piece-wise linearization, of a nonlinear approximation of the error functions that is based on the same number of unknowns as:

$$\tilde{\eta}^{\text{sys}}_{i,j}\left(\frac{I_{i,j,t}}{I^0_{i,j}}\right) = \begin{cases} \eta_{i,j,\bar{\kappa}_{i,j}}\% + m_{\eta,i,j}\left(\frac{\bar{\kappa}_{i,j}}{100} - \frac{I_{i,j,t}}{I^0_{i,j}}\right)^{\chi} & \text{if } \frac{\kappa_{i,j}}{100} I^0_{i,j} < I_{i,j,t} < \frac{\bar{\kappa}_{i,j}}{100} I^0_{i,j} \\ \eta_{i,j,\bar{\kappa}_{i,j}}\% \quad \text{if } I_{i,j,t} \geq \frac{\bar{\kappa}_{i,j}}{100} I^0_{i,j} \end{cases} \tag{3.10}$$

$$\tilde{\psi}^{\text{sys}}_{i,j}\left(\frac{I_{i,j,t}}{I^0_{i,j}}\right) = \begin{cases} \psi_{i,j,\bar{\lambda}_{i,j}}\% + m_{\psi,i,j}\left(\frac{\bar{\lambda}_{i,j}}{100} - \frac{I_{i,j,t}}{I^0_{i,j}}\right)^{\chi} & \text{if } \frac{\lambda_{i,j}}{100} I^0_{i,j} < I_{i,j,t} < \frac{\bar{\lambda}_{i,j}}{100} I^0_{i,j} \\ \psi_{i,j,\bar{\lambda}_{i,j}}\% \quad \text{if } I_{i,j,t} \geq \frac{\bar{\lambda}_{i,j}}{100} I^0_{i,j} \end{cases} \tag{3.11}$$

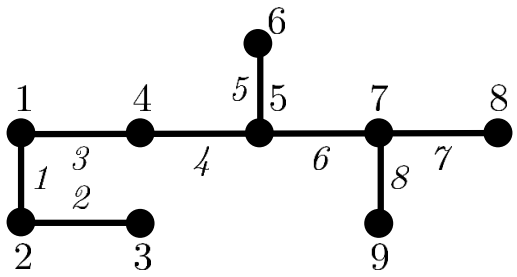

Figure 3.10: Topology of the 15 kV test network.

In (3.10) and (3.11), a possible choice of the additional parameter χ is 2 and the corresponding model will be named DynCTsquare. All the steps described for DynCTlin can be done also for DynCTsquare with the definition of a new measurement model and a new weighing matrix.

3.1.4 Improved method estimation performance

To assess the validity and the performance of the enhanced method presented in the previous section, tests have been carried out using the 15 kV test network shown in Fig. 3.10 (node and branch indices are reported), which is a portion of a larger distribution network (see, for details, Appendix III).

The same assumptions about the DG generation plant and the test set-up of Section 3.1.2 have been considered, with the only difference that the CT errors are obtained by means of the experimental tests shown in Section 3.1.1. The first series of tests have been carried out comparing the estimation results for magnitude and phase CT errors obtained with the method in [84] (named as "Static") and the methods DynCTlin and DynCTsquare proposed in [85]. To do that, Fig. 3.11 and Fig. 3.12 show the η^{sys} and ψ^{sys} estimation results, considering CT1 of Fig. 3.5 and Fig. 3.6, for Static, DynCTlin and DynCTsquare methods, indicated with red, blue and black colors, respectively. The estimation results have been compared with or without the inclusion in the estimation problem of the ZI constraints equations (2.31). From the figures, it is possible to emphasize two aspects:

- DynCTlin and DynCTsquare improve the results of Static for both magnitude and phase-angle errors and this permits concluding that the refined modeling of CT systematic errors (which takes into account the CT complex behavior) leads to estimate these errors more accurately.
- The inclusion of ZI constraints halved, for all the three considered methods, the estimation RMSEs with respect to those without these additional

constraints.

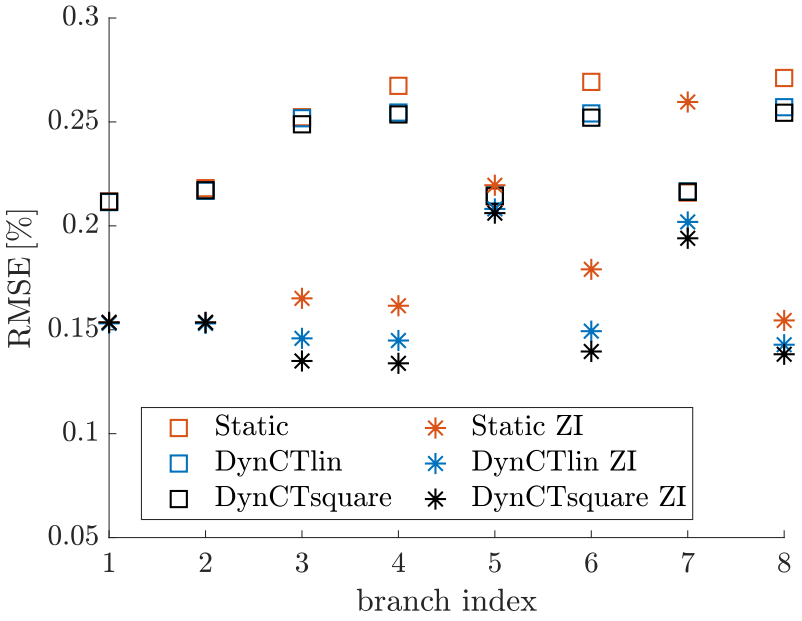

Figure 3.11: Comparison of η^{sys} estimation results (PMU01 and $C = 200$).

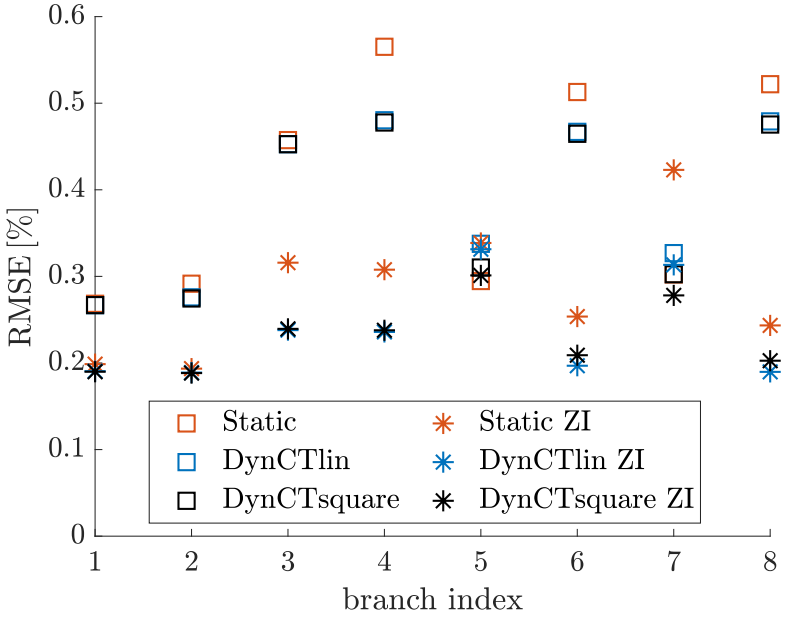

Figure 3.12: Comparison of ψ^{sys} estimation results (PMU01 and $C = 200$).

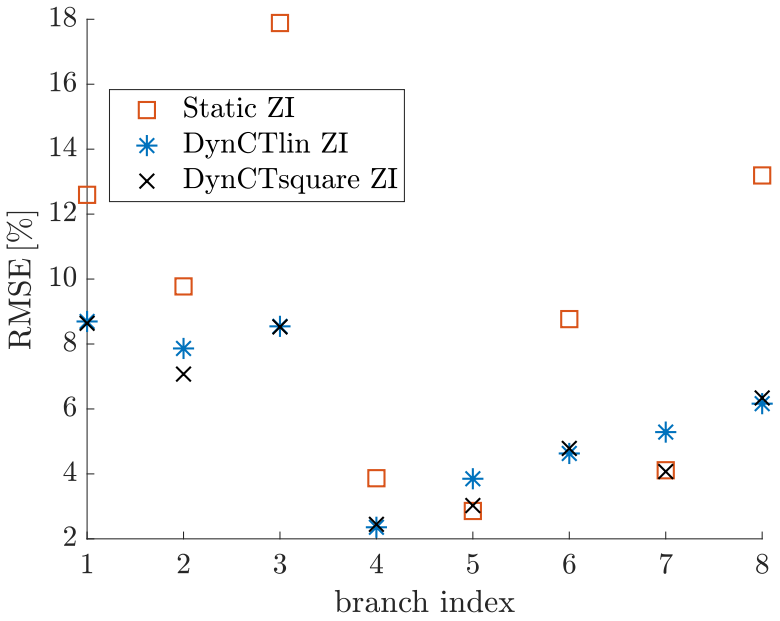

Figure 3.13: Comparison of δ estimation results (PMU01 and $C = 200$).

Further tests have been carried out to evaluate the improvements that can be achieved on the main target of the proposed estimation method, i.e. the estimation of line parameters. In particular, from the results of Section 3.1.2, it was already clear that the most relevant impact should be on the transversal susceptance estimation. In this regard, Fig. 3.13 shows δ estimates (with CT1 errors) obtained introducing ZI constraints. These errors must be compared with the prior standard deviations of these parameters (i.e., also in this case, equal to $15/\sqrt{3} = 8.66\,\%$).

An important consideration that can be drawn from the results in Fig. 3.13 is that, the Static method (indicated with red squares) has RMSEs for branches 1, 2, 3, and 8 higher than prior errors, while DynCTlin and DynCTsquare (indicated with blue stars and black cross, respectively) allow reaching RMSEs lower than the corresponding prior standard deviation. In particular, among all the branches of the grid, branch 8 has an improvement of about 29 % with respect to the prior standard deviation and the maximum improvement is of about 72 % for branch 4. As a general comment, it is possible to see that all δ estimations have better results than those of Section 3.1.2. Other tests have been carried out to show the impact of the PMU accuracy level on the estimation performance. To illustrate that, Table 3.3 shows γ and β estimation results with CT1 and both PMU01 and PMU02. These results confirm the conclusions of Section 3.1.2 and, in particular, that the longitudinal parameters do not suffer

Table 3.3: Comparison of γ and β estimations

Method	**PMU Accuracy**	**RMSE [%]**					
		$\gamma_{4,5}$ [%]	$\beta_{4,5}$ [%]	$\gamma_{5,7}$ [%]	$\beta_{5,7}$ [%]	$\gamma_{7,9}$ [%]	$\beta_{7,9}$ [%]
Static	PMU01	7.70	3.85	5.60	6.16	6.23	7.35
	PMU02	8.31	6.04	7.33	7.6	7.79	8.29
DynCTlin	PMU01	7.59	3.62	5.34	5.91	5.96	7.16
DynCTsquare	PMU02	8.27	5.79	7.17	7.52	7.67	8.22

from the presence of CT errors not constant across multiple cases. Proposed methods DynCTlin and DynCTsquare have identical RMSE performance, while Static method has slightly worse results. Finally, as expected, moving from PMU01 to PMU02, RMSEs degrade but remain below prior standard deviations of γ and β in all the tests.

Final tests have been carried out to summarize the results of the proposed estimation approach by means of a comprehensive analysis. Table 3.4 shows the results for CT errors (indicated with the pair of indices $_{i,j}$) and δ estimation, varying the PMU accuracies and using all the three CT types presented in Section 3.1.1 (i.e., dashed line CT1, dashed line CT2 and solid line CT3 in Figs. 3.5 and 3.6). As a further confirmation, the complex behavior of CTs has a negative impact on the Static approach. The proposed dynamic methods DynCTlin and DynCTsquare overcome the problem reaching good estimation results with slight differences between them. This can be explained by the fact that they give different approximations of the CT model in the estimation framework. In particular, for CT1 and CT3, DynCTlin is better than DynCTsquare, while the latter is marginally better when CT2 is considered. This behavior can be analyzed observing Fig. 3.6 in the lowest part of the measurement range (the region where I/I^0 is lower) where the error function of CT2 appears steeper than CT1 and CT3 and thus it is better matched with a nonlinear representation. Focusing on CT estimation results, as expected, the impact of CTs is larger on ψ^{sys} than η^{sys} due to the wider variation of the phase error function with respect to the ratio error function. As for the results, it is possible to highlight that for both PMU01 and PMU02, the RMSE values are more than halved with respect to the prior standard deviations associated with the actual operating conditions (i.e., the actual current ratio) corresponding to a specific region of the measurement range. Also in this case, the results of the adaptive methods DynCTlin and DynCTsquare are always equal or better than Static.

Table 3.4: Performance comparison in the presence of different PMU and CT configurations

CT	PMU	Method	RMSE					
			$\delta_{4,5}$ [%]	$\eta^{sys}_{4,5}$ [%]	$\psi^{sys}_{4,5}$ [crad]	$\delta_{7,9}$ [%]	$\eta^{sys}_{7,9}$ [%]	$\psi^{sys}_{7,9}$ [crad]
CT1	PMU01	Static	3.87	0.16	0.31	13.19	0.15	0.24
		DynCTlin	2.36	0.14	0.24	6.16	0.14	0.19
		DynCTsquare	2.45	0.13	0.24	6.34	0.14	0.20
	PMU02	Static	3.67	0.15	0.27	9.69	0.15	0.24
		DynCTlin	2.65	0.15	0.25	6.86	0.15	0.21
		DynCTsquare	2.79	0.14	0.25	6.96	0.15	0.22
CT2	PMU01	Static	4.49	0.18	0.34	15.28	0.16	0.26
		DynCTlin	2.89	0.16	0.25	6.95	0.15	0.19
		DynCTsquare	2.83	0.14	0.24	6.67	0.14	0.20
	PMU02	Static	4.17	0.16	0.28	10.74	0.16	0.24
		DynCTlin	3.15	0.16	0.26	7.33	0.16	0.21
		DynCTsquare	3.14	0.15	0.25	7.18	0.15	0.22
CT3	PMU01	Static	3.27	0.15	0.29	11.17	0.15	0.24
		DynCTlin	1.84	0.14	0.23	5.52	0.14	0.19
		DynCTsquare	2.15	0.13	0.24	6.13	0.14	0.21
	PMU02	Static	3.23	0.15	0.27	8.79	0.15	0.25
		DynCTlin	2.20	0.14	0.24	6.50	0.16	0.22
		DynCTsquare	2.53	0.14	0.25	6.82	0.15	0.23

3.2 Realistic model of PMU errors

From all the previous discussions, it is evident that the sources of uncertainty of the measurement chain must be properly taken into account to understand their impact on line parameters estimation methods and exploit their characteristics in the estimation process. In this context, the methods presented in Chapter 2 aim at reducing the impact of systematic measurement errors ([53], [68]) and at dealing with an estimation process over multiple branches at the same time that uses measurements corresponding to different operating conditions of the network [54]. It is worth recalling that the methods shown in Section 2.1.3 and Section 2.2.3 rely on the definition of a measurement model that considers random errors related to PMUs and systematic errors to ITs. Both errors are assumed to be independent.

Then, while Section 3.1 has presented a refined model for CTs, in this section the main purpose is to discuss how the PMU error model can be framed in a more general and realistic way. In this regard, systematic errors associated with PMUs have been considered and investigated in [90] and their impact on the

simultaneous estimation of systematic measurement errors and line parameters has been evaluated. Then, another aspect that can affect the PMU behavior has been investigated: different channels of the same PMU can share a common error in phase-angle measurements since they share the time-base [91]. An enhanced version of the algorithm of Section 2.1.3, where correlation of phase-angle errors is included in real-time in the estimation model, is thus introduced in the next section.

PMU errors

Considering a branch (i, j), the error covariance matrix $\mathbf{\Sigma}_{\boldsymbol{\epsilon}_{i,j,\text{tot}}}$ used in the estimation algorithm (see (2.21) and (2.66)) is built assuming prior information about the unknown parameters and random error of PMU measurements, which, in absence of specific information, are supposed uncorrelated. In particular, considering the matrix of prior variances $\Sigma_{\mathbf{e}_{\text{prior}}}$, two considerations can be made:

- As for line parameters, prior variances $\sigma^2_{\gamma_{iq,jq}}$, $\sigma^2_{\beta_{iq,jq}}$ and $\sigma^2_{\delta_{iq,jq}}$ (with $q = 1, \ldots, N_{\text{br}}$ that represents the index of the branch) are chosen based on considerations on the uncertainty of line parameters and are assumed uncorrelated. It is worth underlining that, if further information is available, it can be seamlessly integrated in the estimation model. A mismatch between actual uncertainty and assumed values can occur and in Section 3.4 such issue is investigated [92]).

- Systematic errors are considered uncorrelated and, similarly to line parameters, if any prior knowledge is available it can be easily added in the estimation model.

Considering instead the first matrix $\mathbf{\Sigma}_{\boldsymbol{\epsilon}_{i,j}}$ in the diagonal of the covariance matrix $\mathbf{\Sigma}_{\boldsymbol{\epsilon}_{i,j,\text{tot}}}$ (see (2.21)), it represents the covariance matrix of random measurement errors, which in Sections 2.1.4 and 2.2.4 have been considered as uncorrelated and related to PMU uncertainty. Despite the fact that, in absence of specific information, the assumption of considering uncorrelated PMU random errors is the only possible choice, PMU errors in a realistic scenario can be actually composed of both systematic and random errors. The presence of systematic errors of PMUs would result in a transfer of uncertainty from the random error covariance matrix $\mathbf{\Sigma}_{\boldsymbol{\epsilon}_{i,j}}$ to the matrix of prior variances $\Sigma_{\mathbf{e}_{\text{prior}}}$.

In general, if the assumption of having both systematic and random error contributions [90] is reasonably valid for magnitude PMU errors, phase-angle PMU errors should be treated more carefully. In this context, a more detailed PMU error model of phase-angle error is considered and, called λ^{PMU} a generic phase-angle error of a PMU installed at node i, the expression of the error is

defined as:

$$\lambda^{\mathrm{PMU}} = \lambda_s + \lambda_c + \lambda_r \tag{3.12}$$

In (3.12), λ_s is the systematic error contribution brought by the PMU (i.e., the average of the phase-angle error), λ_c is the common phase-angle error related to the specific PMU and, thus, shared among all the channels of the same PMU, and λ_r is the random error contribution independent from other errors and specific of the considered PMU channel. Equation (3.12) is a realistic representation of the phase-angle error of a PMU. In fact, phase-angle error, particularly for high-quality instruments, is strongly related to the time-base error [77], which is often reported in PMU datasheet. Such error is common to all the channels of the same PMU and cannot be neglected. The variance $\sigma^2_{\lambda^{\mathrm{PMU}}}$ of the PMU phase-angle error λ^{PMU} can be obtained by the sum of the two random error contributions (λ_c and λ_r, which can be assumed uncorrelated). In particular, considering two phase-angle measurements of two generic channels (1 and 2) of the same PMU, the corresponding phase-angle errors λ_1^{PMU} and λ_2^{PMU} can be defined and their covariance can be written by means of the expectation operator $\mathrm{E}[\cdot]$ as:

$$\begin{aligned} &\mathrm{E}\left[\left(\lambda_1^{\mathrm{PMU}} - \mathrm{E}\left[\lambda_1^{\mathrm{PMU}}\right]\right)\left(\lambda_2^{\mathrm{PMU}} - \mathrm{E}\left[\lambda_2^{\mathrm{PMU}}\right]\right)\right] = \\ &\qquad = \mathrm{E}\left[\left(\lambda_c + \lambda_{r1}\right)\left(\lambda_c + \lambda_{r2}\right)\right] = \mathrm{E}\left[\lambda_c^2\right] = \sigma_c^2 \end{aligned} \tag{3.13}$$

where the two independent random contribution λ_{r1} and λ_{r2} are related to the first and second channel, respectively. The final expression is obtained exploiting the null correlation between the common error and the random contributions. From (3.13), the covariance between the two channels depends on the variance σ_c^2 of λ_c. It is worth highlighting that, differently from the assumptions made in Section 2.1.3 and Section 2.2.3, if a more realistic representation of PMU phase-angle errors is used, correlation arises in the measurement model.

3.2.1 Method proposed to deal with correlation in phase-angle measurements

Following from above considerations, the assumption presented in this section is to associate each PMU i installed at node i with a correlation coefficient between its channels (for phase-angle errors). The correlation is thus described through Pearson correlation coefficient, which is added in the covariance matrix of PMU random errors. Considering $\sigma_{\lambda_1^{\mathrm{PMU}}}$ and $\sigma_{\lambda_2^{\mathrm{PMU}}}$, the standard deviations of the errors in the two channels, the Pearson correlation coefficient ρ_{12} (an index that is not known in advance and, thus, it needs to be estimated) depends on the ratio of σ_c^2 to $\sigma_{\lambda_1^{\mathrm{PMU}}}\sigma_{\lambda_2^{\mathrm{PMU}}}$.

The estimation, as already mentioned, is built based on N_t timestamps (with

$N_t = M \cdot C$) that correspond to different load conditions or repeated measurements of the same operating condition. The generic timestamp t_n can be also indicated with $t_{\chi,m} = [(\chi-1)M+m-1]T_{\mathrm{RR}}$ with $m = 1,\ldots,M$ and $\chi = 1,\ldots,C$ (the procedure can be applied when $M > 1$). Then, for each case χ and each channel, the reference phase-angle is different and, to compute the correlation between the channels of the same PMU, a pre-processing of the measured values is needed.

Defining the average of the phase-angle measurements for the generic case χ of channel 1 as:

$$\nu_{1,t_{\chi,\bullet}} \triangleq \frac{\sum_{m=1}^{M} \nu_{1,t_{\chi,m}}}{M} \tag{3.14}$$

where $\nu_{1,t_{\chi,m}}$ is the mth measure, it is possible to make the measurements unbiased using (3.14) as follows:

$$\tilde{\lambda}_{c+r1,t_{\chi,m}} = \nu_{1,t_{\chi,m}} - \nu_{1,t_{\chi,\bullet}} \tag{3.15}$$

In (3.15), $\tilde{\lambda}_{c+r1,t_{\chi,m}}$ is an estimate of the overall random contribution at $t_{\chi,m}$ for channel 1 and, with similar definitions and computations, it is possible to find also $\tilde{\lambda}_{c+r2,t_{\chi,m}}$ for channel 2. Pearson correlation coefficient ρ_{12} can thus be estimated at run time as:

$$\hat{\rho}_{12} = \frac{\sum_{\chi=1}^{C}\sum_{m=1}^{M} \tilde{\lambda}_{\chi+r1,t_{\chi,m}} \cdot \tilde{\lambda}_{\chi+r2,t_{\chi,m}}}{\sqrt{\sum_{\chi=1}^{C}\sum_{m=1}^{M} \tilde{\lambda}^2_{\chi+r1,t_{\chi,m}} \cdot \sum_{\chi=1}^{C}\sum_{m=1}^{M} \tilde{\lambda}^2_{\chi+r2,t_{\chi,m}}}} \tag{3.16}$$

If all the channels of PMU i have the same accuracy, it is possible to define and consider a unique correlation coefficient $\hat{\rho}^{\mathrm{PMU}_i}$ as:

$$\hat{\rho}^{\mathrm{PMU}_i} = 2\frac{\sum_{ch_1=1}^{N_{\mathrm{ch},i}} \sum_{\mathrm{ch}_2=\mathrm{ch}_1+1}^{N_{\mathrm{ch},i}} \hat{\rho}_{\mathrm{ch}_1 ch_2}}{N_{\mathrm{ch},i}(N_{\mathrm{ch},i}-1)} \tag{3.17}$$

where the estimated correlation coefficient between two generic channels ch_1 and ch_2 is $\hat{\rho}_{\mathrm{ch}_1\mathrm{ch}_2}$ (for a generic PMU i with a number of channels $N_{\mathrm{ch},i}$). Thus, using (3.17) for all the PMUs considered, the covariance matrix of random errors can be modified by inserting the tailored coefficients and following the same steps as in Section 2.1.3 and Section 2.2.3.

It is worth underlining that, despite, in this context, the main source of correlation for the different channels of the same PMU is the synchronization process, other types of correlation can be similarly included in the estimation model.

3.2.2 Analysis of the performance of the proposed method

In this section, the results found using the realistic model of PMU errors above described are discussed. In this regard, the performance achieved with the proposed modification of the estimation model and an ad hoc treatment of the correlation is assessed through simulation, in MATLAB environment, on the single-phase version of the IEEE 14 bus test system (see Fig. 2.3). In particular, two set of branches have been considered:

- The high voltage portion of the network ("6 branches" configuration) .
- The whole network ("All branches" configuration).

To assess the performance of the proposed method, $N_t \in \{100, 1000\}$ measurement timestamps have been considered (i.e., $M = 10$ and $C \in \{10, 100\}$), in a MC simulation with $N_{\mathrm{MC}} = 5000$ trials. For each MC trial, maximum deviations of line parameters are assumed to be of $\pm 15\,\%$, while CTs and VTs belong to Class 0.5. The errors have been extracted from uniform distributions as well as loads and generators, which vary within $\pm 10\,\%$ among the C cases considered. In addition, the following assumptions have been considered for PMUs:

- PMUs follow the synchrophasor standard IEC/IEEE 60255-118-1:2018 [93] and maximum magnitude and phase-angle errors vary from "PMU01" to "TVE1"[1].
- The maximum errors of the considered PMUs are assumed as limits of confidence intervals with a probability > 0.97. In fact, differently from [90], here PMU phase-angle errors are described as in (3.12), whereas magnitude errors are split only into systematic and random contributions. In both cases, however, instead of splitting the maximum values, for sake of a fairer comparison of the different error model combinations, an approach based on variance splitting is used here. For the phase-angle errors, the total error variance derived from the information of the datasheets and thus including also the variability of systematic errors is divided as:

$$\sigma^2_{\lambda^{\mathrm{PMU}}} = \sigma_s^2 + \sigma_c^2 + \sigma_r^2 = \frac{p_s \sigma^2_{\lambda^{\mathrm{PMU}}} + p_c \sigma^2_{\lambda^{\mathrm{PMU}}} + p_r \sigma^2_{\lambda^{\mathrm{PMU}}}}{100} \tag{3.18}$$

  where p_s, p_c and p_r represent the percentages of variance for the different contributions and, they can vary, in the tests, from $0\,\%$ to $100\,\%$. σ_s^2 is the variance of the systematic error contributions across the N_{MC} trials and σ_r^2 is the variance of λ_r. The different errors are all extracted from uniform

[1] In these tests, also the accuracy levels "PMU02" and "PMU05" ($\pm 0.5\,\%$ for the magnitude errors and $\pm 0.5\,\mathrm{crad}$ for the phase-angle errors) have been considered.

distributions, but it is worth underlining that λ^{PMU} presents a different distribution depending on the configured error mix of p_s, p_c and p_r. For this reason, as mentioned above, a coverage factor is used to guarantee the given confidence level to the error. Finally, magnitude errors are treated similarly to (3.12) but without common errors.

According to the more general model, it is possible to state that systematic errors in the measurements are the sum of the PMU and IT contributions. The tests have been carried out comparing the performance of the method that does not include in the estimation model any PMU correlation ([54], indicated below as "Method 0") with the method presented in Section 3.2.1, named "Proposed" in the following sections. Furthermore, for sake of a comprehensive view of the performance, the method proposed in [28, Sec. IV] is also applied (i.e., "Method B" of Section 2.1.4) since it considers the systematic errors at least on one end of the branch. For completeness, the results have been compared also with "Method E": a simplified version of the proposal that considers an a priori fixed Pearson correlation coefficient of $\rho^{\mathrm{PMU}} = 0.75$.

Test results: presence of systematic errors

The first tests have been carried out on the "6 branches" network configuration taking into account the possible presence of a systematic contribution in PMU errors varying the value of p_s (with $p_c = 0\,\%$).

In Fig. 3.14, the average RMSE of the estimated systematic magnitude errors ξ_h^{sys} (with $h = 1, \ldots, 5$) are shown as a function of p_s. It is worth recalling that the RMSEs represent the residual errors after estimation and, thus, give an idea of the capability of the method to compensate for the systematic measurement errors. Figure 3.14 shows the comparison, for $C = 100$ and PMU01, of the estimation results for Proposed and Method B (indicated with orange asterisks and green squares, respectively). Prior errors are also reported and they are indicated with blue crosses. The results show that prior values only slightly increase with p_s due to the fact that the additional PMU systematic contribution is on average significantly lower than the VT systematic contribution (i.e., equal to $0.5/\sqrt{3}\,\%$ as shown in Table 2.2) when PMU01 is considered. Thus, it is possible to emphasize the improvement of Proposed with respect to prior errors also when a mismatch in the prior definition is present in the estimation model, and, in particular, these improvements are of about 48 % and 52% moving from $p_s = 0\,\%$ to $p_s = 75\,\%$. Similar conclusions can be drawn if α_h^{sys}, $\eta_{i,j}^{\mathrm{sys}}$ and $\psi_{i,j}^{\mathrm{sys}}$ are considered. Estimation results of Method B are slightly different but do not improve the prior values.

The same tests have been performed considering TVE1 and the results are

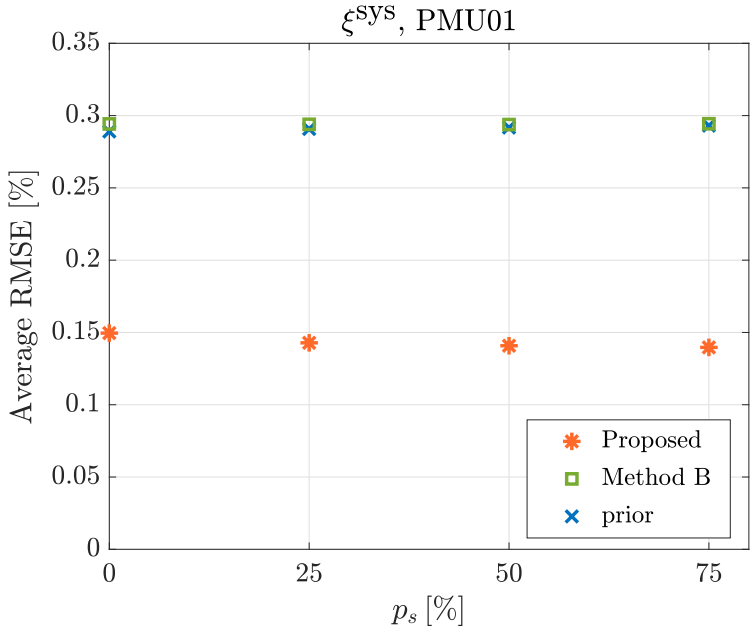

Figure 3.14: Average RMSE of voltage synchrophasor magnitude estimation as a function of PMU systematic error percentage (PMU01 and $C = 100$).

reported in Fig. 3.15. In this figure, the results of Method B are not reported because they are far beyond the prior values. In Fig. 3.15, differently from Fig. 3.14, the prior values increase with p_s due to the larger contribution of PMU systematic errors. Despite that, it is possible to observe that the reduction with respect to the prior values is still significant thanks to the parallel reduction of the random error contribution. In fact, the RMSE reduction is of about 40 % and 45 % for $p_s = 0\,\%$ and $p_s = 75\,\%$, respectively.

Then, it is important to understand the effect of the mismatch on prior definition also on the main target of the method, i.e., line parameters. Figures 3.16 and 3.17 report γ_q estimation RMSE averaged among all the branches (i.e. $q = 1, \ldots, 6$), varying the PMU accuracy and p_s for Proposed and Method B, respectively. The results, as expected, are better in the presence of higher PMU accuracy (left part of the figures) but different behaviors can be observed for the two methods. In particular:

- Figure 3.16 shows, for Proposed method, that, although the estimation accuracy decreases with larger PMU errors, the results still remain below the prior values (i.e., in this case equal to $\frac{15}{\sqrt{3}} \simeq 8.66\,\%$). As a further comment, it is possible to observe that with the best PMU accuracy, increasing systematic errors lead to better estimation results. This is explained (as

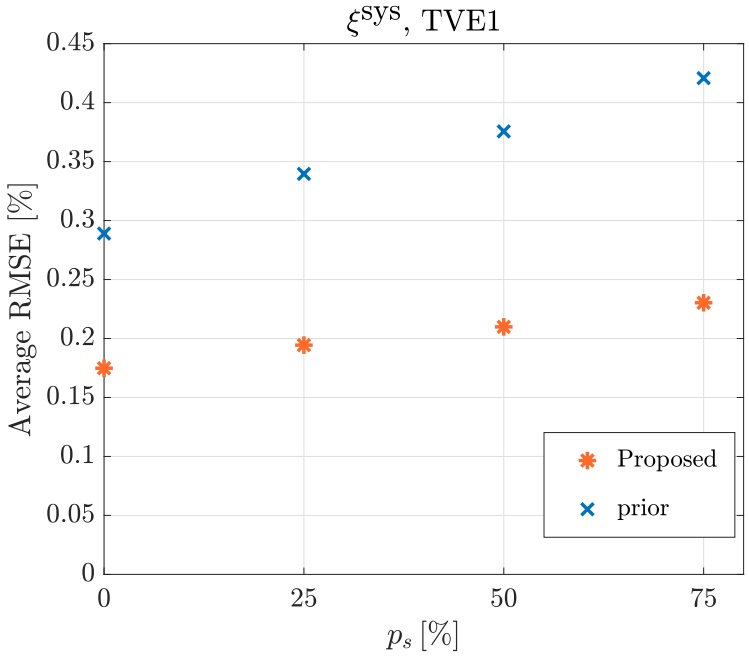

Figure 3.15: Average RMSE of voltage synchrophasor magnitude estimation as a function of PMU systematic error percentage (TVE1 and $C = 100$).

already observed in Fig. 3.14) by the reduced random error contribution and by the compensation capabilities of the method. On the contrary, when TVE1 is considered, increasing systematic error means introducing an additional systematic contribution due to PMUs that becomes comparable with that introduced by the IT. Notwithstanding such degradation, the increase in the maximum RMSE is less than 5 % with $p_s = 75\,\%$ and worst PMU accuracy. This confirms the robustness of the method even in the presence of a large mismatch on the uncertainty model (high mismatch between prior assumptions on systematic errors and actual errors).

- Figure 3.17 shows, for Method B, that the overall trend is very different and it is mainly related to the strong sensitivity of Method B to random errors. Indeed, it is possible to observe that, even with PMU02, the estimates are basically unreliable. Thus, in general, it is possible to affirm that the estimation error increases when PMU accuracy gets worse and PMU random errors are higher.

Test results: presence of common phase-angle errors

In this section, the tests carried out to evaluate the impact of a common phase-angle error in the channels of a PMU are described. To investigate this aspect,

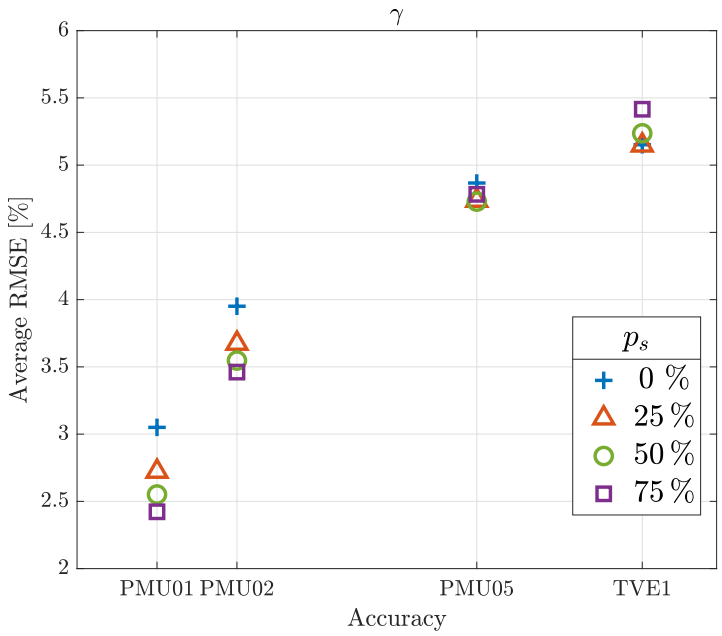

Figure 3.16: Proposed method. Average RMSE of line resistance deviation estimation as a function of PMU systematic error percentage and of PMU accuracy, $C = 100$.

p_c is considered individually (it goes from 0 % up to 95 %) with the exclusion of p_s ($p_s = 0\,\%$), using the whole network and a variation of the accuracy of the PMU from PMU01 to TVE1. Figures 3.18 (for PMU01) and 3.19 (for TVE1) report the average RMSE of γ estimation (similar results can be found for β and δ), comparing the results for Proposed, Method 0 and Method E indicated with orange asterisks, green diamonds and blue squares, respectively.

Figures 3.18 and 3.19 show that, for both levels of PMU accuracy, the impact of p_c and the overall trends are the same:

- RMSEs for Method 0 decrease when p_c increases with a minimum for $p_c = 50\,\%$, then get worse for higher values of p_c but still remain below those for $p_c = 0\,\%$. This can be explained by the fact that, despite the presence of p_c is far from the assumptions of Method 0, the presence of shared error basically limits the error variability and this behavior makes the constraints of the estimation method more effective.

- RMSEs for Method E have, for $p_c = 0\,\%$, results 14 % worse in the PMU01 scenario and about 16 % worse for TVE1 with respect to Method 0 and Proposed. This behavior reveals the limits of assuming a fixed Pearson correlation coefficient. Nevertheless, observing the trend when p_c increases,

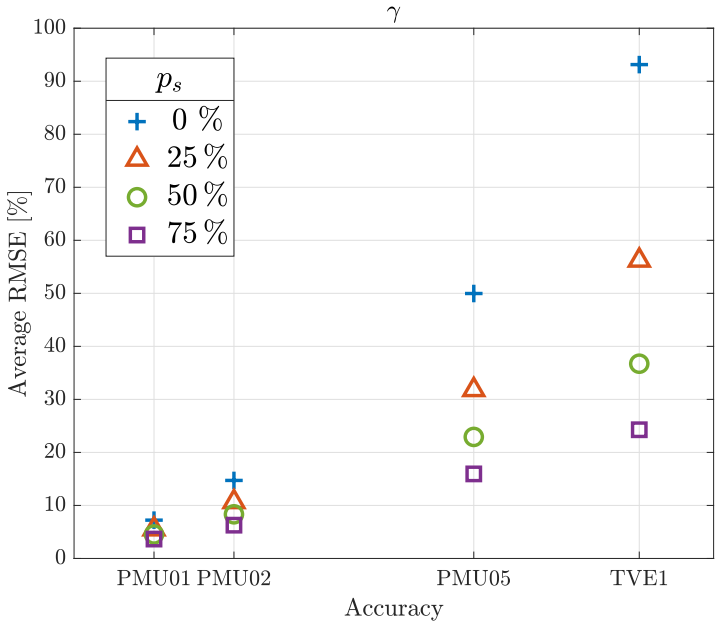

Figure 3.17: Method B. Average RMSE of line resistance deviation estimation as a function of PMU systematic error percentage and of PMU accuracy, $C = 100$.

the results improve getting closer to $p_c = 75\,\%$ (the assumption of Method E) and continue to improve (remaining worse than Proposed) also beyond $p_c = 75\,\%$.

- RMSEs for Proposed have, compared with other methods, the same results of Method 0 for $p_c = 0$ % and those of Method E for $p_c = 75$ %. They are better than those of the other methods in all the other conditions. For instance, as an example, Proposed improves Method 0 of about 25 % when $p_c = 95\,\%$ and TVE1 are considered.

It is also interesting to check the estimation results for all line parameters (without averaging) of the whole network. Figure 3.20 reports the RMSE of γ_q, β_q and δ_q (with $q = 1, \ldots, 20$), comparing Proposed and Method 0 (at the top and bottom of the figure, respectively) when $p_c = 90\,\%$ and PMU01 are considered. Figure 3.20 shows that Proposed have RMSEs lower than Method 0 for all the considered parameters and, in particular, the average improvements of Proposed with respect to Method 0 are of about 21 %, 18 % and 43 % for γ_q, β_q and δ_q, respectively. An interesting conclusion that can be drawn from Fig. 3.20 is that Proposed and Method 0 have, for β_{14}, almost the same results. This can be explained observing the topology of the grid in Fig. 2.3, where it

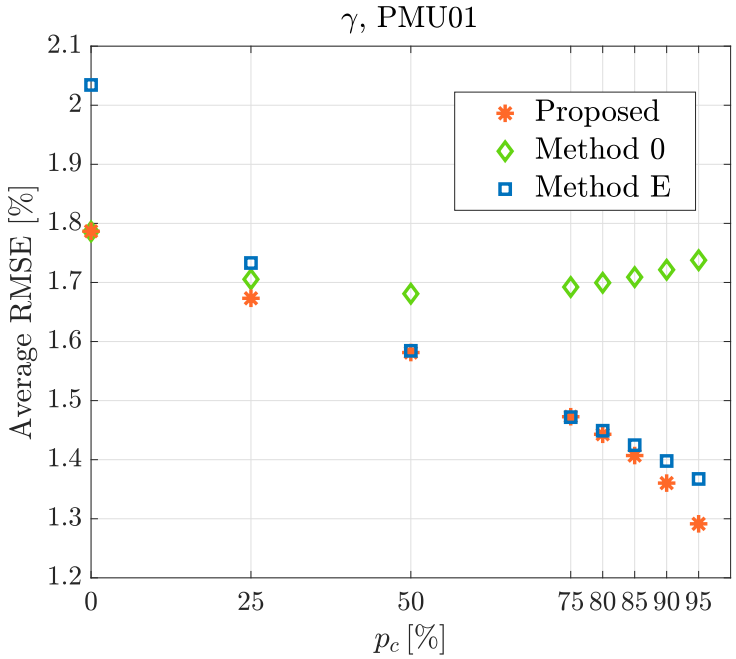

Figure 3.18: Average RMSE of line resistance deviation as a function of the PMU common phase error percentage, entire network (PMU01 and $C = 10$).

is possible to see that this branch between nodes 7 and 8 is a terminal branch: i.e., PMU in node 8 monitors only this branch and, thus, it is isolated with few channels involved.

For completeness, other tests have been performed considering PMU01 and PMU02, $C = 10$ and $C = 100$, and three different p_c values (0, 50, and 90 %). Table 3.5 shows RMSE values for γ_4, β_4, γ_5 and β_5, for the systematic phase-angle errors for voltages of node 4 and 5 and for the systematic phase-angle errors for currents $i_{4,2}$ and $i_{5,2}$ of branches $(2, 4)$ and $(2, 5)$, respectively. The results are reported for Proposed, Method 0 and Method B. As further confirmation of the previous results, it is possible to highlight that in all the considered scenarios when $p_c = 0\,\%$, Proposed behaves like Method 0.

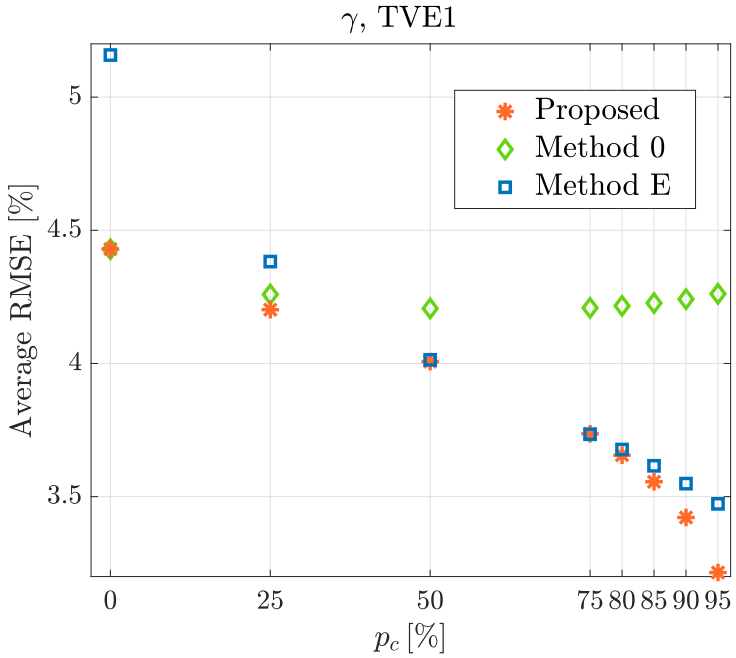

Figure 3.19: Average RMSE of line resistance deviation as a function of the PMU common phase error percentage, entire network (TVE1 and $C = 10$).

Table 3.5: Estimation results in the presence of different accuracies, errors, and cases

Method	**PMU accuracy**	**C**	**p_c** [%]	**RMSE** γ_4 [%]	β_4 [%]	γ_5 [%]	β_5 [%]	α_4 [crad]	$\psi_{4,2}$ [crad]	α_5 [crad]	$\psi_{5,2}$ [crad]
Proposed	PMU01	10	0	1.81	0.61	2.09	0.73	0.09	0.38	0.09	0.38
			50	1.68	0.57	1.87	0.68	0.09	0.37	0.09	0.37
			90	1.49	0.54	1.59	0.63	0.09	0.36	0.09	0.36
		100	0	1.34	0.37	1.41	0.40	0.09	0.37	0.09	0.36
			50	1.29	0.35	1.32	0.37	0.09	0.36	0.09	0.35
			90	1.21	0.34	1.20	0.37	0.08	0.36	0.08	0.35
	TVE1	100	0	3.13	2.00	3.74	2.47	0.12	0.41	0.13	0.42
			50	2.88	1.75	3.41	2.17	0.11	0.40	0.12	0.41
			90	2.51	1.47	2.81	1.82	0.10	0.39	0.11	0.38
Method 0	PMU01	10	0	1.81	0.61	2.09	0.73	0.09	0.38	0.09	0.38
			50	1.74	0.58	1.96	0.69	0.09	0.37	0.09	0.37
			90	1.75	0.60	1.94	0.71	0.09	0.37	0.09	0.38
		100	0	1.34	0.37	1.41	0.40	0.09	0.37	0.09	0.36
			50	1.32	0.35	1.37	0.37	0.09	0.36	0.09	0.35
			90	1.32	0.35	1.37	0.37	0.09	0.36	0.09	0.35
	TVE1	100	0	3.13	2.00	3.74	2.47	0.12	0.41	0.13	0.42
			50	3.00	1.72	3.67	2.13	0.12	0.41	0.12	0.41
			90	2.98	1.67	3.66	2.04	0.12	0.41	0.13	0.41
Method B	PMU01	10	0	7.83	2.69	11.66	4.31	0.46	0.58	0.49	0.60
			50	7.60	2.32	11.18	3.78	0.43	0.56	0.46	0.58
			90	7.68	2.50	11.49	4.12	0.45	0.57	0.48	0.60
		100	0	3.02	1.16	4.30	2.16	0.36	0.52	0.38	0.53
			50	2.93	1.01	4.06	1.84	0.36	0.52	0.37	0.52
			90	2.98	1.09	4.21	2.01	0.36	0.52	0.38	0.53

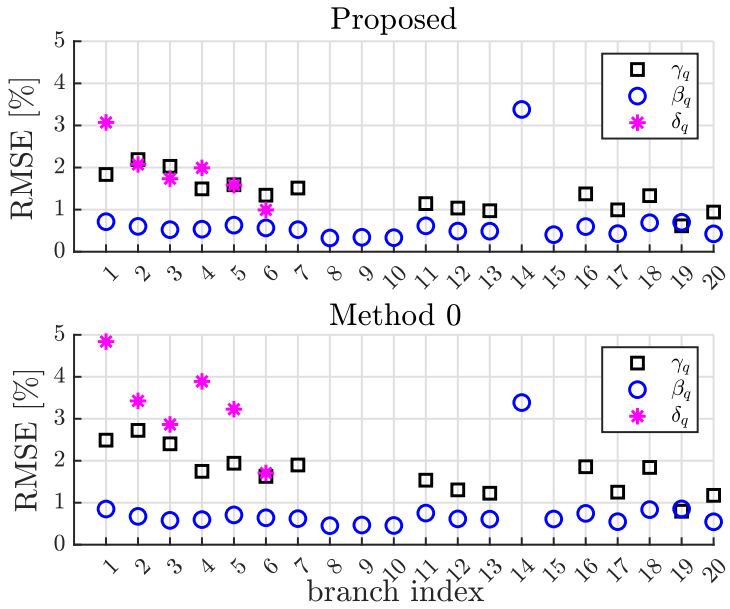

Figure 3.20: RMSE of line parameters deviation considering 90 % of phase-angle common error for each channel of the same PMU, entire network (PMU01 and $C = 10$).

Focusing on the impact of p_c, an increase of this parameter leads, in general, better estimation results for all the methods with different trends. For instance, considering γ_5 estimation with PMU01, $C = 10$ and $p_c = 90\,\%$, the improvements of Proposed, Method 0 and Method B with respect to $p_c = 0\,\%$ are of about 24 %, 7 % and 2 %, respectively. Another important conclusion is that, when the cases increase ($C = 100$), the results improve but the impact of a larger p_c is reduced. Focusing on systematic errors α_4 and α_5, RMSEs for Method 0 are lower than prior uncertainty (reduction up to 72 %), whereas for Method B are close or beyond the prior values. It is worth underlining that, for each considered scenario, the estimates of Proposed and Method 0 degrade with lower PMU accuracies but they still remain below the prior values, whereas Method B results go far beyond prior values and, for this reason, are not reported in Table 3.5.

Test results: presence of both systematic and common errors

To conclude this analysis, some tests have been carried out considering, for PMU phase-angle errors, the simultaneous presence of both systematic and common contributions. In particular, Table 3.6 reports the results for $p_s = 25\,\%$ and $p_c = 70\,\%$, PMU01 and TVE1, and both $C = 10$ and $C = 100$, comparing

the estimation performance of the same parameters of Table 3.5 for Proposed, Method 0 and Method B.

Table 3.6: Estimation results considering $p_s = 25\,\%$ and $p_c = 70\,\%$, in the presence of different accuracies and cases

Method	**PMU accuracy**	**C**	**RMSE**							
			γ_4 [%]	β_4 [%]	γ_5 [%]	β_5 [%]	α_4 [crad]	$\psi_{4,2}$ [crad]	α_5 [crad]	$\psi_{5,2}$ [crad]
Proposed	PMU01	10	1.35	0.44	1.41	0.51	0.09	0.36	0.09	0.36
		100	1.17	0.31	1.17	0.34	0.09	0.36	0.09	0.35
	TVE1	100	2.42	1.21	2.69	1.49	0.11	0.41	0.11	0.40
Method 0	PMU01	10	1.61	0.49	1.74	0.58	0.09	0.37	0.09	0.37
		100	1.29	0.32	1.34	0.33	0.09	0.37	0.09	0.36
	TVE1	100	3.06	1.52	3.77	1.88	0.13	0.43	0.13	0.43
Method B	PMU01	10	5.76	1.87	8.53	2.89	0.41	0.56	0.43	0.56
		100	2.56	0.80	3.21	1.30	0.35	0.52	0.36	0.52

It is possible to observe that, as already found in Section 2.1.4, Method B benefits from the increase of C, but its RMSEs are always the worst with respect to the other methods. As a final comment, it is possible to affirm that Proposed, due to the inclusion in the estimation model of a realistic representation of PMU errors, has the best estimation results. For instance, with $C = 100$ and TVE1, the improvements for γ_5, β_5, α_5 and $\psi_{5,2}$ with respect to Method 0 are of 28 %, 21 %, 15 % and 8 %, respectively.

3.3 Generalized model of tap-changing transformer

Besides the impact of a mismatch on the assumptions concerning the errors in the measurement chain (already discussed in Section 3.1 and Section 3.2), an inaccurate model of the tap-changing transformer can also have a significant influence on the line parameters estimation performance of the presented methodology. In this context, this section shows the impact on the estimation results of a mismatch occurring in the model of the tap-changing transformer. In particular, first it is emphasized how the estimates can be affected by such a model deficiency, then a trade-off solution to improve the estimator is proposed and validated as in [94].

3.3.1 Tap-changing transformer model extension and integration in the estimation method

In literature, tap-changing transformers are commonly represented by means of an impedance in series with off-nominal turns ratio [51] as shown in Fig. 3.21 (for the sake of an effective and simpler introduction, the single-phase model is considered from here on). In this figure, according to the considered model, it is possible to define, for the generic branch (s, r) associated with a tap-changing transformer[2], the off-nominal short circuit admittance $y^{\text{off}}_{\text{sc}_{s,r}}$. In particular it possible to introduce, aiming at a generalization of the model of a tap-changing transformer, a parameter k that represents the ratio between the impedances of the nominal and tapped windings [94].

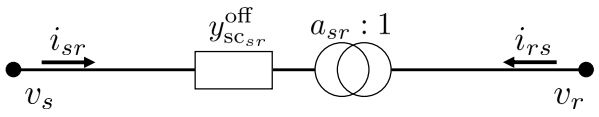

Figure 3.21: Tap-changing transformer model with short circuit impedance at the off-nominal turns side.

The off-nominal short circuit admittance $y^{\text{off}}_{\text{sc}_{s,r}}$ can be written as:

$$y^{\text{off}}_{\text{sc}_{s,r}} = \frac{1}{z_{\text{tap}} + a^2_{s,r} z_{\text{nom}}} = \frac{(1+k)}{(1+a^2_{s,r}k)} y_{\text{sc}_{s,r}} \tag{3.19}$$

where $y_{\text{sc}_{s,r}}$ is the short circuit admittance of the power transformer, which is a parameter provided by the manufacturer, $a_{s,r}$ is the tap ratio and k is defined as $k = \frac{z_{\text{nom}}}{z_{\text{tap}}}$. Using this approach, it is possible to build the equivalent π-model of a tap-changing transformer as a function of the value of k as shown in Fig. 3.22.

It is worth highlighting that shunt admittances y_{sh_s} and y_{sh_r} in Fig. 3.22 are not negligible in case of off-nominal turns ratio. This model can be represented by means of its nodal admittance matrix $\mathbf{Y}_{\text{tap}}$, defined as:

$$\mathbf{Y}_{\text{tap}} = \begin{bmatrix} \mathbf{Y}_{\text{tap}_{s,s}} & \mathbf{Y}_{\text{tap}_{s,r}} \\ \\ \mathbf{Y}_{\text{tap}_{r,s}} & \mathbf{Y}_{\text{tap}_{r,r}} \end{bmatrix} = \begin{bmatrix} y_{\text{tap}_{s,s}} & y_{\text{tap}_{s,r}} \\ \\ y_{\text{tap}_{r,s}} & y_{\text{tap}_{r,r}} \end{bmatrix} \tag{3.20}$$

where the nodal admittance matrix $\mathbf{Y}_{\text{tap}}$ can be splitted into its submatrices associated with the start node s and the end node r. The last equality is based on the single-phase model and thus each submatrix is a complex value. In particular, the components of this tap-changing transformer π-model can be

[2]In this chapter, the pair of nodes (s, r) replaces (l, k) (see Chapter 2) for the notation of the generic tap-changing transformer branch to avoid confusion with the parameter k, which comes from the literature [51].

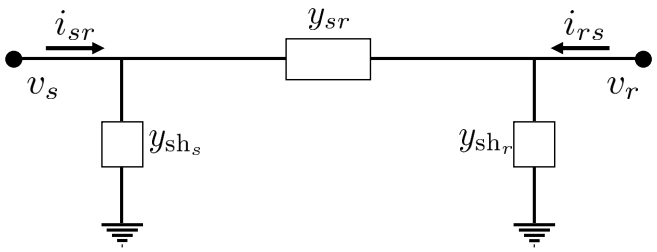

Figure 3.22: Equivalent single-phase general π-model of a transformer equipped with tap changer.

defined as:

$$\begin{aligned} y_{s,r} &= -y_{\mathrm{tap}_{s,r}} = \frac{a_{s,r}(1+k)}{(1+a_{s,r}^2 k)} y_{\mathrm{sc}_{s,r}} \\ y_{\mathrm{sh}_s} &= y_{\mathrm{tap}_{s,s}} + y_{\mathrm{tap}_{s,r}} = \frac{(1-a_{s,r})(1+k)}{(1+a_{s,r}^2 k)} y_{\mathrm{sc}_{s,r}} \\ y_{\mathrm{sh}_r} &= y_{\mathrm{tap}_{r,r}} + y_{\mathrm{tap}_{s,r}} = \frac{a_{s,r}(a_{s,r}-1)(1+k)}{(1+a_{s,r}^2 k)} y_{\mathrm{sc}_{s,r}} \end{aligned} \tag{3.21}$$

Thus, besides the parameter k, the general model of the tap-changing transformer here considered is function of $a_{s,r}$ and $y_{\mathrm{sc}_{s,r}}$ (see [51], [50]).

In this context, the unknowns to be estimated are the same of the transformer of Section 2.1.2, in particular: ξ_s^{sys}, ξ_r^{sys}, α_s^{sys}, α_r^{sys}, $\eta_{s,r}^{\mathrm{sys}}$, $\eta_{r,s}^{\mathrm{sys}}$, $\psi_{s,r}^{\mathrm{sys}}$, $\psi_{r,s}^{\mathrm{sys}}$, $\beta_{s,r}$ and $\tau_{s,r}$. Nevertheless, it is important to define new constraints equations, which are the counterpart of (2.8) and (2.9), to estimate these parameters. To do that, considering (3.20), which links the branch current and voltage measurements, it is possible to write the following two complex equations for the generic branch (s,r):

$$(1+k)(v_s^R - a_{s,r} v_r^R) = (1+k a_{s,r}^2) z_{s,r} i_{s,r}^R \tag{3.22}$$

$$i_{r,s}^R = -a_{s,r} i_{s,r}^R \tag{3.23}$$

using the same notation as before.

Then, it is possible to define the linearized measurement functions for the voltage drop and current balance constraints using the first order approximation for the reference values of voltage and current phasors reported in (2.3) and also the transformer parameters definitions (see (2.7)). Substituting (2.3) and (2.7) in (3.22) and (3.23), it is possible to obtain, considering the rectangular coordinates, four real-valued equations. For (3.22), the following two real-valued

equations are found:

$$\begin{aligned}
&(1+k)V_s^r - a_{s,r}^0\,(1+k)\,V_r^r + \left(1+k{a_{s,r}^0}^2\right) X_{s,r}^0 I_{s,r}^x \\
&\quad\simeq \left(\xi_s^{\text{sys}}+\xi_s^{\text{rnd}}\right)(1+k)\,V_s^r - \left(\alpha_s^{\text{sys}}+\alpha_s^{\text{rnd}}\right)(1+k)\,V_s^x + \\
&\quad- \left(\xi_r^{\text{sys}}+\xi_r^{\text{rnd}}\right) a_{s,r}^0\,(1+k)\,V_r^r + \left(\alpha_r^{\text{sys}}+\alpha_r^{\text{rnd}}\right) a_{s,r}^0\,(1+k)\,V_r^x + \\
&\quad+ \left(\eta_{s,r}^{\text{sys}}+\eta_{s,r}^{\text{rnd}}\right)\left(1+k{a_{s,r}^0}^2\right) X_{s,r}^0 I_{s,r}^x + \\
&\quad+ \left(\psi_{s,r}^{\text{sys}}+\psi_{s,r}^{\text{rnd}}\right)\left(1+k{a_{s,r}^0}^2\right) X_{s,r}^0 I_{s,r}^r + \\
&\quad- \beta_{s,r}\left(1+k{a_{s,r}^0}^2\right) X_{s,r}^0 I_{s,r}^x + \tau_{s,r}\left[a_{s,r}^0\,(1+k)\,V_r^r - 2k{a_{s,r}^0}^2 I_{s,r}^x X_{s,r}^0\right]
\end{aligned} \tag{3.24}$$

$$\begin{aligned}
&(1+k)V_s^x - a_{s,r}^0\,(1+k)\,V_r^x - \left(1+k{a_{s,r}^0}^2\right) X_{s,r}^0 I_{s,r}^r \\
&\quad\simeq \left(\xi_s^{\text{sys}}+\xi_s^{\text{rnd}}\right)(1+k)\,V_s^x + \left(\alpha_s^{\text{sys}}+\alpha_s^{\text{rnd}}\right)(1+k)\,V_s^r + \\
&\quad- \left(\xi_r^{\text{sys}}+\xi_r^{\text{rnd}}\right) a_{s,r}^0\,(1+k)\,V_r^x - \left(\alpha_r^{\text{sys}}+\alpha_r^{\text{rnd}}\right) a_{s,r}^0\,(1+k)\,V_r^r + \\
&\quad- \left(\eta_{s,r}^{\text{sys}}+\eta_{s,r}^{\text{rnd}}\right)\left(1+k{a_{s,r}^0}^2\right) X_{ij}^0 I_{s,r}^r + \\
&\quad+ \left(\psi_{s,r}^{\text{sys}}+\psi_{s,r}^{\text{rnd}}\right)\left(1+k{a_{s,r}^0}^2\right) X_{s,r}^0 I_{s,r}^x + \\
&\quad+ \left(1+k{a_{s,r}^0}^2\right)\beta_{s,r} X_{s,r}^0 I_{s,r}^r + \tau_{s,r}\left[a_{s,r}^0\,(1+k)\,V_r^x + 2k{a_{s,r}^0}^2 I_{s,r}^r X_{s,r}^0\right]
\end{aligned} \tag{3.25}$$

Focusing on the current balance equation (3.23) and replacing the pair of nodes (l,k) with (s,r) in (2.16)-(2.17), the following two real-valued equations can be obtained:

$$\begin{aligned}
I_{r,s}^r + a_{s,r}^0 I_{s,r}^r \simeq{}& \left(\eta_{r,s}^{\text{sys}}+\eta_{r,s}^{\text{rnd}}\right) I_{r,s}^r - \left(\psi_{r,s}^{\text{sys}}+\psi_{r,s}^{\text{rnd}}\right) I_{r,s}^x + \\
&+ \left(\eta_{s,r}^{\text{sys}}+\eta_{s,r}^{\text{rnd}}\right) a_{s,r}^0 I_{s,r}^r - \left(\psi_{s,r}^{\text{sys}}+\psi_{s,r}^{\text{rnd}}\right) a_{s,r}^0 I_{s,r}^x + \\
&- \tau_{s,r} a_{s,r}^0 I_{s,r}^r
\end{aligned} \tag{3.26}$$

$$\begin{aligned}
I_{r,s}^x + a_{s,r}^0 I_{s,r}^x \simeq{}& \left(\eta_{r,s}^{\text{sys}}+\eta_{r,s}^{\text{rnd}}\right) I_{r,s}^x + \left(\psi_{r,s}^{\text{sys}}+\psi_{r,s}^{\text{rnd}}\right) I_{r,s}^r + \\
&+ \left(\eta_{s,r}^{\text{sys}}+\eta_{s,r}^{\text{rnd}}\right) a_{s,r}^0 I_{s,r}^x + \left(\psi_{s,r}^{\text{sys}}+\psi_{s,r}^{\text{rnd}}\right) a_{s,r}^0 I_{s,r}^r + \\
&- \tau_{s,r} a_{s,r}^0 I_{s,r}^x
\end{aligned} \tag{3.27}$$

These equations can be used in the estimation framework as an enhanced version of (2.10)-(2.13). In the next section, the performance of this proposed extension is investigated.

3.3.2 Analysis of the performance of the proposed extension

In this section, the assessment of the estimation results is obtained through tests carried out, in MATLAB environment, on the single-phase version of the IEEE 14 bus test system in Fig. 2.3. In particular, for the grid under analysis, tap ratio values (i.e., $a_{s,r}^0$) for the tap-changing transformers are shown in Table 3.7.

Table 3.7: Tap ratios of the IEEE 14 bus test system

Branch	$a^0_{s,r}$
8	0.978
9	0.969
10	0.932

For the three tap-changing transformers in Fig. 2.3, the general model depending on the parameter k is used. In the tests, $C \in \{10, 200\}$ cases (with a maximum variability of $\pm 10\,\%$ for loads or generators), $M = 10$ repeated measurements for each case and $N_{\mathrm{MC}} = 5000$ MC trials have been considered. Line parameters deviations, systematic errors for ITs (0.5 accuracy class), and PMU errors (considering PMU01 and purely random contribution) have been extracted according to uniform distributions. The following assumptions are applied:

- As for transmission line parameters, maximum deviations of $\pm 10\,\%$ with respect to the nominal values have been considered.
- As for transformer parameters, $\pm 10\,\%$ and $\pm 1\,\%$ are the maximum deviations from $X^0_{s,r}$ and $a^0_{s,r}$, respectively. Thus, the prior standard deviations for $X_{s,r}$ and $a_{s,r}$ are of about $5.77\,\%$ and $0.57\,\%$, respectively.
- In the following tests, the values for the ratio between the impedance of the nominal winding and that of the tapped winding are chosen varying $k \in \{0, 0.1, 0.25, 0.50, 0.75, 1, 1.25, 2, 5, 100, 10000\}$.

In the tests, the performance evaluation metric is again the RMSE in (2.45) and k_m indicates the value of k assumed in the measurement process (i.e., in the estimation model). In particular, the estimation performance has been compared using two different approaches. The first one is "$k_m = k$", which is the best possible option when k is known, for instance from the manufacturer or from dedicated analyses. This method can be considered as a benchmark method since it assumes the "correct" value in the estimation process. The second method is the proposed solution "$k_m = 1$", which is a compromise adopted when the value of k is unknown, as suggested by [51] and [95]. In addition, the comparison has been conducted considering also the method that assumes "$k_m = \infty$" [55] (which corresponds to the method described in Section 2.1.2). The results, as usual, have been also compared with the prior standard deviations (named as "Prior") of the considered parameters.

The first tests have been carried out considering the single-branch approach for the branches associated with tap-changing transformers, i.e., branches with

indices 8, 9 and 10 in Fig. 2.3 (in this section, the branches will be indicated with the index $q \in \{1, \ldots, 20\}$). Figure 3.23 shows the estimation results for β_{10} obtained with different values of k, comparing "$k_m = 1$", "$k_m = \infty$" and also the estimates of the benchmark method "$k_m = k$". As expected, "$k_m = k$" has the best results among all the values of k. It is important to highlight that "$k_m = 1$" shows greater robustness with respect to "$k_m = \infty$" when a strong mismatch between the assumed value of k and the actual one occurs. In fact, "$k_m = \infty$" has errors far beyond prior values in the presence of low values of k. It has to be noticed that, among the three tap-changing transformers, branch

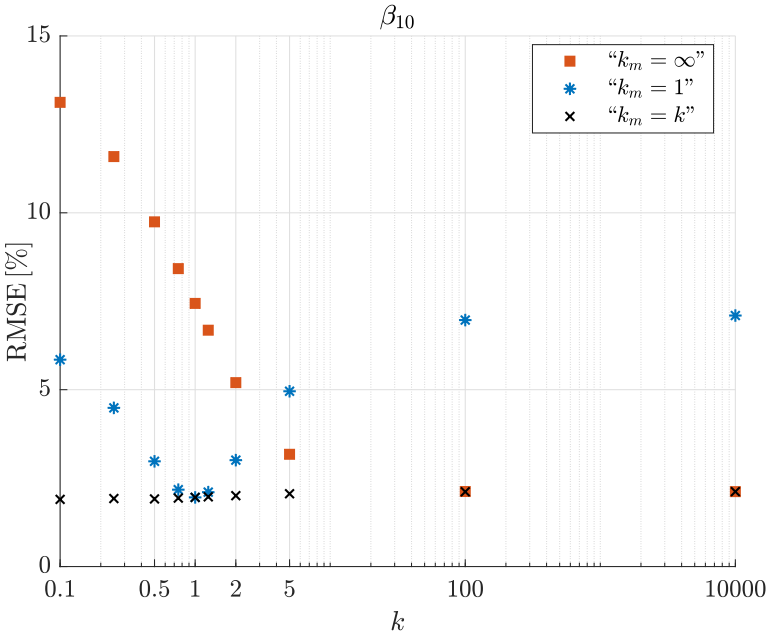

Figure 3.23: Single-branch approach, RMSE of estimated transformer reactance deviations of branch 10 for different values of k.

10 is the one that operates at a ratio farthest from $a_{s,r} = 1$. Indeed, the impact of the mismatch (the difference between k_m and k) due to the tap-changing transformer modeling is greater when tap ratio values deviate from $a_{s,r} = 1$, as discussed in [51]. Thus, despite branches 8 and 9 have similar trends (not reported here for the sake of brevity), branch 10 has the worst estimation results.

Table 3.8 shows the RMSEs for β_q and τ_q (with $q \in \{8, 9, 10\}$) varying $k \in \{0.5, 1, 2\}$. As a further confirmation of the trends observed in Fig. 3.23 for β_{10} results, it is possible to notice that prior values are exceeded for $k = 0.5$ and $k = 1$ when $k_m = \infty$ is applied. Instead, looking at β_8, for instance, the estimation results with $k_m = 1$ are close to those with $k_m = k$ when $k = 0.5$ and $k = 2$, and obviously they are the same for $k = 1$. Focusing on τ_q estimation

results instead, it is possible to underline that the results for the three estimation methods are similar and, thus, it can be concluded that these estimates are robust with respect to a possible mismatch between k and k_m.

Table 3.8: Single-branch approach, estimation results for different values of k

Method	$\boldsymbol{k}$	**RMSE [%]**					
		β_8 [%]	τ_8 [%]	β_9 [%]	τ_9 [%]	β_{10} [%]	τ_{10} [%]
"$k_m = \infty$"	0.5	3.52	0.26	4.44	0.26	9.74	0.27
	1	3.07	0.26	3.53	0.26	7.44	0.27
	2	2.73	0.26	2.70	0.26	5.20	0.26
"$k_m = 1$"	0.5	2.45	0.26	1.98	0.26	2.98	0.26
	1	2.37	0.26	1.74	0.26	1.95	0.26
	2	2.49	0.26	2.04	0.26	3.00	0.26
"$k_m = k$"	0.5	2.38	0.26	1.72	0.26	1.91	0.26
	1	2.37	0.26	1.74	0.26	1.95	0.26
	2	2.40	0.26	1.77	0.26	2.00	0.26

Other tests have been carried out considering the multi-branch approach when the whole network is considered, considering only methods "$k_m = 1$" and "$k_m = \infty$". Figures 3.24 and 3.25 report the β_q RMSE results for $k = 1$ and $k = 2$, respectively. It is interesting to notice that, for both $k = 1$ and $k = 2$, "$k_m = 1$" has the best estimation results, especially for β_8, β_9 and β_{10}. Moving from the match condition in Fig. 3.24 to Fig. 3.25, the RMSEs obtained with the proposed method worsen by at least 72 % for β_8 up to a maximum of 335 % for β_{10}, but still remaining far below the prior values. The estimation of the reactances of the transformers obtained with "$k_m = \infty$" in Fig. 3.25 has an improvement of about 34 % with respect to Fig. 3.24 but, some errors are still significantly higher than those achieved with the proposed method.

As a further test, a comparison of the estimation results for α_h has been carried out, considering PMU01 and TVE1. In fact, Fig. 3.26 shows the RMSE values for the voltage phase-angle systematic errors when $k = 1$. It has to be noticed that, when the measurement scenario PMU01 is considered, the two methods have basically the same estimation results. On the contrary, focusing on TVE1, the proposed method proves to be better: in particular, a maximum RMSE reduction of about 17 % for α_5 with respect to "$k_m = \infty$" and an average improvement, among all the nodes of network, of about 7 % are achieved.

Figure 3.27 shows instead the estimation results for β_q using TVE1 and $k = 0.5$. Once again, β_q estimates with $k_m = 1$ are better than those obtained with the "$k_m = \infty$" approach and, in particular, the RMSE for branch 10 goes beyond the prior value.

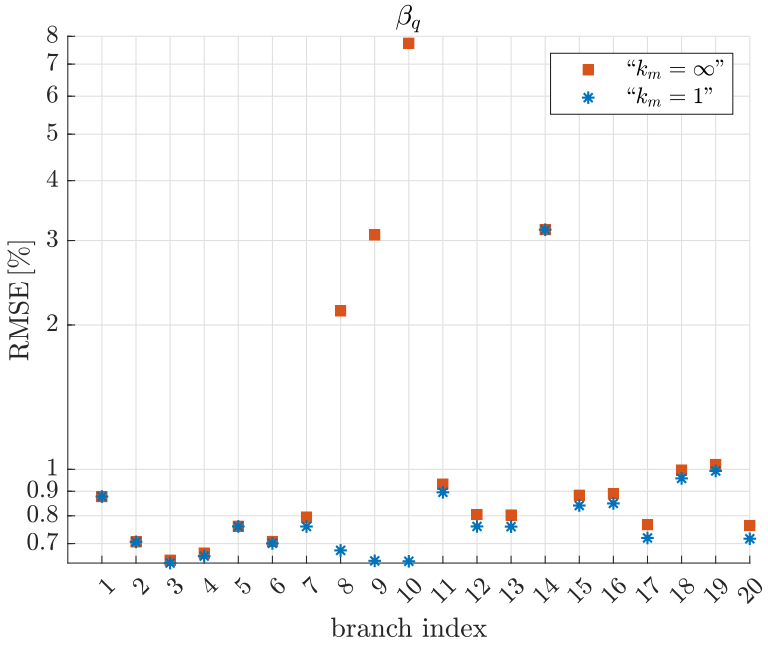

Figure 3.24: Multi-branch approach, RMSE of reactance deviations of the entire network and $k = 1$.

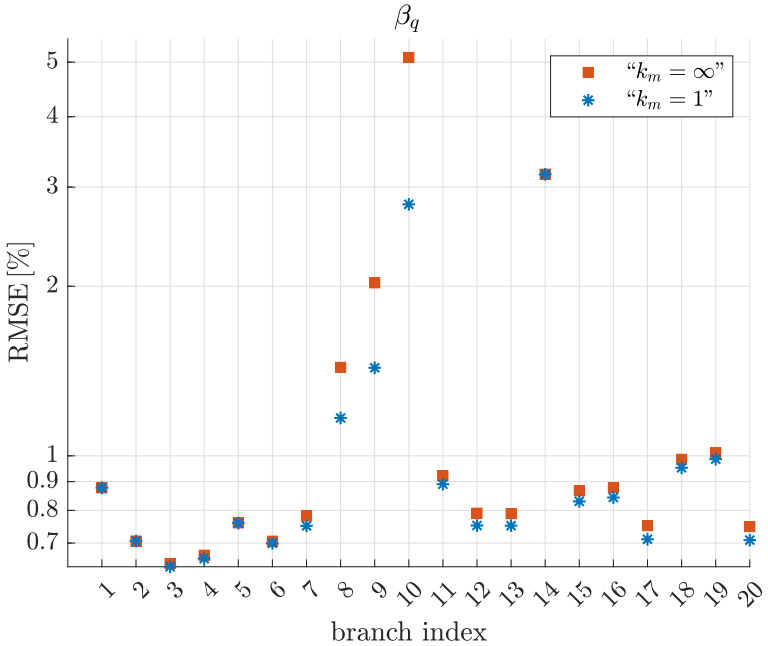

Figure 3.25: Multi-branch approach, RMSE of reactance deviations of the entire network and $k = 2$.

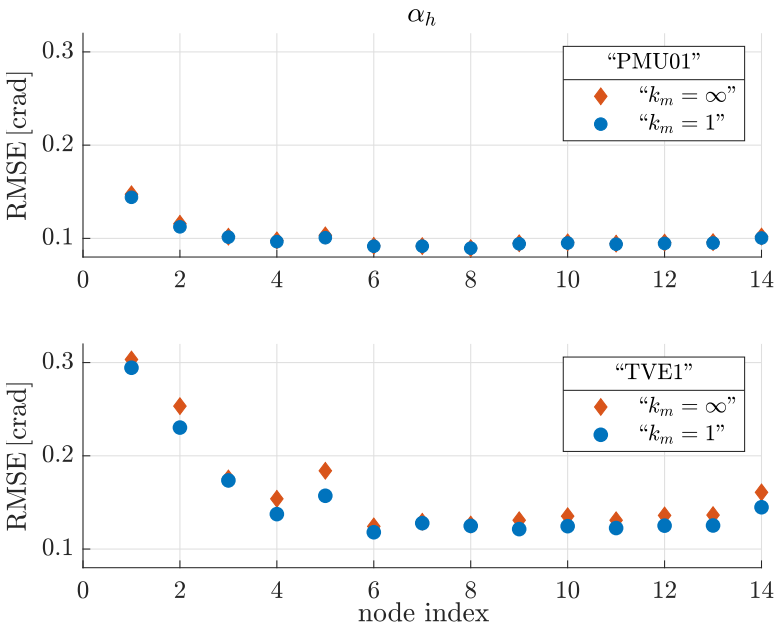

Figure 3.26: Multi-branch approach, RMSE of voltage phase-angle error of the entire network, $k = 1$ and PMU01 (above) and TVE1 (below).

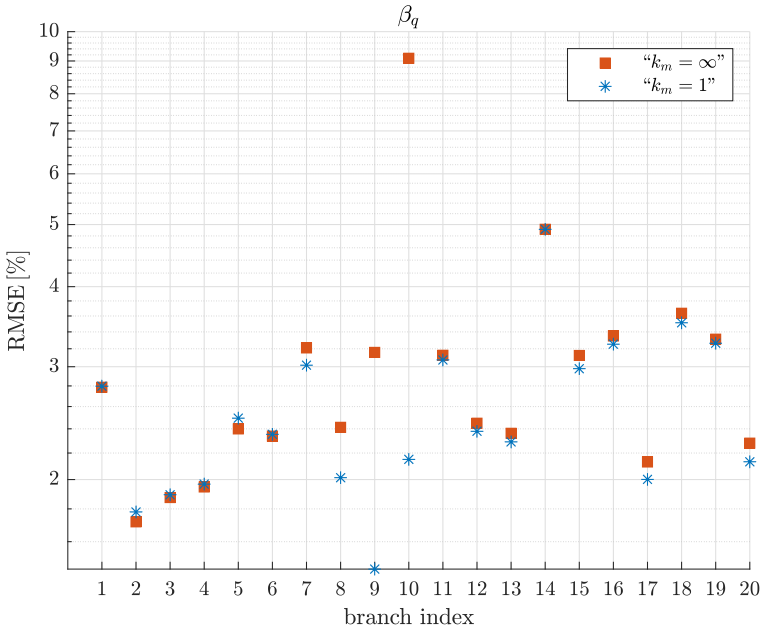

Figure 3.27: Multi-branch approach, RMSE of reactance deviations of the entire network, $k = 0.5$ and TVE1.

For sake of a comprehensive investigation of the performance, the results for both single-branch and multi-branch approaches have been compared for $k = 1$ and for different number of cases ($C \in \{10, 200\}$). Table 3.9 shows the RMSE for the following parameters: γ_7, β_7, β_8, β_9, β_{10} and the systematic errors for the voltage at node 4 (ξ_4^+ and α_4^+). Superscript $^+$ indicates that, in the single-branch approach, RMSEs are obtained averaging the results of all the branches converging on node 4. It is possible to observe that the performance for "$k_m = \infty$" and "$k_m = 1$" has an average improvement, moving from the single-branch approach and $C = 10$ to the multi-branch approach and $C = 200$, of about 41 % and 81 %, respectively. Focusing on the voltage systematic errors estimation, it is possible to notice that moving from the single-branch approach to the multi-branch approach, the α_4^+ RMSEs are more than halved for all the methods and the ξ_4^+ RMSEs are close to be halved.

Table 3.9: Comparison of estimation performance for $k = 1$, different approaches and test configurations

Method	**Approch**	**C**	**RMSE**						
			γ_7 [%]	β_7 [%]	β_8 [%]	β_9 [%]	β_{10} [%]	ξ_4^+ [%]	α_4^+ [crad]
"$k_m = \infty$"	Single branch	10	5.56	4.28	3.07	3.53	7.44	0.22	0.25
		200	4.93	2.27	2.33	3.30	7.70	0.22	0.24
	Multi branch	10	2.10	0.80	2.14	3.08	7.64	0.12	0.10
		200	1.30	0.48	2.07	3.06	7.74	0.13	0.09
"$k_m = 1$"	Single branch	10	5.56	4.28	2.37	1.74	1.95	0.22	0.25
		200	4.93	2.27	0.80	0.57	0.73	0.22	0.24
	Multi branch	10	2.08	0.76	0.68	0.64	0.64	0.12	0.10
		200	1.29	0.44	0.42	0.41	0.43	0.13	0.09

The results for tap ratios estimation are not reported but it is important to underline that the multi-branch approach, also in this case, halves the RMSEs of the single-branch approach. It is possible to emphasize that Table 3.9 shows how the appropriate model of the tap-changing transformer, in the presence of different values of k, improves the estimation results for both approaches.

Finally, further tests (the results are summarized in Table 3.10) have been carried out to assess the proposal performance with respect to other methods in literature, with the same measurement set-up used above. In particular, the Proposed Method ("$k_m = 1$") has been compared, for both PMU01 and TVE1, and using $C \in \{10, 200\}$, with the two following methods:

- Method A, already described in Section 2.1.4. For this comparison, an extension of such direct method has been designed and applied (see [55]) to

Table 3.10: Comparison of estimation performance between the Proposed method and other methods, $k = 1$

Method	**PMU accuracy**	**C**	**RMSE** γ_1 [%]	β_1 [%]	ξ_2 [%]	α_2 [crad]	β_9 [%]	τ_9 [%]	β_{10} [%]	τ_{10} [%]
Proposed Method	PMU01	10	2.37	0.88	0.12	0.11	0.64	0.13	0.64	0.13
		200	1.38	0.41	0.13	0.09	0.41	0.13	0.43	0.12
	TVE1	10	4.33	2.75	0.14	0.23	1.60	0.14	1.54	0.15
		200	3.77	1.98	0.16	0.28	1.75	0.13	1.69	0.15
Method A	PMU01	10	13.69	5.35	–	–	6.32	0.41	9.43	0.41
		200	13.81	5.39	–	–	6.32	0.41	9.33	0.40
	TVE1	10	13.83	5.37	–	–	6.35	0.42	9.43	0.42
		200	13.82	5.39	–	–	6.32	0.41	9.33	0.40
Method B	PMU01	10	7.79	2.55	0.37	0.41	–	–	–	–
		200	2.63	1.04	0.30	0.36	–	–	–	–

deal with tap-changing transformer branches (using the traditional model, i.e., "$k_m = \infty$") and to obtain τ and β estimates.

- Method B, already presented in Section 2.1.4, can be applied only with the single-branch approach. This method is chosen since line parameters and systematic measurement errors of the end node in a branch can be estimated (considering voltage and current measurements at the start node as the reference ones).

In Table 3.10, the symbol '$-$' refers to the fact that ξ_2 and α_2 (the systematic errors of the end node voltage v_2 of the branch with branch index 1 in Fig. 2.3) are not available for Method A, as well as β_9, τ_9, β_{10} and τ_{10} for Method B. Method B estimation results for the TVE1 scenario are not reported since they are far beyond the prior values. For all test configurations, RMSEs for Method A are higher than those of the Proposed Method for both line parameters and tap ratios and, in particular, those of γ_1, β_9 and β_{10} exceed the prior values. A further behavior that can be highlighted is that the results of Method A are stable varying the number of cases and the PMU accuracy considered. This can be explained by the fact that the method is not able to exploit the benefits of the additional constraints brought by the number of cases or to leverage a higher PMU accuracy. The performance of Method B, unlike Method A, takes advantage of a higher C, specifically for γ_1 and β_1 estimation results, while it is strongly and negatively sensitive to the increase in PMU measurement errors (its estimates are critically affected by the accuracy of "TVE1"). Method B allows estimating also systematic errors ξ_2 and α_2 (systematic errors in v_2) but

it is possible to notice that the corresponding RMSE values are beyond prior standard deviations for both $C = 10$ and $C = 200$ cases. Similar results (not reported here for the sake of brevity) can be observed for $\eta_{2,1}$ and $\psi_{2,1}$. It is possible to conclude that the Proposed Method leverages multiple cases and multiple branches and achieves the best performance for all considered line and transformer parameters. Furthermore, as proven above, it shows, compared to others, also a significant robustness with respect to an increase of measurement uncertainty.

3.4 Mismatch on line parameters uncertainty

In the context of the analysis of the behavior of the presented method under different types of mismatch, this section shows a characterization of its performance under incorrect prior information on line parameter uncertainty. In particular, the impact of a mismatch between the assumed parameter variability and the actual one (as proposed in [92]) has been evaluated by means of simulations carried out in MATLAB environment and again on the IEEE 14 bus test system of Fig. 2.3. The high voltage portion of the network "6 branches", is here considered.

The tests have been carried out considering $C = 10$, $N_{\mathrm{MC}} = 5000$ MC trials, ITs of Class 0.5, PMU accuracy ranging from PMU01 to TVE1 and loads and generators variability of $\pm 10\,\%$ with respect to active and reactive power nominal values. In addition, deviations of line parameters $R_{i,j}$, $X_{i,j}$ and $B_{\mathrm{sh},i,j}$ vary from $\pm 5\,\%$ to $\pm 30\,\%$ in different tests.

Figure 3.28 shows the results of some tests performed to investigate the robustness of the proposed method (γ estimation RMSE is reported in the figure) with respect to prior knowledge on line parameters. Maximum variability of the line parameters is increased from 5 % to 30 %. The comparison of three different prior information settings of the proposed method is considered: correct prior assumption (indicated with blue squares), a value fixed to 5 % for prior maximum deviation (red circles) and value fixed to 15 % (indicated with green stars). Actual prior is also reported in the figure (black crosses).

The best estimation performance is obtained, as expected, when the correct prior information is used (i.e., when the prior standard deviation in the weighting matrix matches actual variability). In addition, if a mismatch in prior information occurs, RMSEs have an almost linear increase with the variability, whereas the trend becomes sub-linear when prior information is correct.

As a comprehensive evaluation of the robustness of the proposed method, Figs. 3.29 and 3.30 report the average results for β and δ assuming a mismatch between the prior knowledge on line parameters and the actual line parameters

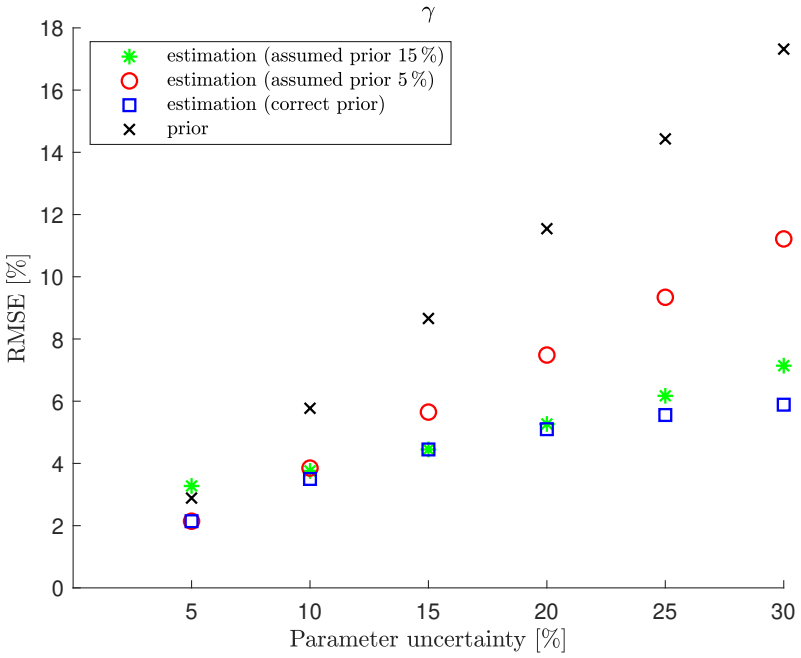

Figure 3.28: RMSE of γ estimation in the presence of prior information mismatch on line parameters.

variability. The same comparison between the three different prior information settings in Fig. 3.28 is carried out with same colors, markers and line parameters uncertainty. As expected, also for β and δ, the best estimation performance is in case of correct prior assumption. It is important to emphasize that, except for the method that assumes correct prior information, in general the best results are obtained for the method that assumes a maximum prior deviation of 15 %. In fact, this choice allows better estimates when a strong mismatch occurs in both methods (e.g., in the case of a parameter uncertainty of 30 %). Nevertheless, it is important to emphasize that the results are below the prior values in all the prior information settings of the proposed method reported in the figures.

Finally, as a further confirm of the conclusions drawn from previous results, Table 3.11 shows the comparison for the average estimation of ξ among all the nodes of the network configuration "6 branches" for the three different prior information settings of the proposed method. It is possible to notice that assuming a fixed prior value equal to 15 % permits limiting the impact of a mismatch on the actual line parameters variability on the ξ estimates with respect to the assumption of a prior value fixed to 5 %. In fact, is it possible to notice that this assumption allows having results close to the best choice about the prior knowledge (correct prior assumption) for almost all the parameters uncertain-

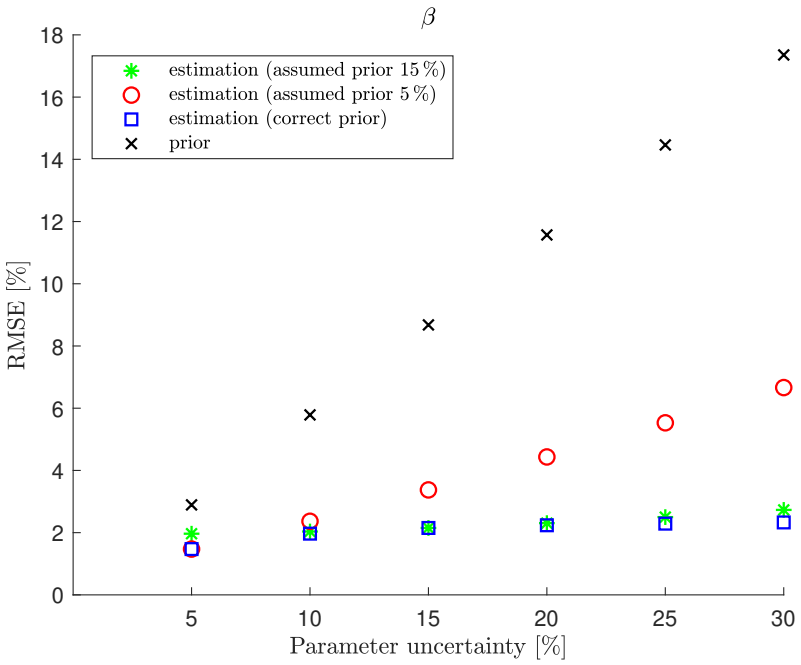

Figure 3.29: RMSE of β estimation in the presence of prior information mismatch on line parameters.

ties considered. For example, if a parameters uncertainty of 25 % is considered, the assumption of a prior value equal to 15 % improves the results of about 23 % with respect to the assumption of a prior value fixed to 5 %.

Table 3.11: Estimation performance of ξ with different line parameters uncertainties and prior values

Parameters uncertainty	**Average RMSE of ξ [%]** prior 15 %	prior 5 %	correct prior
5 %	0.16	0.14	0.14
10 %	0.16	0.16	0.16
15 %	0.17	0.19	0.17
20 %	0.18	0.22	0.18
25 %	0.20	0.26	0.19
30 %	0.21	0.30	0.19

As a final comment, despite different behaviors can be observed according to the type of the mismatch, the method proves to be robust in the presence of an increasing uncertainty on the line parameters and even in the presence of a mismatch with respect to prior knowledge on line parameters.

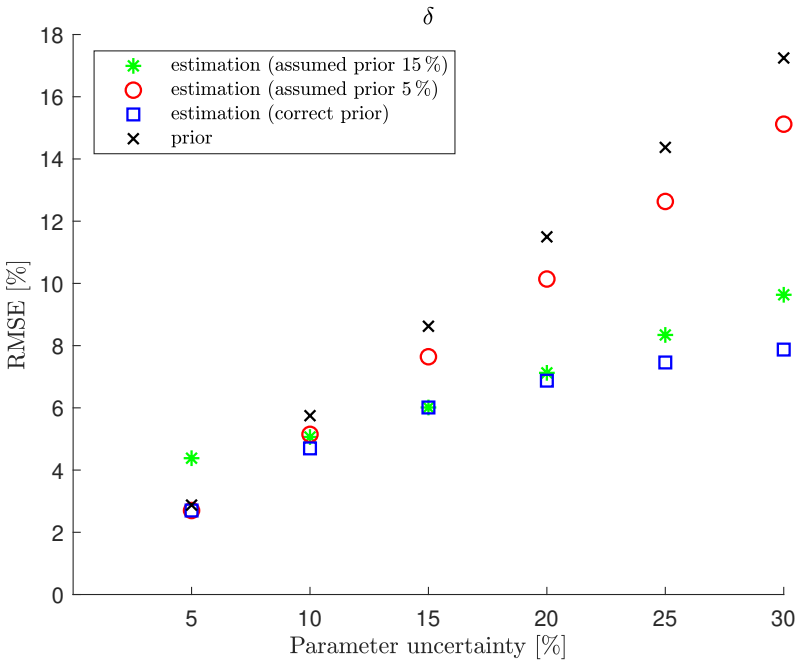

Figure 3.30: RMSE of δ estimation in the presence of prior information mismatch on line parameters.

Chapter 4

Validation of the methodology on grid emulators

For a wider understanding of the potentiality of the estimation method introduced and discussed in the previous chapters, this section presents the next step of the validation analysis. So far, the assessment of the performance has been carried out in MATLAB environment, mainly on benchmark networks (e.g., the IEEE test systems) defined by simplified models, while, in general, it would benefit from more realistic validation possibilities. In this context, software-in-the-loop and hardware-in-the-loop (HIL) would provide the possibility to expand the types and methods of testing, and the simulation of the power system in real-time can also be considered.

In this regard, this section provides an overall view of the performance of the proposed estimation methodology considering in particular:

- Tests carried out by means of grid simulators, as presented in [96].
- Estimation results obtained in the presence of photovoltaic (PV) plants and vehicle-to-grid technology (V2G), as discussed in [97].

The method presented in Section 2.1.3 and applied to a Distribution Network (DN) is discussed and validated. The tests have been performed on the digital twin of the Forschungszentrum Jülich (FZJ) campus. The real grid is connected to the 110 kV DN of North-Rine Westphalia (NRW) and the distribution is performed by means of 10 kV underground cables. The campus is organized in rings (each of them with 3 to 4 buildings). In particular, the low-voltage supply is carried out through 130 MV/LV transformers, in which each side is monitored with class 1 devices (following the specifics of the standard IEC 61036 [98]).

4.1 Validation of the methodology on grid simulators

In the considered tests, the digital twin of the campus runs on the real-time simulator Opal-RT [99] with a time-step of 100 µs. Opal-RT is a simulator capable of design, test and optimize the control and protection of systems used, for example, in power grids before implementing them on the real system. The grid model has been developed relying on nominal data and real measurements collected from the field (these measurements are stored in a database with a time resolution of 5 minutes). Then, the validation of the digital twin is obtained by comparing the voltages and currents measured from all the MV/LV transformers and their corresponding values from the simulated model, using active and reactive power consumption in order to replicate the dynamic behavior of the loads.

Different parts of the network of the campus have been considered. Initially, the analysis has been performed on three buildings connected with a ring scheme to a 10 kV busbar as shown in Fig. 4.1.

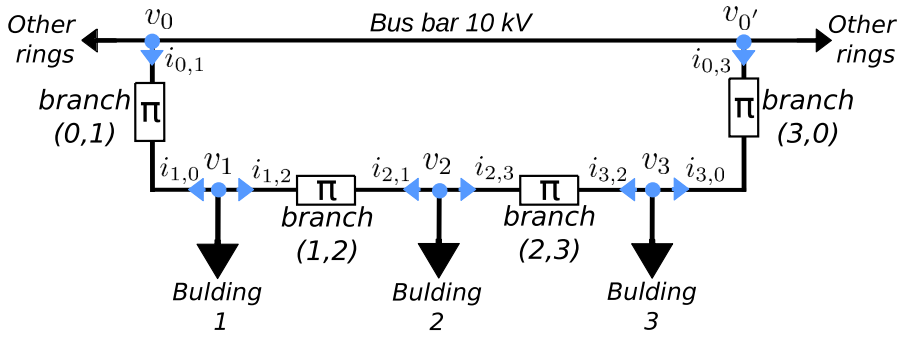

Figure 4.1: Considered section of the FZJ power network.

Then, the three-phase lines have been modeled as π-lines (as in Fig. 2.15) neglecting the mutual capacitance between the lines.

For the validation of the procedure in the real time simulation environment, the three-phase measurements collected from the outputs of the digital twin (running in Opal-RT) have been taken into account as reference values for voltages and currents (indicated in Fig. 4.1 for each node and branch). Starting from the three-phase model, the positive sequence equivalent network has been considered for both grid modeling and voltage and current measurements. IT and PMU uncertainties have been considered, before the application of the described methodology, adding to the reference values of voltages and currents

of the Opal-RT simulation the errors as in (2.1). The estimation performance has been evaluated considering different realistic test cases in a typical working day of July 2017, which is taken as reference load scenario. Active and reactive power consumption for the three considered buildings are shown in Fig. 4.2 considering the MV/LV transformers of each building.

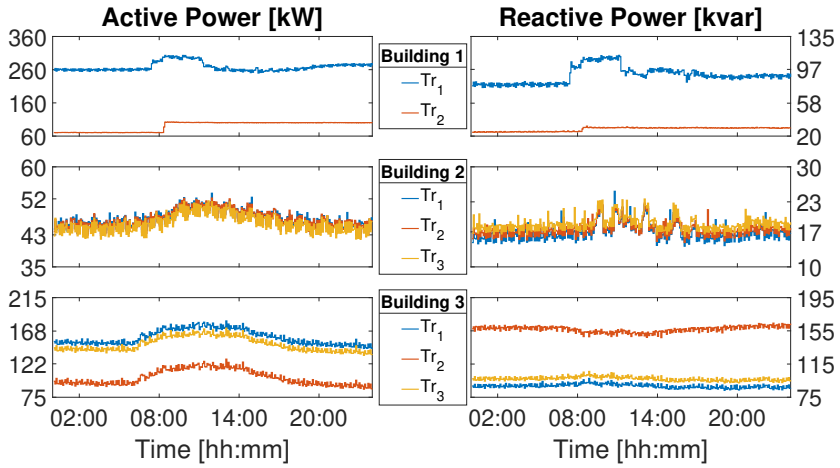

Figure 4.2: Active and reactive power demand of Buildings 1-3.

In the tests, obtained by means of $N_{MC} = 5000$ MC trials and considering all the branches of the grid under analysis, the following set-up has been used:

- Maximum deviations of line parameters equal to $\pm 15\,\%$.
- PMUs of accuracies "PMU01", "PMU05" and "TVE1".
- ITs of Class 0.2 and 0.5.
- 24-hour simulation, as divided into intervals of 1 hour each. Thus, due to the time resolution of the measurements stored in the database, 12 different variations of load occur for each hour (i.e., $C = 12$).

All the PMUs, ITs and line parameter errors have been extracted from uniform distributions.

For each hour an estimation according to (2.29) has been performed.

4.1.1 Validation results

The results for the time of the day between 9:00 and 10:00 am are shown in Table 4.1. In particular, RMSEs of series line parameters have been evaluated for all the branches of the grid with ITs of accuracy Class 0.2 and for both PMU01 and PMU05[1]. It has to be underlined that, when PMU accuracy degrades,

[1]In this section, the results of γ, β and δ will be referred to the pair of nodes associated with the estimated branch: i.e., $\gamma_{i,j}$, $\beta_{i,j}$ and $\delta_{i,j}$

Table 4.1: Estimation performance under different measurement uncertainty scenarios - line parameters

IT class	**PMU accuracy**	**RMSE** [%]							
		$\gamma_{0,1}$	$\beta_{0,1}$	$\gamma_{1,2}$	$\beta_{1,2}$	$\gamma_{2,3}$	$\beta_{2,3}$	$\gamma_{3,0}$	$\beta_{3,0}$
0.2	PMU01	4.71	5.11	4.92	5.19	5.22	5.30	4.79	5.15
	PMU05	5.52	5.80	6.76	6.48	7.72	7.07	5.81	6.18

the degradation of RMSEs ranges between 12 % and 32 %. Another important aspect is that the impact of ITs is limited thanks to the estimation of their contributions to the measurement error. Without a proper treatment of these errors the RMSEs can exceed the prior values. Similar considerations can be drawn focusing on the percentiles of the absolute values of these estimation errors. In particular, if ITs of Class 0.2 and PMU01 are considered, the 90th percentile is always less than 9 %.

Other tests, whose results can be found in Table 4.2, have been carried out considering, for different IT classes and with PMU05, the estimates for magnitude and phase-angle systematic errors of voltages (ξ_h and α_h) and currents flowing from the start node ($\eta_{i,j}$ and $\psi_{i,j}$). In particular, the application of the methodology halves the ξ_h and α_h estimation errors with respect to the accuracy class limits. For $\eta_{i,j}$ and $\psi_{i,j}$ estimation results, the most significant improvement is on branch $(2, 3)$ where a RMSE improvement of about 31 % can be observed.

Table 4.2: Estimation performance under different IT uncertainty scenarios - systematic errors

		Voltage measurements - RMSE							
IT class	**PMU accuracy**	ξ_0 [%]	α_0 [crad]	ξ_1 [%]	α_1 [crad]	ξ_2 [%]	α_2 [crad]	ξ_3 [%]	α_3 [crad]
0.2	PMU05	0.06	0.09	0.06	0.09	0.06	0.09	0.06	0.09
0.5	PMU05	0.15	0.17	0.15	0.17	0.15	0.17	0.15	0.17
		Current measurements - RMSE							
IT class	**PMU accuracy**	$\eta_{0,1}$ [%]	$\psi_{0,1}$ [crad]	$\eta_{1,2}$ [%]	$\psi_{1,2}$ [crad]	$\eta_{2,3}$ [%]	$\psi_{2,3}$ [crad]	$\eta_{3,0}$ [%]	$\psi_{3,0}$ [crad]
0.2	PMU05	0.09	0.15	0.11	0.13	0.08	0.16	0.09	0.13
0.5	PMU05	0.21	0.39	0.25	0.38	0.20	0.39	0.21	0.37

For sake of a comprehensive view of the achievable estimation results, other tests have been carried out on another portion of the digital twin of the FZJ campus (considering other four buildings) shown in Fig. 4.3 [97]. In particular, to further demonstrate the potentialities of the methodology presented in

Chapter 2, in this tests, smart meters (SMs) with synchronized measurement capability have been considered [100]. Indeed, devices that provide synchronized phasor measurements with respect to a common time reference [101, 102] can bring, in some cases, similar benefits to PMU measurements [103] and are often well-suited for DSs. Also in this case, a summer working day of July 2017 has been considered as a base load scenario. In what follows, data and results associated with this scenario will be referred to as "*Base*". Assumptions as those described for the previous tests have been made on how reference values of voltages and currents, errors and line parameters variability have been taken into account.

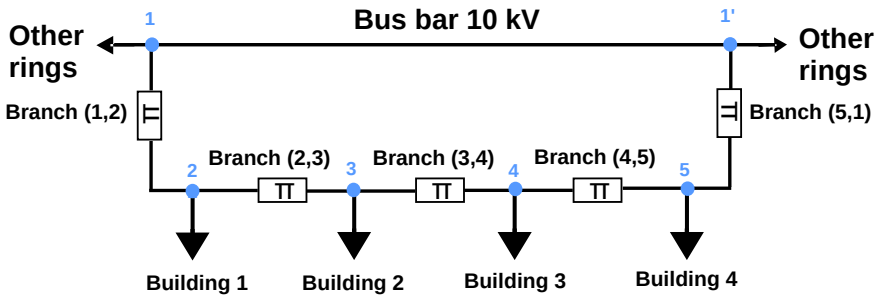

Figure 4.3: Section of the FZJ power network monitored with SMs.

For SMs, two accuracy levels have been considered. The first one is characterized by an accuracy equal to $\pm 0.1\,\%$ and $\pm 0.1\,\mathrm{crad}$ for magnitude and phase-angle measurement (of both voltage and current), respectively, and it is referred to as "SM01". The second one, indicated as "SM02" in the following tests, has double error limits than "SM01".

Table 4.3 reports the estimation results for $\eta_{i,j}$, $\psi_{i,j}$, $\gamma_{i,j}$ and $\beta_{i,j}$ of the branches $(1,2)$, $(2,3)$, $(3,4)$ and $(4,5)$ of the grid in Fig. 4.3, considering the "*Base*" load scenario and measurement uncertainty "SM01" for the time of the day between 08:00 and 09:00 am. In particular, the RMSE results are reported considering the inclusion, or exclusion, of the injection constraints (see, for details, (2.31)) associated with Building 1. It has to be noticed that, considering or not the injection constraint, the RMSEs of the systematic measurement errors of the currents are below the prior values and, in addition, the considered injection constraint brings, as expected, a significant improvement (in the range between $20 - 35\,\%$) for the branches $(1,2)$ and $(2,3)$ that are adjacent to Building 1. Focusing on line parameters estimation, it is possible to see that the results are not significantly affected by the introduction of the injection constraint equation (2.31) since this constraint is mainly related to CT errors.

Table 4.3: Comparison of the estimation performances with and without injection constraint

	RMSE							
Injection Constraint	$\eta_{1,2}$ [%]	$\psi_{1,2}$ [crad]	$\eta_{2,3}$ [%]	$\psi_{2,3}$ [crad]	$\eta_{3,4}$ [%]	$\psi_{3,4}$ [crad]	$\eta_{4,5}$ [%]	$\psi_{4,5}$ [crad]
NO	0.20	0.37	0.20	0.37	0.21	0.38	0.20	0.37
YES	0.14	0.24	0.16	0.27	0.20	0.38	0.20	0.37
Injection Constraint	$\gamma_{1,2}$ [%]	$\beta_{1,2}$ [%]	$\gamma_{2,3}$ [%]	$\beta_{2,3}$ [%]	$\gamma_{3,4}$ [%]	$\beta_{3,4}$ [%]	$\gamma_{4,5}$ [%]	$\beta_{4,5}$ [%]
NO	5.01	5.43	8.49	8.40	4.81	5.19	6.66	5.99
YES	4.97	5.36	8.51	8.27	4.80	5.13	6.41	5.87

4.2 Photovoltaic and Vehicle-to-Grid technologies: impact on the estimates

In this section, further analyses are presented to discuss estimation performance in the presence of modern technologies like PV plants and V2G charging stations, which are getting everyday more common in DSs.

It is worth mentioning that the considered PV system was still not installed in the field at the considered time, but it was simulated according to the nominal data of the installation planned for the considered ring. Thus, active and reactive powers generated by the PV plant have been obtained by considering a nominal power of 100 kVA, with a constant power factor of 0.95, and weather data, i.e. ambient temperature and solar radiance, of the above-mentioned day. In the following tests, the results of this scenario will be always referred to as "*PV*". In the tests performed for the scenarios including V2G, 4 electric vehicles (EVs) have been represented by means of the demand/supply of their batteries, working in charging/discharging mode [104]. The EVs are assumed to be connected to bi-directional charging stations and, thus, able to operate in V2G mode. More specifically, the Tesla Model S [105] has been considered with a maximum battery capacity of 85 kWh. In particular, EVs are assumed to be charged (or discharged) in around 7 hours (in line with the typical duration of a working day). In the following tests, "*V2G-Ch*" and "*V2G-Disch*" indicate the charging and discharging modes, respectively. "*PV*", "*V2G-Ch*" and "*V2G-Disch*" scenarios have been realized considering the technology installed in Building 1. In addition, the injection constraint for Building 1 has been considered in the estimation problem. For all these scenarios, the same procedure and implementation details presented in Section 4.1 are used to obtain the estimation of line parameters.

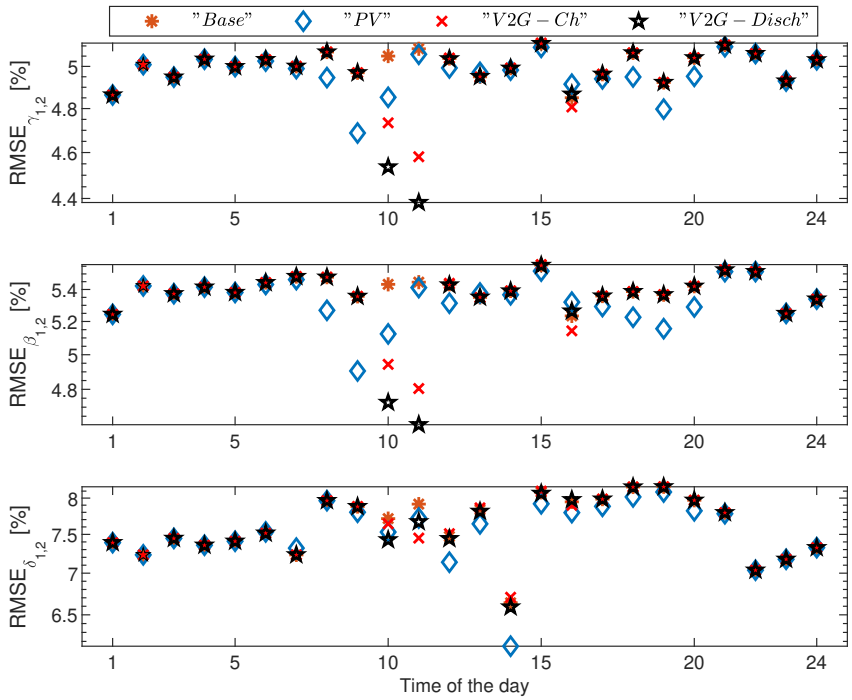

Figure 4.4: Line parameters estimation results of branch $(1, 2)$ in different scenarios.

Figure 4.4 shows the RMSEs for the estimation of line parameters of branch $(1, 2)$, considering all the above-define scenarios and for all the time intervals of the working day considered. The "Time of the day" on the x-axis represents the hour of day at which the methodology is applied and thus the associated interval (e.g., 19 is the interval between 18:00 and 19:00 AM).

In Fig. 4.4, values corresponding to *Base*, *PV*, *V2G-Ch*, and *V2G-Disch* are indicated with red asterisks, blue diamonds, red crosses and black stars, respectively. Focusing on the results, it can be highlighted that the main differences in the estimations can be observed, as expected, when PV plant or V2G are assumed to participate in the power-flows. More specifically, the differences are in the interval between 06:00 and 20:00 AM for *PV*, and between 09:00 and 16:00 AM for *V2G-Ch* (or *V2G-Disch*). Thus, on one hand, the presence of PV generation is characterized by RMSEs for γ, β, and δ estimation generally lower than those calculated in the *Base* case. The reason is the introduction, especially in the hours with high production of the PV plant, of a higher variability of the power-flows, helping the improvement of the estimation with a better "independence" in the constraints given by the C cases. On the other hand, the presence of V2G leads to the absolute lowest RMSEs in specific intervals. In particular, focusing on the estimation of the longitudinal parameters,

Table 4.4: Comparison of estimation performance for different scenarios and hour of the day

Time of the day	**Scenario**	**Accuracy**	**RMSE**					
			$\gamma_{1,2}$ [%]	$\beta_{1,2}$ [%]	$\delta_{1,2}$ [%]	$\gamma_{3,4}$ [%]	$\beta_{3,4}$ [%]	$\delta_{3,4}$ [%]
from 09 : 00 to 10 : 00	"$Base$"	SM01	5.05	5.43	7.71	4.78	5.14	5.18
	"PV"		4.85	5.12	7.53	4.72	4.99	5.07
	"$V2G-Ch$"		4.73	4.94	7.64	4.65	4.85	5.46
	"$V2G-Disch$"		4.54	4.73	7.43	4.56	4.75	4.51
	"$Base$"	SM02	5.31	5.83	8.32	5.04	5.50	6.71
	"PV"		5.15	5.57	8.26	5.04	5.44	6.66
	"$V2G-Ch$"		5.12	5.54	8.29	5.01	5.36	6.84
	"$V2G-Disch$"		4.89	5.16	8.23	4.99	5.25	6.30
from 10 : 00 to 11 : 00	"$Base$"	SM01	5.09	5.45	7.91	4.78	5.14	5.27
	"PV"		5.06	5.41	7.72	4.77	5.13	5.56
	"$V2G-Ch$"		4.58	4.80	7.45	4.64	4.85	4.82
	"$V2G-Disch$"		4.38	4.60	7.67	4.48	4.69	4.56
	"$Base$"	SM02	5.31	5.84	8.38	5.04	5.52	6.81
	"PV"		5.29	5.80	8.31	5.03	5.52	6.99
	"$V2G-Ch$"		4.93	5.31	8.24	5.05	5.41	6.53
	"$V2G-Disch$"		4.72	4.98	8.29	4.95	5.19	6.39

V2G-Ch presents the best results in correspondence of the 16-th interval while *V2G-Disch* in the 10-th and 11-th. This can be explained by the fact that, V2G scenarios have charging and discharging modes of EVs characterized by strong variations of load or generated powers and this helps the estimation process for the above mentioned reason. More specifically, these variations influence the power-flows (voltage and current profiles) bringing lower (or higher) voltage drops according to the considered scenario.

To sum up and conclude, Table 4.4 shows the line parameters estimation results for branches $(1, 2)$ and $(3, 4)$ and different SM accuracies and time intervals. In Table 4.4 the results basically confirm the conclusions drawn by the previous analyses: PV and V2G permit having lower errors with respect to the *Base* case in all of the considered conditions. For $\beta_{1,2}$ estimation, considering the 10-th time interval and SM01, *V2G-Disch* scenario leads to an improvement of about 13 % with respect to *Base* case, while for PV and *V2G-Ch* the improvement is 6 % and 9 %, respectively. Focusing on SM accuracy, it is possible to observe that, despite the fact that, as expected, when SM02 accuracy is considered, the performance decreases with respect to SM01, the trends for both SM accuracies are the same.

As a general comment, it is possible to highlight that the presence of PV and V2G positively affects the estimation performance, due to the presence of

both higher variability and strong variations of the power-flows.

According to the above results, the conclusion is that the presented method can benefit from the dynamics introduced by PV and V2G. In this regard, the operator, on the basis of its own experience and of expected network load profiles, can define guidelines for the application of the methodology, customizing it for the specific load or generator conditions and the technologies installed in the grid.

Chapter 5

Benefits of the application of the proposed method: fault location

5.1 PMU-based fault location

In the context of modern power systems, the fault detection and location is one of the most important challenges since it regards critical operating conditions and high currents flowing in the grid. In order to reduce issues associated with these critical conditions, the fault should be extinguished quickly. Accurate and fast fault location is essential to reduce the maintenance time and the restoration costs and obtaining the desired efficiency in power systems.

In literature, one of the most used fault location criterion is based on impedance matrix [106]. The corresponding methods rely on Kirchhoff's laws and, for the resolution of the problem, the measurements before and after the occurrence of a fault are taken into account. Most of the latest methodologies address the fault location based on synchronized measurements provided by PMUs and/or SMs [107–110], as it is now recognized that synchronized measurements can significantly help these applications.

In this context, a critical point common to basically all methods in the literature is that of an underestimation of the uncertainty related to the measurement chain, which is instead a fundamental aspect in the fault detection and location process. In this regard, few proposals for fault location designed for DNs face the problem, considering also a given level of uncertainty (see, as an example, [111–115]). In particular, [111] proposes a fault location method based on power system status estimation evaluated by means of PMUs. In this paper, the

method is tested by means of a sensitivity analysis considering different network loading states and varying PMU number and accuracy. In [112], a single-phase approach is presented to identify event locations (occurrence of power quality events or changes in the state of the switches). Different values of uncertainties in current phasor measurements, line parameters and pseudo-measurements have been considered. In particular, possible deviations in line parameters have been assumed in the range between ±10 % to ±50 %. The extension of [112] for three-phase power systems has been presented in [113], with a more in-depth analysis on several aspects regarding the uncertainty of input data to the algorithm. In this paper, the authors, based on field experience and manufacturers' data-sheets, assume that in distribution power systems PMUs have high accuracy (i.e., ±0.01 % in magnitude and ±0.003° in phase-angle). For this reason, they emphasize that, in practice, errors in the measurement chain are basically associated with ITs. As a result of that, in [113], CTs and VTs errors are roughly constant for consecutive measurements made over a short period of time. This makes the authors conclude that measurement differences at the same location are not significantly influenced by measurement errors. In [114], an algorithm for the detection and location of faults based on pre- and during-fault measurements is presented. In this paper, current measurements are not used in the process of fault location to rule out the CT saturation and related inaccurate measurements. As for voltage measurements, zero-mean Gaussian noises with standard deviations equal to 2 % and 0.1° for magnitude and phase-angle errors, respectively, have been considered as worst case. The same noise type with a 10 % standard deviation is instead assumed for line impedance uncertainty.

In [115], a graph-based fault location method for DSs has been presented. The algorithm works with distribution system state estimations (DSSEs) integrating limited PMU measurements. Only during-fault PMU data are considered. However, the method is tested considering PMU measurements with an error of 2 % in magnitude and 0.02 rad for phase-angles as worst case, while assuming the maximum errors of pseudo-measurements as 50 %. Maximum variations in line parameters variation ranges from 2 % to 10 %.

DSSE is also the base process to detect fault in [116] and [117]. In [117], the same approach presented in [116] is applied using the minimum necessary number of PMUs. Both papers consider the knowledge on line parameters to be exact and, in addition, a measurement chain based on experimental data provided by a particularly accurate measurement infrastructure.

5.2 Integration of the proposed estimation method in fault location

It is clear that an accurate knowledge of line parameters is one of the most important factors for the success of monitoring and control applications and, among them, of the fault location methods. This is the reason why the methodology discussed in the previous sections appears promising to improve accuracy and efficacy of fault location algorithms [3]. To address this problem, this chapter presents the application of the previously discussed line parameters estimation algorithm to design an enhanced three-phase fault detection and location method.

In particular, the integration of the methodology presented in previous sections in a fault location algorithm introduced in literature (presented in [116] and modified in [117]) is analyzed [118]. This algorithm is interesting to study because it merges monitoring and protection applications, basing fault detection on distribution system state estimation results. Therefore, the idea is to obtain information on the possible presence of faults from an established network monitoring procedure running in a grid monitoring center, potentially before there is an actual fault notification from a protection system. In this scenario, in-depth analyses have been carried out to understand how the accuracy of grid information and available data can influence this type of network monitoring.

One of the main contributions to the improvement of the procedures [116] and [117] has been obtained using the outputs of the three-phase line parameters and systematic measurement errors estimation of Section 2.2.3, thus getting better knowledge on the line parameters and better fault location results. Moreover, another critical aspect that has been considered concerns the monitoring system capable of providing data in the presence of a fault and its uncertainty. For these studies, the idea has been therefore to feed the state estimation algorithm with data provided by a protection system. Finally, the impact of the corresponding large measurement uncertainties on the fault location performance has been analyzed.

It is important to emphasize that the proposed procedure is not intended to replace existing protection systems, but it aim at integrating information provided to the system operator, which are needed particularly when challenging faults occur in the system, such as those non-destructive or, in general, difficult to detect.

The validation of the presented enhanced fault location method has been carried out considering the three-phase version of the CIGRE European Medium Voltage distribution network, simulated in a Real Time Digital Simulator (RTDS)

in combination with the associate software RSCAD.

5.2.1 Problem definition and proposed solution

The fault location method is intended for a three-phase DSSE equipped with PMUs, which monitor node voltages and nodal currents in all the grid buses of the network. This assumption can be considered realistic in smart grids, the next generation of distribution grids, and permits the analysis to be focused on the impact of the measurement chain. For the distribution network lines, a three-phase π-model (see Fig. 2.15) is considered. The problem, differently from [116] and [117], is investigated by assuming a measurement chain composed of protection transformers and class P PMUs, i.e., the key elements of an advanced protection system, which makes the assumption of such pervasive monitoring on the network even more realistic. Line parameters are supposed known with a given level of uncertainty and, as a consequence, uncertainty has been associated also with the nodal admittance matrix $\mathbf{Y}$.

A three-phase power grid with n buses and N_{br} branches can be described with the state vector $\mathbf{x_v}$:

$$\mathbf{x_v} = [\mathbf{V}_{1,r}^{abc\intercal}, \mathbf{V}_{1,x}^{abc\intercal}, ..., \mathbf{V}_{n,r}^{abc\intercal}, \mathbf{V}_{n,x}^{abc\intercal}]^\intercal \tag{5.1}$$

where $\mathbf{V}_{i,r}^{abc}$ and $\mathbf{V}_{i,x}^{abc}$ represent, for the bus i, the real and imaginary parts of the three-phase voltage vectors, respectively. For the state estimation, the measurement vector $\mathbf{z}$ used as input is defined as:

$$\mathbf{z} = \left[\mathbf{z}^{v\intercal}, \mathbf{z}^{i\intercal}\right]^\intercal \tag{5.2}$$

where $\mathbf{z}^v$ and $\mathbf{z}^i$ represent the nodal voltage and current measurements (real and imaginary parts). The state $\mathbf{x_v}$ can be related to the measurements according to the following equation:

$$\mathbf{z} = \mathbf{H}\mathbf{x_v} + \mathbf{e_{x_v}} \tag{5.3}$$

where $\mathbf{H}$ is the measurement matrix linking $\mathbf{x_v}$ to the voltage and current measurements, while $\mathbf{e_{x_v}}$ is the measurement error associated with the uncertainties of the entire measurement chain.

The estimated state vector $\hat{\mathbf{x}}_\mathbf{v}$ is obtained by applying the WLS method, which formally corresponds to finding:

$$\hat{\mathbf{x}}_\mathbf{v} = \left(\mathbf{H}^\intercal \mathbf{W}_{\mathbf{x_v}} \mathbf{H}\right)^{-1} \mathbf{H}^\intercal \mathbf{W}_{\mathbf{x_v}} \mathbf{z} \tag{5.4}$$

where the weight matrix $\mathbf{W}_{\mathbf{x_v}}$ is chosen as the inverse of the covariance matrix of measurements.

The evaluation metric associated with the state estimation process is the Weighted Measurement Residual (WMR), which, for an estimation at time in-

stant t, can be calculated as:

$$w_t = \sqrt{(\mathbf{z} - \mathbf{H}\hat{\mathbf{x}}_\mathbf{v})^\intercal \mathbf{W}_{\mathbf{x_v}} (\mathbf{z} - \mathbf{H}\hat{\mathbf{x}}_\mathbf{v})} \tag{5.5}$$

and represents the objective function of the state estimation process.

The algorithm in [116, 117] consider that, for fault location purposes, the presence of a fault causes a change in the grid topology. In particular, considering a branch (i, j), the fault point at distance p from node i is represented by means of a virtual bus as shown in Fig. 5.1, which means that, in the grid, an additional bus must be taken into account. This virtual bus $n + 1$ absorbs, through the fault resistance R_f, the fault current.

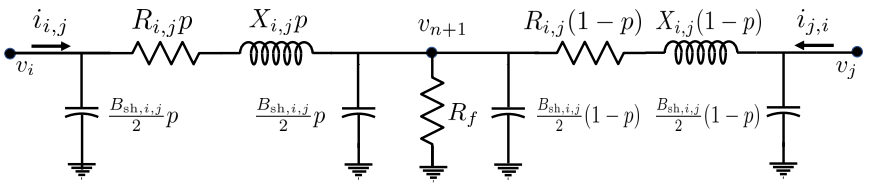

Figure 5.1: Equivalent model of the fault in a generic branch.

For fault location, the idea is to run N_{br} parallel state estimators like (5.4), each of them assuming the presence of the fault in the center of a specific branch. It has to be noticed that, in absence of specific information, different assumptions about the position of the fault can be done but here the simplest choice is to suppose the fault in the middle of the line [116], [117]. Thus, each of the N_{br} state estimations is then associated with an augmented nodal admittance matrix $\mathbf{Y}^{s_{i,j}}$ (where $s_{i,j} \in \{1, ..., N_{br}\}$ is the index of the branch split in the middle of its end nodes (i, j)), thus dealing with an augmented topology with $n+1$ buses. According to the findings of [116], in normal operating conditions, the WMRs are all very close to each other. On the contrary, if a fault occurs, the WMR considering the virtual bus in the faulted branch results in the lowest value. This applies in the absence or with a low level of uncertainty, but, when uncertainty sources occur in the system (related to line parameters, modeling or measurements uncertainty etc.), the problem requires a different approach, as also underlined in [117].

In realistic conditions, it can be useful to consider WMRs in case of both original and augmented topology, indicated as w_t^0 and $w_t^{s_{i,j}}$, respectively. The fault location procedure is composed of two phases:

- The detection of the fault is performed to notify the system operator that a fault in the system is present.

- The location of the fault is performed to find out the faulted branch among all the branches of the considered grid.

The first step of the procedure is carried out when a strong variation $(w_t^0 - w_{t-1}^0)$, between two consecutive time instants, is detected. In particular, a fault event is raised at the time instant t_{F} when:

$$\left|w_{t_{\mathrm{F}}}^0 - w_{t_{\mathrm{F}}-1}^0\right| > th_w^0 \cdot \mu_{w_{\mathrm{PF}}}^0 \tag{5.6}$$

In (5.6), th_w^0 is a positive threshold, the subscript $_{\mathrm{PF}}$ indicates the pre-fault operating conditions and $\mu_{w_{\mathrm{PF}}}^0$ is the mean of WMRs obtained considering N_{PF} pre-fault evaluation instants and the original topology.

After the detection of the fault, the location is obtained analyzing the N_{br} parallel state estimations obtained considering the nodal admittance matrix $\mathbf{Y}^{s_{i,j}}$ and the corresponding updated measurement matrix $\mathbf{H}_+$ for each branch. The generic augmented state vector can be estimated according:

$$\hat{\mathbf{x}}_{\mathbf{v}^+} = \left(\mathbf{H}_+^{\intercal}\mathbf{W}_{\mathbf{x_v}}\mathbf{H}_+\right)^{-1}\mathbf{H}_+^{\intercal}\mathbf{W}_{\mathbf{x_v}}\mathbf{z} \tag{5.7}$$

Once the augmented estimated state vectors are obtained, it is possible to evaluate each of the N_{br} parallel state estimations $w_t^{s_{i,j}}$ like in (5.5) and to obtain the location of the faulted branch s_{ij_F} evaluating:

$$s_{i,j_F} = \arg\min_{s_{i,j}} \left|w_{t_{\mathrm{F}}}^{s_{i,j}} - \mu_{w_{\mathrm{PF}}}^{s_{i,j}}\right| \tag{5.8}$$

In (5.8), $w_{t_{\mathrm{F}}}^{s_{i,j}}$ is the WMR obtained for the time instant t_{F} and the nodal admittance matrix $\mathbf{Y}^{s_{i,j}}$, while $\mu_{w_{\mathrm{PF}}}^{s_{i,j}}$ defines the mean of N_{PF} pre-fault WMRs.

5.2.2 Procedure for fault location on grid simulators

The presented method has been validated by means of different tests carried out on the three-phase version of the CIGRE European MV distribution network, rated frequency of 50 Hz [119], shown in Fig. 5.2 and simulated in RTDS environment. RTDS [120] is a power system simulator capable of reproducing power system dynamics, from DC up to 3 kHz and thus of providing realistic operating conditions before and after the occurrence of a fault. RTDS can also provide synchronized phasors of voltages and currents on the nodes of the network. These synchrophasors, obtained from the RTDS component "GTNET-PMU24" and based on the P-class algorithm suggested in [121], have been considered as the basis for all the measurements in this study.

In particular, RTDS generates the reference values of voltage and current measurements starting from the active and reactive power profiles. These measurements are provided for the operating conditions before and after the occurrence of the fault and, once the reference values are obtained, measurement errors are added to these values according to the the uncertainty configuration

considered (see, for details, the next Section). For the application of the line parameters estimation method, a procedure like that of Section 4.1 is carried out.

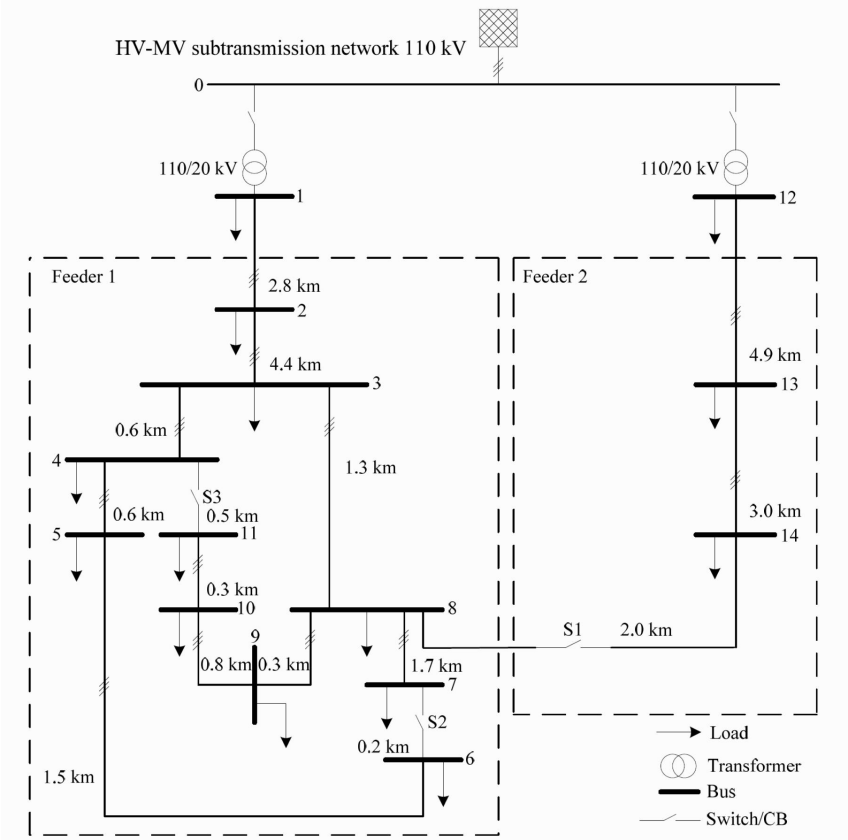

Figure 5.2: CIGRE European MV distribution network.

5.3 Performance assessment of the improved fault detection and location

The faults have been simulated considering fixed load operating conditions for both pre- and post-fault scenarios and assuming resistive faults. For the fault analysis, in order to exploit significant data from PMUs, the measurements have been acquired at the end of the activation transient of the fault (post-fault condition).

To test the advantages of including the line parameters and systematic measurement errors estimation method presented in Chapter 2, single-phase to

ground fault (which is the most frequent fault in power distribution systems [106]) has been considered, assuming it can occur at different branches and positions within the branch, and with different fault resistances. In what follows, this fault type is indicated as $\mathrm{LG}_{p_\mathrm{F}}$ with $p_\mathrm{F} \in \{a, b, c\}$ the system phase.

The two level of uncertainties assumed in [116] for the fault detection and location are indicated as M_1 and M_2 and described in Table 5.1.

Table 5.1: Comparison of uncertainty configurations from literature

Accuracy	σ_{V_ξ} [%]	σ_{V_α} [crad]	σ_{I_η} [%]	σ_{I_ψ} [crad]	$\sigma_{I_{\eta_P}}$ [%]	$\sigma_{I_{\psi_P}}$ [crad]
M_1	0.0016	0.0051	0.4	0.58	4	5.8
M_2	0.016	0.051	4	5.8	12	17

In this thesis, the operating conditions and measurement uncertainties considered for the test set-up are instead:

- Line parameters maximum deviations are equal to $\pm 15\,\%$.
- Normal operating conditions used for the application of the line parameters estimation method have a variability of $\pm 10\,\%$ with respect to nominal values for both active and reactive powers.
- $N_\mathrm{PF} = 10$ and $th_w^0 = 1$.
- ITs of the measurement chain are for protection purposes. In particular, VTs are of Class 3P [122], and have maximum errors of $3\,\%$ and $3.5\,\mathrm{crad}$ for ratio error and phase-angle displacement error (for both pre-fault and post-fault scenarios), respectively. CTs are considered to be of Class 5P [123]: in steady-state conditions (pre-fault), they are assumed to have maximum ratio and phase-angle errors of $1\,\%$ and 1.8 crad, respectively. The post-fault condition is followed with maximum errors of $3.54\,\%$ for magnitude and 3.54 crad for phase-angle (i.e., they reach a composite error of $5\,\%$).
- PMUs in steady-state conditions have maximum magnitude error of $0.1\,\%$ and maximum phase-angle error of $0.1\,\mathrm{crad}$, whereas, in post-fault condition, they have a maximum TVE of $3\,\%$.

Fourth and final items of the tests assumptions are supposed to represent realistic uncertainty behavior of the measurement chain that is required to follow signal dynamics in the transition between pre-fault (basically steady-state) and post-fault (unknown dynamics) conditions. This uncertainty configuration will be indicated as M_3 and, when no other information except the data-sheets is

available, it is applied to all the measurements on all the nodes of the considered grid.

In Table 5.1 [116], the measurement errors are indicated in terms of standard deviations summarizing the combination of measurement transducers and PMUs. In particular, σ_{V_ξ}, σ_{V_α} and σ_{I_η}, σ_{I_ψ} are the standard deviations for amplitude and phase-angle errors of voltages and currents, respectively. In addition, this table provides also the standard deviations adopted for the combination of current protection transducers and PMUs assumed to be installed in the buses at the low voltage side of the 110/20 kV transformers in Fig. 5.2: $\sigma_{I_{\eta_P}}$ and $\sigma_{I_{\psi_P}}$ are the corresponding ratio and phase-angle errors of current measurements.

To validate statistically the results, tests have been performed considering $N_{MC} = 5000$ trials and, in absence of specific information, possible deviations in the values of all the parameters involved and measurement errors are extracted from uniform distributions. The methodology of Section 2.2.3 has been applied during normal operating conditions and assuming measurement errors related to steady-state conditions. The performance of the enhanced fault identification algorithm is evaluated considering the number of the correct locations of the faulted line N_{Loc} with respect to all the MC trials. The associated index L is obtained as:

$$L = 100 \times \frac{N_{Loc}}{N_{MC}} \tag{5.9}$$

In the tests, different estimation approaches have been evaluated and compared and the following indices represent their performance:

- L_{LPE} (the proposed method), indicating the fault location that uses the outputs of the method in Section 2.2.3 (i.e., the estimated line parameters) to update the nodal admittance matrix $\mathbf{Y}$ (and $\mathbf{Y}^{s_{i,j}}$), and assuming as maximum uncertainty level the actual one.

- L_{DSO}, indicating the fault location that uses the nodal admittance matrix obtained from the values available from the network operator database (in this case DSO) and assuming as maximum uncertainty level the actual one.

- $L_{DSO_{M_2}}$, indicating the fault location that uses the same nodal admittance matrix of L_{DSO} and, in addition, it assumes always as maximum uncertainty level M_2.

- L_{Act}, indicating the fault location that uses the best possible knowledge of $\mathbf{Y}$ (and $\mathbf{Y}^{s_{i,j}}$), i.e., the actual value of the nodal admittance matrix and it considers as maximum uncertainty level the actual one. It will be used as benchmark method.

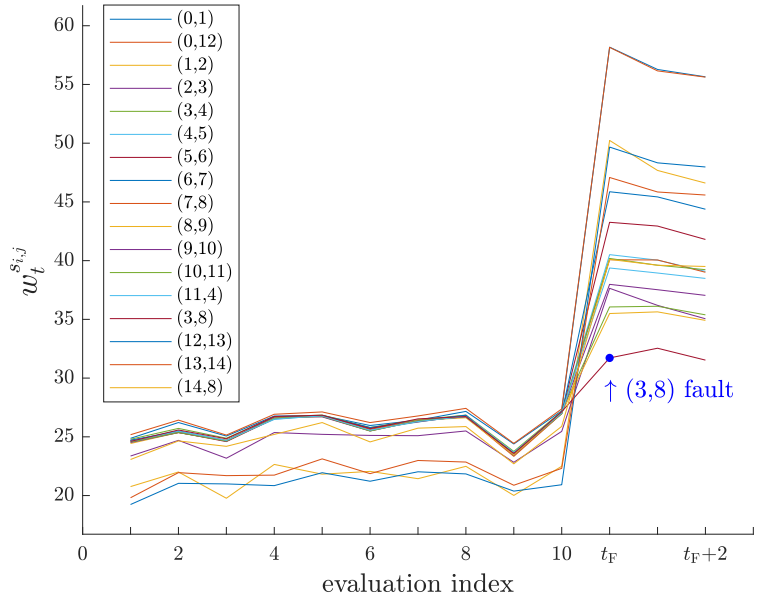

Figure 5.3: L_{DSO}, WMRs of the state estimations considering M_2, fault on branch $(3, 8)$, $R_f = 100\,\Omega$.

The first series of tests have been performed in order to evaluate the impact of possible deviations of the line parameters. Since the fault detection and location algorithm relies on the WMRs evaluation, understanding the impact of a possible uncertainty on line parameters on the WMR is a key point. Figures 5.3 and 5.4 show for the branch $(3, 8)$, considering $R_f = 100\,\Omega$, M_2 and $p = 0.5$, the trends of $w_t^{s_{i,j}}$ for L_{DSO} and L_{LPE}, respectively. In the figures, "evaluation index" is the index of the retained evaluation instants related to the considered pre- and post-fault instants. It is worth underlining that the time interval between consecutive instants represents the PMU reporting rate, but a time gap exists between steady-state pre- and post-fault useful measurements. From Fig. 5.3, it is possible to see that L_{DSO} has variable trends for $w_t^{s_{i,j}}$. On the contrary, in Fig. 5.4, L_{LPE} has almost identical pre-fault $w_t^{s_{i,j}}$. Moreover, in post-fault conditions, the faulted branch keeps a $w_t^{s_{i,j}}$ substantially unchanged compared to those obtained in pre-fault conditions.

This behavior can be explained by the fact that L_{LPE} allows, in general, a better reproduction of the actual nodal admittance matrix, which affects the WMRs and, as a consequence, a better reproduction of the actual network. Thus, the resulting estimates are more accurate leading to an improvement of the fault location performance. Table 5.2 shows the fault location results considering a fault resistance $R_f \in \{10\,\Omega, 100\,\Omega\}$ (0.625 and 6.25 pu, respectively), fault

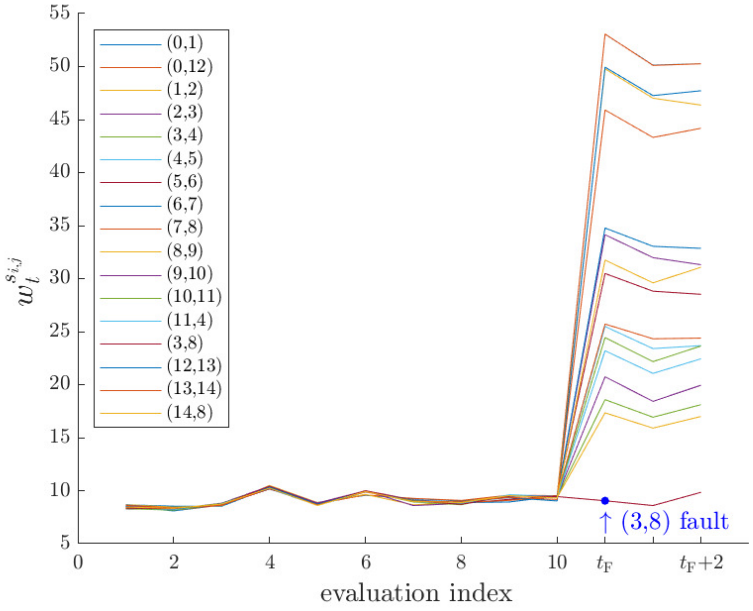

Figure 5.4: L_{LPE}, WMRs of the state estimations considering M_2, fault on branch $(3, 8)$, $R_f = 100\,\Omega$.

position that occurs halfway or at a quarter of the branch ($p = 0.5$ and $p = 0.25$ are the distances relative to the line length), and uncertainty configuration M_2. It has to be noticed that same tests have been carried out also with M_1, but similar results are obtained and, thus, they are not reported in the table, as well as the results of $L_{DSO_{M_2}}$, since it obviously produces, in this configuration, the same results of L_{DSO}. In this context, it is worth underlining that a fault position of $p = 0.25$ represents a mismatch on the assumption at the base of the N_{br} augmented topologies used for DSSEs.

In Table 5.2, it is possible to notice that L_{LPE} and L_{Act} have similar results in the considered branches. This behavior can be explained by the fact that, if line parameters are estimated with the presented method, this is enough to have a valid fault location process as if they were accurately known *a priori*. Thus, in the presence of low uncertainty levels line parameters estimation method has a significant effect. In Table 5.2, L_{DSO} has the worst performance: in particular, when a fault occurs with $R_f = 100\,\Omega$ at position $p = 0.25$, L_{LPE} improves with respect to L_{DSO} of about 17 % and 24 % for branches $(9, 10)$ and $(3, 8)$, respectively.

Other tests have been performed to emphasize another important aspect of the fault location problem: the impact on the identification process of a measurement chain typical for protection purposes as M_3. Since the combination

Table 5.2: Location performance for a single-phase to ground fault LG_a, considering M_2 accuracy

Fault position	**Branch**	R_f	**Location** L_{LPE} [%]	L_{DSO} [%]	L_{Act} [%]
$p = 0.5$	$(3,4)$	$10\,\Omega$	100	100	100
	$(9,10)$		100	100	100
	$(3,8)$		100	100	100
	$(3,4)$	$100\,\Omega$	100	98.2	100
	$(9,10)$		100	99.0	100
	$(3,8)$		100	96.2	100
$p = 0.25$	$(3,4)$	$10\,\Omega$	100	100	100
	$(9,10)$		100	98.6	100
	$(3,8)$		100	96.9	100
	$(3,4)$	$100\,\Omega$	100	96.8	100
	$(9,10)$		94.7	77.7	96.6
	$(3,8)$		95.8	70.7	95.9

of high fault resistances and M_3 makes the fault detection and location more challenging and requires specific analyses, the results obtained for a lower fault resistance are discussed. In Table 5.3, the results for M_3 and fault resistance $R_f = 1\,\Omega$ (0.0625 pu) are shown.

Table 5.3: Location performance for a single-phase to ground fault LG_a, considering M_3 accuracy

Fault position	**Branch**	R_f	**Location** L_{LPE} [%]	L_{DSO} [%]	L_{Act} [%]
$p = 0.5$	$(3,4)$	$1\,\Omega$	100	100	100
	$(5,6)$		100	100	100
	$(3,8)$		100	100	100
$p = 0.25$	$(3,4)$	$1\,\Omega$	100	100	100
	$(5,6)$		99.6	97.9	99.6
	$(3,8)$		93.8	92.5	94.8

It has to be noticed that also in these challenging conditions the uncertainty in the line parameters values shows an impact: L_{LPE} and L_{Act} have basically the same results, while L_{DSO} still suffers from the lack of knowledge on the nodal admittance matrix.

The tests in Table 5.3, which are performed considering a measurement chain appropriate for these dynamic conditions, highlight the importance of making the right assumptions on the errors to avoid misinterpreting the actual operating conditions. It can therefore be reiterated that the obtained results confirm the

utility of the application of line parameters estimation in a fault identification process and, the estimation algorithm proves to be valid considering the presence of both measurement and parameters realistic uncertainties.

Conclusions

Power transmission and distribution systems have transitioned and are undergoing significant changes. This evolution requires an enhancement in monitoring and control applications at the basis of an efficient operation of power systems. In this context, management and control of power systems are based on tools that can be affected by many sources of uncertainty. Among these it is possible to mention the uncertainty on the network parameters, on the used network models down to all the sources of uncertainty in the measurement chain.

To reduce the impact of these factors, the research activity carried out for this thesis led to the development of a simultaneous estimation of network (lines and power transformers) parameters and systematic measurement errors, which can be applied to both transmission and distribution systems and in the presence of single-phase or three-phase models of the power grid.

Differently from the literature, the proposed approaches include in the vector of parameters to estimate not only the network parameters but also the systematic errors of all the measurements involved. Another fundamental point is that the framework has been conceived to deal, potentially simultaneously, with all the branches of the grid under test and to leverage the high reporting rate of the PMUs.

The presented algorithms are built considering a monitoring infrastructure composed of Instrument Transformers feeding PMUs, which are assumed to be installed at both ends of each branch, but some tests have been carried out exploiting also other types of devices with synchronized measurement capability. As for the errors of the measurement chain, the general assumption is that random errors are mainly associated with PMUs, while systematic errors are mainly associated with Instrument Transformers, but also more complex errors combination are taken into account and analyzed.

The performance of the proposed algorithms has been evaluated and validated by means of both simulations carried out in MATLAB environment and grid emulators. Moreover, the performance assessment has been carried out also with respect to relevant methods published in literature.

The base version of the algorithms proved to be capable to reduce the uncertainty on network parameters and systematic measurement errors and to be robust under realistic measurement uncertainties and different network conditions.

Then, further analyses have been carried out to understand how the assumptions about the models of the measurement chain and the grid could be improved. Specifically, the methodology has been tested by assuming different types of mismatches on the base assumptions. Based on the results obtained, the methods have been improved with the integration of more detailed and generalized models of the error of both the PMUs and the Current Transformers and with a generalization of the tap-changing transformer model. After these updates, the methods showed a significant improvement in estimation accuracy.

In general, all the results obtained for both single-phase and three-phase formulations have shown the capability of the approach to reduce the uncertainty on both targets of the method: network parameters and systematic measurement errors.

The proposed approach proved to be effective also in its integration in one of the most important power system management and control applications, the fault location. In this context, an in-depth analysis was carried out starting from a fault detection and location procedure present in the literature.

In conclusion, it can be highlighted that the proposed approach and the presented estimation framework can be considered as a valid and robust tool, which can be used by System Operators to update their data and model with a certain periodicity and to compensate for systematic errors in their measurements. This can improve the efficacy and flexibility of their monitoring and control applications.

Appendix

I IEEE 14 Bus test system

The main characteristics of the IEEE 14 bus test system are reported in Fig. 1, Table 1 and Table 2.

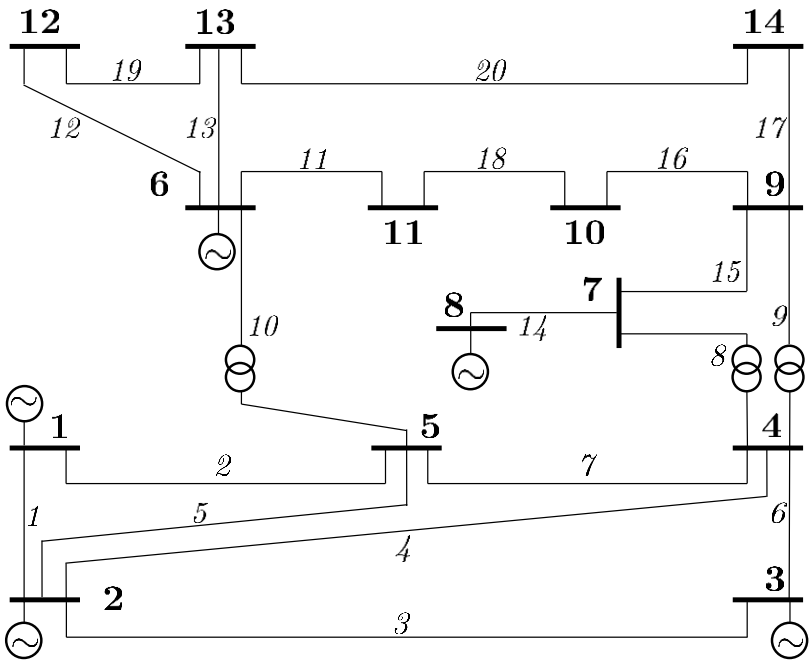

Figure 1: Topology of the IEEE 14 bus test system.

Table 1: Nominal linedata of the IEEE 14 bus test system

Branch	$R^0_{i,j}$	$X^0_{i,j}$	$B^0_{sh,i,j}$
		[pu]	
1	0.01938	0.05917	0.0264
2	0.05403	0.22304	0.0246
3	0.04699	0.19797	0.0219
4	0.05811	0.17632	0.0170
5	0.05695	0.17388	0.0173
6	0.06701	0.17103	0.0064
7	0.01335	0.04211	0.0
8	0.0	0.20912	0.0
9	0.0	0.55618	0.0
10	0.0	0.25202	0.0
11	0.09498	0.19890	0.0
12	0.12291	0.25581	0.0
13	0.06615	0.13027	0.0
14	0.0	0.17615	0.0
15	0.0	0.11001	0.0
16	0.03181	0.08450	0.0
17	0.12711	0.27038	0.0
18	0.08205	0.19207	0.0
19	0.22092	0.19988	0.0
20	0.17093	0.34802	0.0

Table 2: Active and reactive power of the loads

Node index	P_h **[MW]**	Q_h **[Mvar]**
2	−18.3	−30.86
3	94.2	−6.08
4	47.8	−3.9
5	7.6	1.6
6	11.2	−5.23
7	0	0
8	0	−17.62
9	29.5	16.6
10	9	5.8
11	3.5	1.8
12	6.1	1.6
13	13.5	5.8
14	14.9	5

II Modified version of the 95 nodes UKGDS system

The main characteristics of the modified version of 95 UKGDS system are reported in Fig. 2, Table 3 and Table 4.

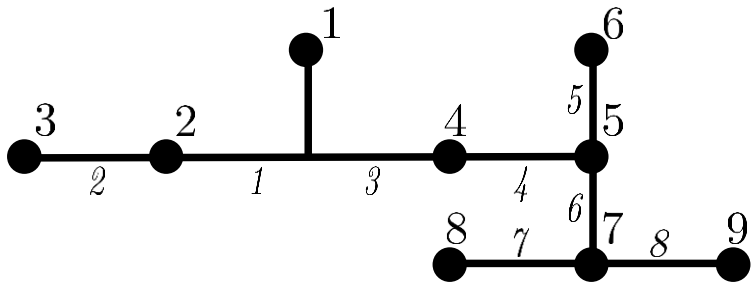

Figure 2: Topology of the modified version of 95 UKGDS system.

Table 3: Nominal linedata values of the modified version of 95 UKGDS system

Branch	$R^0_{i,j}$	$X^0_{i,j}$	$B^0_{sh,i,j}$
	[pu]		
1	0.055	0.057	0.000073
2	0.039	0.10	0.000052
3	0.049	0.051	0.000065
4	0.098	0.33	0.00013
5	0.17	0.076	0.00023
6	0.21	0.20	0.00028
7	0.24	0.11	0.00032
8	0.26	0.18	0.00035

Table 4: Active and reactive power of the loads

Node index	P_h **[MW]**	Q_h **[Mvar]**
2	0	0
3	3.28	0.57
4	0	0
5	0	0
6	0.058	0.0083
7	0	0
8	0.12	0.017
9	4	4

III 15 kV test network

The main characteristics of the 15 kV test network are reported in Fig. 3, Table 5 and Table 6.

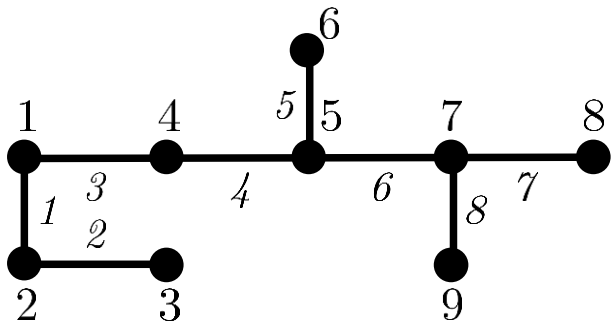

Figure 3: Topology of the 15 kV test network.

Table 5: Nominal line parameters of the 15 kV test network

Branch	$R^0_{i,j}$	$X^0_{i,j}$	$B^0_{sh,i,j}$
	[pu]		
1	0.055	0.057	0.00017
2	0.039	0.12	0.00065
3	0.049	0.051	0.00015
4	0.098	0.33	0.0016
5	0.17	0.066	0.00012
6	0.21	0.20	0.00066
7	0.24	0.09	0.00017
8	0.26	0.18	0.00048

Table 6: Active and reactive power of the loads

Node index	P_h **[MW]**	Q_h **[Mvar]**
2	0	0
3	3.28	0.57
4	0	0
5	0	0
6	0.12	0.017
7	0	0
8	0.24	0.035
9	4	4

Bibliography

[1] H. Wang, H. Jiao, J. Chen, and W. Liu, "Parameter identification for a power distribution network based on MCMC algorithm," *IEEE Access*, vol. 9, pp. 104 154–104 161, Jun. 2021.

[2] D. H. Tungadio, J. A. Jordaan, and M. W. Siti, "Power system state estimation solution using modified models of PSO algorithm: Comparative study," *Measurement*, vol. 92, pp. 508–523, Oct. 2016.

[3] J. Fu, G. Song, and B. De Schutter, "Influence of measurement uncertainty on parameter estimation and fault location for transmission lines," *IEEE Trans. Autom. Sci. Eng.*, vol. 18, no. 1, pp. 337–345, Jan. 2021.

[4] Z. Wu, H. Long, and C. Chen, "Line aging assessment in distribution network based on topology verification and parameter estimation," *J. Mod. Power Syst. Clean Energy*, vol. 10, no. 6, pp. 1658–1668, Nov. 2022.

[5] M. Asprou and E. Kyriakides, "Identification and estimation of erroneous transmission line parameters using PMU measurements," *IEEE Trans. Power Del.*, vol. 32, no. 6, pp. 2510–2519, Dec. 2017.

[6] G. Kusic and D. Garrison, "Measurement of transmission line parameters from SCADA data," in *IEEE PES Power Syst. Conf. and Expo.*, New York City, NY, USA, Oct. 2004, pp. 344–349.

[7] H. Zhang, Z. Diao, and Y. Cui, "Identification of Power Network Branch Parameters Based on State Space Transformation," *IEEE Access*, vol. 7, pp. 91 720–91 730, Jul. 2019.

[8] M. Asprou, E. Kyriakides, and M. M. Albu, "Uncertainty bounds of transmission line parameters estimated from synchronized measurements," *IEEE Trans. Instrum. Meas.*, vol. 68, no. 8, pp. 2808–2818, Aug. 2019.

[9] S. Vlahinić, D. Franković, M. Ž. Durovič, and N. Stojković, "Measurement uncertainty evaluation of transmission line parameters," *IEEE Trans. Instrum. Meas.*, vol. 70, pp. 1–7, Apr. 2021.

[10] A. Xue, F. Xu, K. E. Martin, H. You, J. Xu, L. Wang, and G. Wei, "Robust identification method for transmission line parameters that considers PMU phase angle error," *IEEE Access*, vol. 8, pp. 86 962–86 971, May 2020.

[11] H. Haiyan, K. He, G. Lei, M. Jing, X. Feiyang, and X. Ancheng, "Steady-state PMU data selection for parameter identification of transmission line considering the influence of measurement error," *IET Gener. Transm. Distrib.*, vol. 16, pp. 4549–4562, Sep. 2022.

[12] J. Lin, J. Song, and C. Lu, "Synchrophasor data analytics: Transmission line parameters online estimation for energy management," *IEEE Trans. Eng. Manag.*, vol. 69, no. 3, pp. 671–681, Jun. 2022.

[13] J. Sun, M. Xia, and Q. Chen, "A classification identification method based on phasor measurement for distribution line parameter identification under insufficient measurements conditions," *IEEE Access*, vol. 7, pp. 158 732–158 743, Oct. 2019.

[14] Y. Hou, T. Fang, F. Shi, and H. Zhang, "Parameter estimation method of distribution network based on PMU measurement data," in *2020 5th Asia Conference on Power and Electrical Engineering (ACPEE)*, Chengdu, China, Jun. 2020, pp. 1620–1625.

[15] Y. Wang, M. Xia, Q. Yang, Y. Song, Q. Chen, and Y. Chen, "Augmented state estimation of line parameters in active power distribution systems with phasor measurement units," *IEEE Trans. Power Del.*, vol. 37, no. 5, pp. 3835–3845, Oct. 2022.

[16] A. Wehenkel, A. Mukhopadhyay, J.-Y. L. Boudec, and M. Paolone, "Parameter estimation of three-phase untransposed short transmission lines from synchrophasor measurements," *IEEE Trans. Instrum. Meas.*, vol. 69, no. 9, pp. 6143–6154, Sep. 2020.

[17] F. P. De Albuquerque, E. C. M. Da Costa, R. F. R. Pereira, L. H. B. Liboni, and M. C. De Oliveira, "Nonlinear analysis on transmission line parameters estimation from noisy phasorial measurements," *IEEE Access*, vol. 10, pp. 1720–1730, Dec. 2021.

[18] M. Xiao, W. Xie, C. Fang, S. Wang, Z. Ullah, X. Zheng, R. Arghandeh, Y. Li, and S. Liu, "Distribution line parameter estimation driven by probabilistic data fusion of d-PMU and AMI," *IET Generation, Transmission & Distribution*, vol. 15, no. 20, pp. 2883–2892, Jun. 2021.

[19] R. K. Gupta, F. Sossan, J.-Y. Le Boudec, and M. Paolone, "Compound admittance matrix estimation of three-phase untransposed power distribution grids using synchrophasor measurements," *IEEE Trans. Instrum. Meas.*, vol. 70, pp. 1–13, Jun. 2021.

[20] E. Satsuk, A. Zhukov, D. Dubinin, I. Ivanov, and A. Murzin, "Analytical approach to phasor-based line parameter estimation verified through real PMU data," in *2022 International Conference on Smart Grid Synchronized Measurements and Analytics (SGSMA)*, Split, Croatia, May 2022, pp. 1–6.

[21] D. Franković, S. Vlahinić, and M. Ž. Durovič, "Application of different least square methods for transmission line parameter estimation," in *2022 IEEE 12th International Workshop on Applied Measurements for Power Systems (AMPS)*, Cagliari, Italy, Sep. 2022, pp. 1–5.

[22] C. Roberts, C. M. Shand, K. Brady, E. M. Stewart, A. W. McMorran, and G. A. Taylor, "Improving distribution network model accuracy using impedance estimation from micro-synchrophasor data," in *2016 IEEE Power and Energy Society General Meeting (PESGM)*, Boston, Massachusetts, USA, Nov. 2016, pp. 1–5.

[23] R. S. Singh, S. Babaev, V. Cuk, S. Cobben, and H. van den Brom, "Line parameters estimation in presence of uncalibrated instrument transformers," in *2019 2nd International Colloquium on Smart Grid Metrology (SMAGRIMET)*, Split, Croatia, Apr. 2019, pp. 1–8.

[24] V. Milojevic, M. V. Aćanski, and D. Colangelo, "Utilization of PMU Measurements for Three-Phase Line Parameter Estimation in Power Systems," *IEEE Trans. Instrum. Meas.*, vol. 67, no. 10, p. 10, Oct. 2018.

[25] A. Pal, P. Chatterjee, J. S. Thorp, and V. A. Centeno, "Online calibration of voltage transformers using synchrophasor measurements," *IEEE Trans. Power Del.*, vol. 31, no. 1, pp. 370–380, Feb. 2016.

[26] C. Wang, V. A. Centeno, K. D. Jones, and D. Yang, "Transmission lines positive sequence parameters estimation and instrument transformers calibration based on PMU measurement error model," *IEEE Access*, vol. 7, pp. 145 104–145 117, Oct. 2019.

[27] Y. G. Kononov, O. S. Rybasova, and K. A. Sidirov, "Identification of overhead-line parameters from PMU data with compensation of systematic measurement errors," in *Int. Conf. on Ind. Eng., Appl. and Manuf. (ICIEAM)*, Moscow, Russia, May 2018, pp. 1–5.

[28] H. Goklani, G. Gajjar, and S. A. Soman, "Instrument transformer calibration and robust estimation of transmission line parameters using PMU measurements," *IEEE Trans. Power Syst.*, vol. 36, no. 3, pp. 1761–1770, May 2021.

[29] K. V. Khandeparkar, S. A. Soman, and G. Gajjar, "Detection and correction of systematic errors in instrument transformers along with line parameter estimation using PMU data," *IEEE Trans. Power Syst.*, vol. 32, no. 4, pp. 3089–3098, Jul. 2017.

[30] P. A. Pegoraro, P. Castello, C. Muscas, K. Brady, and A. von Meier, "Handling instrument transformers and PMU errors for the estimation of line parameters in distribution grids," in *2017 IEEE International Workshop on Applied Measurements for Power Systems (AMPS)*, Liverpool, UK, Sep. 2017, pp. 1–6.

[31] P. A. Pegoraro, K. Brady, P. Castello, C. Muscas, and A. von Meier, "Line impedance estimation based on synchrophasor measurements for power distribution systems," *IEEE Trans. Instrum. Meas.*, vol. 68, no. 4, pp. 1002–1013, Apr. 2019.

[32] P. A. Pegoraro, K. Brady, P. Castello, C. Muscas, and A. von Meier, "Compensation of systematic measurement errors in a PMU-based monitoring system for electric distribution grids," *IEEE Trans. Instrum. Meas.*, vol. 68, no. 10, pp. 3871–3882, Oct. 2019.

[33] C. A. Ferreira and R. B. Prada, "Improved model for tap-changing transformer," *IET Generation, Transmission & Distribution*, vol. 7, no. 11, pp. 1289–1295, Nov. 2013.

[34] R. Yang, D. Zhang, Z. Li, K. Yang, S. Mo, and L. Li, "Mechanical fault diagnostics of power transformer on-load tap changers using dynamic time warping," *IEEE Trans. Instrum. Meas.*, vol. 68, no. 9, pp. 3119–3127, Sep. 2019.

[35] X. Liang, Y. Wang, and H. Gu, "A mechanical fault diagnosis model of on-load tap changer based on same-source heterogeneous data fusion," *IEEE Trans. Instrum. Meas.*, vol. 71, pp. 1–9, Mar. 2021.

[36] G. Korres, P. Katsikas, and G. Contaxis, "Transformer tap setting observability in state estimation," *IEEE Trans. Power Syst.*, vol. 19, no. 2, pp. 699–706, May 2004.

[37] A. Singhal, H. K. Rathour, P. Agarwal, K. V. S. Baba, and S. K. Soonee, "State estimation at all india level," in *2016 National Power Systems Conference (NPSC)*, Bhubaneswar, India, Dec. 2016, pp. 1–6.

[38] M. Rezaei, S. S. Mortazavi, M. Razaz, and M. S. Ghazizadeh, "The statistical interval estimation of the mean and the hypothesis testing of population proportions for transformer tap position estimation," *Electric Power Systems Research*, vol. 164, pp. 212–219, Nov. 2018.

[39] R. C. Pires, L. Mili, and F. A. B. Lemos, "Constrained robust estimation of power system state variables and transformer tap positions under erroneous zero-injections," *IEEE Trans. Power Syst.*, vol. 29, no. 3, pp. 1144–1152, May 2014.

[40] A. S. Dobakhshari, M. Abdolmaleki, V. Terzija, and S. Azizi, "Online non-iterative estimation of transmission line and transformer parameters by SCADA data," *IEEE Trans. Power Syst.*, vol. 36, no. 3, pp. 2632–2641, May 2021.

[41] S. G. Ghiocel, J. H. Chow, G. Stefopoulos, B. Fardanesh, D. Maragal, B. Blanchard, M. Razanousky, and D. B. Bertagnolli, "Phasor-measurement-based state estimation for synchrophasor data quality improvement and power transfer interface monitoring," *IEEE Trans. Power Syst.*, vol. 29, no. 2, pp. 881–888, Mar. 2014.

[42] E. R. Fernandes, S. G. Ghiocel, J. H. Chow, D. E. Ilse, D. D. Tran, Q. Zhang, D. B. Bertagnolli, X. Luo, G. Stefopoulos, B. Fardanesh, and R. Robertson, "Application of a phasor-only state estimator to a large power system using real PMU data," *IEEE Trans. Power Syst.*, vol. 32, no. 1, pp. 411–420, Jan. 2017.

[43] C. Borda, A. Olarte, and H. Diaz, "PMU-based line and transformer parameter estimation," in *2009 IEEE/PES Power Systems Conference and Exposition*, Seattle, Washington, USA, Mar. 2009, pp. 1–8.

[44] B. Vicol, "On-line overhead transmission line and transformer parameters identification based on PMU measurements," in *2014 International Conference and Exposition on Electrical and Power Engineering (EPE)*, Iasi, Romania, Oct. 2014, pp. 1045–1050.

[45] M. R. Rezaei, S. R. Hadian-amrei, and M. R. Miveh, "Online identification of power transformer and transmission line parameters using synchronized voltage and current phasors," *Electric Power Systems Research*, vol. 203, p. 107638, Feb. 2022.

[46] R. S. Luciano V. Barboza, Hans H. Ziirn, "Load tap change transformers: A modeling reminder," *IEEE Power Eng. Rev.*, vol. 21, no. 2, pp. 51–52, Feb. 2001.

[47] A. Abur and A. G. Expòsito, *Power System State Estimation. Theory and Implementation.* Marcel Dekker, New York, 2004.

[48] J. D. Glover, M. S. Sarma, and T. J. Overbye, *Power system analysis and design.* Cengage Learning, 2012.

[49] Jiangshan Scotech Electrical Co.,Ltd, "220kV power transformer with on load tap changer," https://www.scotech-electrical.com/showroom/220kv-Power-Transformer-with-on-Load-Tap-Changer.html, Accessed: 2022-06-15.

[50] J. M. Cano, M. R. R. Mojumdar, and G. A. Orcajo, "On the consistency of tap-changing transformer models in power system studies," in *2020 IEEE Power & Energy Society General Meeting (PESGM)*, Montreal, QC, Canada, Aug. 2020, pp. 1–5.

[51] ——, "Reconciling tap-changing transformer models," *IEEE Trans. Power Del.*, vol. 34, no. 6, pp. 2266–2268, Dec. 2019.

[52] R. Puddu, K. Brady, C. Muscas, P. A. Pegoraro, and A. V. Meier, "PMU-based technique for the estimation of line parameters in three-phase electric distribution grids," in *2018 IEEE 9th Int. Workshop on Applied Measurements for Power Systems (AMPS)*, Sept 2018, pp. 1–5.

[53] C. Muscas, P. A. Pegoraro, C. Sitzia, A. V. Solinas, and S. Sulis, "Compensation of systematic measurement errors in PMU-based monitoring systems for transmission grids," in *IEEE Int. Instrum. and Meas. Technol. Conf. (I2MTC)*, Virtual Event, May 2021, pp. 1–6.

[54] C. Sitzia, C. Muscas, P. A. Pegoraro, A. V. Solinas, and S. Sulis, "Enhanced PMU-based line parameters estimation and compensation of systematic measurement errors in power grids considering multiple operating conditions," *IEEE Trans. Instrum. Meas.*, vol. 71, pp. 1–12, Jan. 2022.

[55] P. A. Pegoraro, C. Sitzia, A. V. Solinas, and S. Sulis, "A PMU-based technique for the simultaneous estimation of systematic measurement errors, line parameters and tap changer ratio," in *2021 IEEE 11th International Workshop on Applied Measurements for Power Systems (AMPS)*, Virtual Event, Sep. 2021, pp. 1–6.

[56] IEC/IEEE, *International Standard- Power transformers - Part 21: Standard requirements, terminology, and test code for step-voltage regulators*, IEC/IEEE IEC 60076-21:2018(E) IEEE Std C57.15-2017, 2018.

[57] P. Ren, H. Lev-Ari, and A. Abur, "Tracking three-phase untransposed transmission line parameters using synchronized measurements," *IEEE Trans. Power Syst.*, vol. 33, no. 4, pp. 4155–4163, July 2018.

[58] JCGM, "Evaluation of data - guide to the expression of uncertainty in measurement," *JCGM 100:2008*, Sep. 2008.

[59] IEC, *Instrument transformers - Part 2: Inductive voltage transformers*, CEI IEC Int. Std. IEC 60044-2, 1997.

[60] ——, *Instrument transformers - Part 1: Current transformers*, CEI IEC Int. Std. IEC 60044-1, 2003.

[61] R. Abu-Hashim, R. Burch, G. Chang, M. Grady, E. Gunther, M. Halpin, C. Harziadonin, Y. Liu, M. Marz, T. Ortmeyer, V. Rajagopalan, S. Ranade, P. Ribeiro, T. Sim, and W. Xu, "Test systems for harmonics modeling and simulation," *IEEE Trans. Power Del.*, vol. 14, no. 2, pp. 579–587, Apr 1999.

[62] P. C. Hansen, "REGULARIZATION TOOLS: A Matlab package for analysis and solution of discrete ill-posed problems," *Numerical Algorithms*, vol. 6, no. 1, pp. 1–35, Mar. 1994.

[63] ——, "The discrete picard condition for discrete ill-posed problems," *BIT Numerical Mathematics*, vol. 30, pp. 658–672, 1990.

[64] P. C. Hansen, "The L-curve and its use in the numerical treatment of inverse problems," *P. Johnston (Ed.), Computational Inverse Problems in Electrocar-diography, WIT Press, Southampton*, pp. 119–142, 2001.

[65] V. A. Morozov, *Methods for Solving Incorrectly Posed Problems.* New York, NY: Springer New York, 1984.

[66] D. Carta, C. Muscas, P. A. Pegoraro, A. V. Solinas, and S. Sulis, "Compressive sensing-based harmonic sources identification in smart grids," *IEEE Trans. Instrum. Meas.*, vol. 70, pp. 1–10, Nov. 2020.

[67] L. Reichel and A. Shyshkov, "A new zero-finder for Tikhonov regularization," *BIT Numerical Mathematics*, vol. 48, no. 3, pp. 627–643, Sep. 2008.

[68] P. A. Pegoraro, C. Sitzia, A. V. Solinas, and S. Sulis, "PMU-based estimation of systematic measurement errors, line parameters, and tap changer ratios in three-phase power systems," *IEEE Trans. Instrum. Meas.*, vol. 71, pp. 1–12, Apr. 2022.

[69] W. H. K. Kersting, *Distribution System Modeling and Analysis, 3rd ed.* Boca Raton, FL, USA: William H. Kersting, 2002.

[70] M. Bazrafshan, N. Gatsis, and H. Zhu, "Optimal power flow with step-voltage regulators in multi-phase distribution networks," *IEEE Trans. Power Syst.*, vol. 34, no. 6, pp. 4228–4239, May 2019.

[71] M. Bazrafshan and N. Gatsis, "Comprehensive modeling of three-phase distribution systems via the bus admittance matrix," *IEEE Trans. Power Syst.*, vol. 33, no. 2, pp. 2015–2029, Mar. 2018.

[72] R. Abu-Hashim, R. Burch, G. Chang, M. Grady, E. Gunther, M. Halpin, C. Harziadonin, Y. Liu, M. Marz, T. Ortmeyer, V. Rajagopalan, S. Ranade, P. Ribeiro, T. Sim, and W. Xu, "Test systems for harmonics modeling and simulation," *IEEE Trans. Power Del.*, vol. 14, no. 2, pp. 579–587, Apr. 1999.

[73] Terna SpA, "Qualità del servizio di trasmissione - rapporto annuale per l'anno 2020 [Quality of service - Annual report for year 2020]," pp. 1–109, 2021, (in Italian). [Online]. Available: https://download.terna.it/terna/Rapporto%20Annuale%20Qualit%C3%A0%202020_8d942c0ff3f9277.pdf

[74] P. Castello, C. Muscas, P. A. Pegoraro, G. Guida, G. M. Giannuzzi, and P. Pau, "Interoperability of phasor measurement units under voltage unbalance conditions," in *2017 AEIT International Annual Conference*, Cagliari, Italy, Sep. 2017, pp. 1–6.

[75] H. Goklani, G. Gajjar, and S. A. Soman, "Quantification of minimum unbalance required for accurate estimation of sequence parameters of transmission line using PMU data," in *2019 IEEE Power & Energy Society General Meeting (PESGM)*, Atlanta, GA, USA, Aug. 2019, pp. 1–5.

[76] P. Castello, G. Gallus, C. Muscas, P. A. Pegoraro, D. Sitzia, and S. Sulis, "A statistical investigation of PMU errors in current measurements," in *2023 IEEE International Instrumentation and Measurement Technology Conference (I2MTC)*, Kuala Lumpur, Malaysia, May 2023, pp. 1–6.

[77] P. Castello, C. Muscas, and P. A. Pegoraro, "Statistical behavior of PMU measurement errors: An experimental characterization," *IEEE Open Journal of Instrumentation and Measurement*, vol. 1, pp. 1–9, Sep. 2022.

[78] A. Mingotti, L. Peretto, R. Tinarelli, A. Angioni, A. Monti, and F. Ponci, "Calibration of synchronized measurement system: from the instrument transformer to the PMU," in *2018 IEEE 9th International Workshop on Applied Measurements for Power Systems (AMPS)*, Bologna, Italy, Sep. 2018, pp. 1–5.

[79] CENELEC, *Voltage characteristics of electricity supplied by public electricity networks*, European Standard EN50160:2010+A3 Std., 2019.

[80] *Instrument transformers - Part 11: Additional requirements for low-power passive voltage transformers*, IEC Int. Std. IEC 61869-11:2017, 2017.

[81] C. Laurano, S. Toscani, and M. Zanoni, "A simple method for compensating harmonic distortion in current transformers: Experimental validation," *Sensors*, vol. 21, no. 9, Apr. 2021.

[82] M. Faifer, C. Laurano, R. Ottoboni, and S. Toscani, "Compensating the harmonic distortion introduced by instrument transformers: An improved method based on frequency-domain polynomials," in *IEEE 11th Int. Workshop on Applied Measurements for Power Systems (AMPS)*, Virtual Event, Sep. 2021, pp. 1–6.

[83] *Instrument transformers - Part 10: Additional requirements for low-power passive current transformers*, IEC Int. Std. IEC 61869-10:2017, 2017.

[84] P. A. Pegoraro, C. Sitzia, A. V. Solinas, S. Sulis, C. Laurano, and S. Toscani, "Impact of current transformers on line parameters estimation based on synchronized measurements," in *2022 IEEE 12th International Workshop on Applied Measurements for Power Systems (AMPS)*, Cagliari, Italy, Sep. 2022, pp. 1–6.

[85] C. Laurano, P. A. Pegoraro, C. Sitzia, A. V. Solinas, S. Sulis, and S. Toscani, "Refined modeling and compensation of current transformers behavior for line parameters estimation based on synchronized measurements," *IEEE Open Journal of Instrumentation and Measurement*, vol. 2, pp. 1–11, Feb. 2023.

[86] D. Tziouvaras, P. McLaren, G. Alexander, D. Dawson, J. Esztergalyos, C. Fromen, M. Glinkowski, I. Hasenwinkle, M. Kezunovic, L. Kojovic, B. Kotheimer, R. Kuffel, J. Nordstrom, and S. Zocholl, "Mathematical models for current, voltage, and coupling capacitor voltage transformers," *IEEE Trans. Power Del.*, vol. 15, no. 1, pp. 62–72, 2000.

[87] A. Mingotti, L. Peretto, L. Bartolomei, D. Cavaliere, and R. Tinarelli, "Are inductive current transformers performance really affected by actual distorted network conditions? An experimental case study," *Sensors*, vol. 20, no. 3, Feb. 2020.

[88] R. Pintelon and J. Schoukens, *System Identification: A Frequency Domain Approach*. Wiley-IEEE Press, 2012.

[89] R. Singh, "State estimation in power distribution network operation," Ph.D. dissertation, Imperial College London, 2009.

[90] P. A. Pegoraro, C. Sitzia, A. V. Solinas, and S. Sulis, "Characterization of a method for transmission line parameters estimation with respect to PMU measurement error modeling," in *25th IMEKO TC4 International Symposium*, Brescia, Italy, Sep. 2022, pp. 1–6.

[91] ——, "Transmission line parameters estimation in the presence of realistic PMU measurement error models," *Measurement*, vol. 218, p. 113175, Aug. 2023.

[92] C. Muscas, P. A. Pegoraro, C. Sitzia, A. V. Solinas, S. Sulis, E. M. Carlini, G. M. Giannuzzi, and C. Pisani, "Characterization of a PMU-based method for transmission line parameters estimation with systematic measurement error modeling," in *AEIT Int. Annual Conf.*, Virtual Event, Oct. 2021, pp. 1–6.

[93] "IEEE/IEC international standard - Measuring relays and protection equipment - part 118-1: Synchrophasor for power systems - Measurements," pp. 1–78, Dec 2018.

[94] P. A. Pegoraro, C. Sitzia, A. V. Solinas, and S. Sulis, "Estimation of line parameters, tap changer ratios, and systematic measurement errors based on synchronized measurements and a general model of tap-changing transformers," *IEEE Open Journal of Instrumentation and Measurement*, vol. 1, pp. 1–11, Sep. 2022.

[95] M. R. R. Mojumdar, J. M. Cano, and G. A. Orcajo, "Estimation of impedance ratio parameters for consistent modeling of tap-changing transformers," *IEEE Trans. Power Syst.*, vol. 36, no. 4, pp. 3282–3292, Jul. 2021.

[96] D. Carta, A. Benigni, C. Sitzia, P. A. Pegoraro, and S. Sulis, "Performance assessment of synchronized phasor measurement-based parameter estimation for distribution networks," in *2022 International Conference on Smart*

Energy Systems and Technologies (SEST), Eindhoven, Netherlands, Sep. 2022, pp. 1–6.

[97] C. Sitzia, D. Carta, A. Benigni, P. A. Pegoraro, and S. Sulis, "Distribution systems line parameter estimation with nodal injection constraints in presence of vehicle-to-grid," in *2023 IEEE Belgrade PowerTech*, Belgrade, Serbia, Jun. 2023, pp. 01–06.

[98] IEC, "Alternating current static watt-hour meters for active energy (classes 1 and 2)," *Standard IEC 61036*, 2000.

[99] Opal-RT Technologies, "Simulator Opal-RT," https://www.opal-rt.it.

[100] a-eberle, "Datasheet pqi-da smart." [Online]. Available: Available:https://www.a-eberle.de/produkte/the-power-quality-allrounder-pqi-da-smart

[101] J.-S. Brouillon, E. Fabbiani, P. Nahata, K. Moffat, F. Dörfler, and G. Ferrari-Trecate, "Bayesian error-in-variables models for the identification of distribution grids," *IEEE Trans. Smart Grid*, pp. 1–1, Oct. 2022.

[102] P. V. H. Seger, F. L. Grando, A. E. Lazzaretti, M. Moreto, G. W. Denardin, and C. R. Pastro, "Power system monitoring through low-voltage distribution network using *freePMU*," *IEEE Trans. Ind. Appl.*, vol. 58, no. 3, pp. 3153–3163, Jun. 2022.

[103] A. von Meier, E. Stewart, A. McEachern, M. Andersen, and L. Mehrmanesh, "Precision micro-synchrophasors for distribution systems: A summary of applications," *IEEE Trans. Smart Grid*, vol. 8, no. 6, pp. 2926–2936, Nov. 2017.

[104] C. Li, D. Carta, and A. Benigni, "A real-time simulation framework to evaluate the scheduling of V2G in distribution networks," in *IECON 2022 – 48th Annual Conference of the IEEE Industrial Electronics Society*, Oct. 2022, pp. 1–6.

[105] S. Bhowmick, "Tesla model s battery system: An engineer's perspective," Dec 2021. [Online]. Available: https://circuitdigest.com/article/tesla-model-s-battery-system-an-engineers-perspective.

[106] P. Stefanidou-Voziki, N. Sapountzoglou, B. Raison, and J. Dominguez-Garcia, "A review of fault location and classification methods in distribution grids," *Electric Power Systems Research*, vol. 209, p. 108031, Aug. 2022.

[107] M. Gholami, A. Abbaspour, M. Moeini-Aghtaie, M. Fotuhi-Firuzabad, and M. Lehtonen, "Detecting the location of short-circuit faults in active distribution network using PMU-based state estimation," *IEEE Trans. Smart Grid*, vol. 11, no. 2, pp. 1396–1406, Mar. 2020.

[108] P. K. Ganivada and P. Jena, "A fault location identification technique for active distribution system," *IEEE Trans. Ind. Informat.*, vol. 18, no. 5, pp. 3000–3010, May 2022.

[109] Q. Cui and Y. Weng, "Enhance high impedance fault detection and location accuracy via μ-PMUs," *IEEE Trans. Smart Grid*, vol. 11, no. 1, pp. 797–809, Jan. 2020.

[110] M. U. Usman and M. O. Faruque, "Validation of a PMU-based fault location identification method for smart distribution network with photovoltaics using real-time data," *IET Generation, Transmission & Distribution*, vol. 12, no. 21, pp. 5824–5833, Oct. 2018.

[111] M. Dashtdar, A. Hussain, H. Z. Al Garni, A. A. Masud, W. Haider, K. M. AboRas, and H. Kotb, "Fault location in distribution network by solving the optimization problem based on power system status estimation using the PMU," *Machines*, vol. 11, no. 1, p. 109, Jan. 2023.

[112] M. Farajollahi, A. Shahsavari, and H. Mohsenian-Rad, "Location identification of distribution network events using synchrophasor data," in *2017 North American Power Symposium (NAPS)*, Morgantown, WV, USA, Sep. 2017, pp. 1–6.

[113] M. Farajollahi, A. Shahsavari, E. M. Stewart, and H. Mohsenian-Rad, "Locating the source of events in power distribution systems using micro-PMU data," *IEEE Trans. Power Syst.*, vol. 33, no. 6, pp. 6343–6354, Nov. 2018.

[114] M. Majidi and M. Etezadi-Amoli, "A new fault location technique in smart distribution networks using synchronized/nonsynchronized measurements," *IEEE Trans. Power Del.*, vol. 33, no. 3, pp. 1358–1368, Jun. 2018.

[115] Y. Zhang, J. Wang, and M. E. Khodayar, "Graph-based faulted line identification using micro-PMU data in distribution systems," *IEEE Trans. Smart Grid*, vol. 11, no. 5, pp. 3982–3992, Sep. 2020.

[116] M. Pignati, L. Zanni, P. Romano, R. Cherkaoui, and M. Paolone, "Fault detection and faulted line identification in active distribution networks us-

ing synchrophasors-based real-time state estimation," *IEEE Trans. Power Del.*, vol. 32, no. 1, pp. 381–392, Feb. 2017.

[117] F. Conte, F. D' Agostino, B. Gabriele, G. P. Schiapparelli, and F. Silvestro, "Fault detection and localization in active distribution networks using optimally placed phasor measurements units," *IEEE Trans. Power Syst.*, vol. 38, no. 1, pp. 714–727, Jan. 2023.

[118] P. A. Pegoraro, C. Sitzia, A. V. Solinas, S. Sulis, A. Benigni, and D. Carta, "Fault identification in three phase distribution networks improved by line parameter estimation," in *2023 IEEE 13th International Workshop on Applied Measurements for Power Systems (AMPS)*, Bern, Switzerland, Sep. 2023, pp. 1–6.

[119] K. Strunz, E. Abbasi, R. Fletcher, N. Hatziargyriou, R. Iravani, and G. Joos, *TF C6.04.02 : TB 575 – Benchmark Systems for Network Integration of Renewable and Distributed Energy Resources.* CIGRE, 2014.

[120] RTDS Technologies Inc., "Real Time Digital Simulator (RTDS)," https://www.rtds.com.

[121] *IEEE Standard for Synchrophasor Measurements for Power Systems*, IEEE IEEE Std C37.118.1-2011 (Revision of IEEE Std C37.118-2005), Dec. 2011.

[122] IEC, *Instrument transformers - Part 3: Additional requirements for inductive voltage transformers*, IEC Int. Std. 61869-3, 2011.

[123] ——, *Instrument Transformers - Part 2: Additional Requirements For Current Transformers*, IEC Int. Std. 61869-2, 2012.

List of Figures

List of Tables

Acronyms

CT Current Transformer

DG distributed generation

DN Distribution Network

DP *Discrepancy Principle*

DS Distribution System

DSO Distribution System Operator

DSSE Distribution System State Estimation

EMS Energy Management System

EV Electric Vehicle

FZJ Forschungszentrum Jülich

GCV *Generalized Cross Validation*

HIL hardware-in-the-loop

IT Instrument Transformers

LCC *L-curve* criterion

LS Least Square

LV Low Voltage

MC Monte Carlo

MV Medium Voltage

NRW North-Rine Westphalia

PMU Phasor Measurement Unit

PV photovoltaic

RMSE root mean square error

RR reporting rate

RRSE relative root square error

RTDS Real Time Digital Simulator

SCADA supervisory control and data acquisition

SM smart meters

SO System Operator

SVD Singular Value Decomposition

SVR step voltage regulator

TSO Transmission System Operator

TVE Total Vector Error

UTC Coordinated Universal Time

V2G Vehicle-to-Grid

VT Voltage Transformer

WLS Weighted Least Square

WMR Weighted Measurement Residual

ZI zero injection

Acknowledgements

I would like to thank my supervisors **Prof. Sara Sulis** and **Prof. Paolo Attilio Pegoraro**, who supervised and guided me during the three years of my PhD, with practical suggestions and advice thanks to which I was able to improve academically and personally.

I would also like to thank **Prof. Carlo Muscas** and **Dr. Paolo Castello** who encouraged me and provided valuable advice during these three years.

Special thanks go to **Dr. Antonio Vincenzo Solinas** for his constant support during our research activities. I also thank my colleagues **Davide** and **Giacomo**, who made my time in the office lighter with their company.

I thank **Prof. Andrea Benigni** and **Dr. Daniele Carta** for supporting me during my visiting PhD period in Jülich and thanks to the **GMEE** association for making this experience possible.

Finally, I sincerely thank my **family** and **Patrizia**. Thank you for the invaluable and continuous support during these three years.